White organic light-emitting diodes: Status and perspective

Sebastian Reineke*

Department of Electrical Engineering and Computer Science, Massachusetts Institute of Technology, 77 Massachusetts Avenue, Cambridge, Massachusetts 02139, USA

Michael Thomschke,† Björn Lüssem, and Karl Leo

Institut für Angewandte Photophysik, TU Dresden, George-Bähr-Strasse 1, 01062 Dresden, Germany

(published 30 July 2013)

White organic light-emitting diodes (OLEDs) are ultrathin, large-area light sources made from organic semiconductor materials. Over the past decades, much research has been spent on finding suitable materials to realize highly efficient monochrome and white OLEDs. With their high efficiency, color tunability, and color quality, white OLEDs are emerging as one of the next-generation light sources. In this review, the physics of a variety of device concepts that have been introduced to realize white OLEDs based on both polymer and small-molecule organic materials are discussed. Owing to the fact that about 80% of the internally generated photons are trapped within the thin-film layer structure, a second focus is put on reviewing promising concepts for improved light outcoupling.

DOI: 10.1103/RevModPhys.85.1245 PACS numbers: 32.50.+d, 78.66.−w, 78.60.Fi, 78.55.−m

CONTENTS

*reineke@mit.edu
†Current address: Fraunhofer Research Institution for Organics, Materials and Electronic Devices COMEDD, Maria-Reiche-Strasse 2, 01109 Dresden, Germany.

I. INTRODUCTION

In 1880, Thomas A. Edison introduced the incandescent bulb—an epochal technical breakthrough that brought new light and comfort into people's everyday lives. Electricity was converted into a photon flux, so that artificial lighting became versatile as never before (Edison, 1880). Ever since, the energy demand of mankind has steadily increased to levels which clearly question our current ways of dealing with natural energy resources. Besides the fact that fossil resources are limited, our current energy consumption will most likely harm the global ecosystem, calling for another revolution in the way energy is used. Today it is one of the most important challenges to find efficient solutions for any energy-consuming process or application.

Edison's light bulb (a Planckian radiator) is still unmatched with respect to its color quality, because it is inherently good at resembling natural sunlight, which is most comfortable for the human perception both of light and, equally important, of the content that is illuminated. However, because incandescent lamps convert only roughly 5% of the consumed electric power into light, new lighting solutions with higher luminous efficacies (LEs), given in lumens per watt ($\mathrm{lm\,W^{-1}}$) (Ohta and Robertson, 2005), need to be developed. At the same time, alternative technologies should match the light quality of incandescent bulbs. With luminous efficacies up to 90 $\mathrm{lm\,W^{-1}}$ (Steele, 2007), fluorescent tubes are widely used as energy-efficient light sources; however, they lack good color quality and contain toxic mercury. In the past decades, a new class of light sources emerged, referred to as solid state lighting (SSL). In contrast to the gas discharge lamps, charge carriers (electrons and holes) are injected into semiconductor materials in their condensed phase, where they recombine under emission of photons.[1] The first light-emitting diodes (LEDs) were realized using inorganic semiconductors, where electroluminescence (EL) was initially observed in silicon carbide by Losev in 1928 (Zheludev, 2007). Similar to fluorescent tubes and compact fluorescent lamps, inorganic white LEDs make use of phosphorus downconversion layers excited by a blue LED to achieve white light (Ohno, 2004). White LEDs show remarkable efficiencies, the latest reported device efficiencies reach up to 169 $\mathrm{lm\,W^{-1}}$, which is almost double the values of typical fluorescent tubes (Narukawa *et al.*, 2006, 2008). Because of the crystallinity of the inorganic semiconductors used, these LEDs are point light sources with forward-directed emission characteristics.

The reports of Tang and VanSlyke (1987) and later of Burroughes *et al.* (1990) on electroluminescence from thin organic films made of small-molecular-weight molecules (devices referred to as OLEDs) and conducting polymers (PLEDs), respectively, opened a new field of research. Early efforts following these pioneering works focused on the improvement of these devices with respect to their efficiency, stability, and color tunability; however, solely monochrome devices[2] have been investigated. Roughly a decade later, the first multicolor OLEDs (Kido *et al.*, 1994) and PLEDs (Wang *et al.*, 1999) were reported, demonstrating that LEDs based on organic materials can become an alternative for general lighting applications.

It is our objective to review the topic of white organic light-emitting diodes[3] made of small molecules and/or polymers. We discuss different concepts that enable white light emission. We first focus on the internal efficiency of converting charges into photons, the most important prerequisite for highly efficient white OLEDs. The discussion of various concepts will show that OLEDs have the potential to reach very high internal efficiencies approaching unity; however, a large fraction of the light generated within the device cannot escape the thin-film layer structure. This results in low light-outcoupling efficiencies, typically on the order of 20% (Greenham, Friend, and Bradley, 1994), bearing great potential for improvement. Therefore, we put a second focus on key concepts for outcoupling enhancement known to date. Despite the fact that material and device stability still is one of the most important challenges for OLEDs to become a mature technology, we will not include the discussion of stability-related issues herein because this topic itself deserves a comprehensive review [see, e.g., So and Kondakov (2010)].

This review is organized as follows. Within Sec. I, fundamentals of organic light-emitting diodes (Sec. I.A) and their characterization (Sec. I.B) are discussed. This is followed by sections discussing concepts for white OLEDs based on polymers (Sec. II) and small molecules (Sec. III). Concepts for enhanced light outcoupling are jointly discussed for polymer- and small-molecule-based devices in Sec. IV. This review concludes by outlining the perspective of white OLEDs with regard to their device efficiency in Sec. V. In order to keep the readability high, rather than stating the complex material's full names in the main text, only the common abbreviations found in literature are used. Only, when it is important or helps clarity, the full chemical names are additionally given. All material abbreviations are defined in the Appendix of this paper.

A. Working principle of OLEDs

1. Device configurations and white light generation

Organic light-emitting diodes are ultrathin, large-area light sources made of thin-film organic semiconductors

[1]Note that luminescence can also be generated without injecting charges, driven by an alternating electric field, in inorganic thin films (Rack and Holloway, 1998), quantum dots (Wood *et al.*, 2011), and organic systems (Perumal *et al.*, 2012). However, to date, these technologies are not considered mainstream for SSL.

[2]Here monochrome is used to describe EL devices where emission stems from one type of emitter molecule only. This occurs even though any organic semiconductor has a certain spectral distribution of its emitted spectrum typically with full width at half maximum in the range of 50 to 100 nm (Pope, 1999).

[3]The abbreviation OLED is jointly used for small-molecule and polymer organic LEDs, simply because both material classes belong to the organic chemistry. The context will clarify whether OLEDs or PLEDs are discussed.

sandwiched between two electrodes. State-of-the-art small-molecule-based OLEDs consist of various layers—each layer having a distinct functionality. These films are prepared by thermal evaporation in high vacuum or organic vapor phase deposition (Baldo *et al.*, 1997; Forrest, 1997, 2004; Zhou *et al.*, 2005). In contrast, polymer OLEDs are typically processed by spin-on or spray-coating techniques (Friend *et al.*, 1999; Forrest, 2004), where the solvent is removed by annealing steps. Polymer OLEDs are limited in their complexity owing to the fact that the solvents used often harm the underlying layers. In order to improve the general complexity of wet-processed devices, tremendous effort is spent on improving polymer processing. These efforts include the use of cross-linking polymers to enable deposition of sequential layers from solution (Rehmann *et al.*, 2008; Zuniga, Barlow, and Marder, 2011), cross-linking in connection with direct photolithography to achieve patterned polymer layers (Gather, Koehnen *et al.*, 2007), and the laser-induced forward transfer of individual device pixels (Stewart *et al.*, 2012). Besides these uniform coating techniques, inkjet printing can be used to process polymer-based devices.

The general architecture of an OLED is shown as a cross section in Fig. 1 (top). The conventional bottom-emitting device comprises a transparent electrode on top of a glass substrate, followed by one or more layers of organic material and capped with a highly reflective metal electrode. By altering the optical properties of the electrodes, top-emitting (Riel *et al.*, 2003; Kanno, Sun, and Forrest, 2005; Q. Huang *et al.*, 2006) and transparent (Bulovic *et al.*, 1996) OLEDs can be fabricated. As organic materials have emission bands with 50–100 nm full width at half maximum (FWHM) (Pope, 1999; Thompson, 2007; Shimizu and Hiyama, 2010), typically more than one emitting material is necessary to realize white light. Figure 1 (bottom) schematically shows the common concepts used to realize white light emission in OLEDs. Stacked OLEDs [cf. Fig. 1(a)], where each unit can host different emitters, can be realized with additional (Burrows *et al.*, 1996) and without (Kanno, Giebink *et al.*, 2006; Kanno, Holmes *et al.*, 2006) electrodes. Here optical optimization is challenging because the emitters placed far apart within the optical cavity must all be located at their respective field antinode for efficient outcoupling (Lin *et al.*, 2006; Mladenovski *et al.*, 2009). Alternatively, the individual device units emitting red, green, and blue can be independently designed in a pixelated approach as shown in Fig. 1(b); however, this approach has major drawbacks because it involves comparably complicated structuring processes and higher current density for each color, which accelerates degradation. Apart from these concepts where high technological efforts are necessary, all other approaches for white OLEDs are based on a single device unit [cf. Figs. 1(c)–1(f)]. These are single-emitter-based devices [cf. Fig. 1(c)] (Adamovich *et al.*, 2002; D'Andrade *et al.*, 2002; Tsai *et al.*, 2003; Cocchi *et al.*, 2007; Kalinowski *et al.*, 2007; Williams *et al.*, 2007), blue OLEDs with external (Krummacher *et al.*, 2006; Gohri *et al.*, 2011) or internal (Schwab *et al.*, 2011) downconversion layers as depicted in Fig. 1(d), OLEDs with single emission layers (EMLs) comprising all emitter molecules [cf. Fig. 1(e)] (Kido, Shionoya, and Nagai, 1995; D'Andrade, Holmes, and Forrest, 2004; Liu *et al.*, 2005), and single white OLEDs comprising an EML containing different sublayers for red, green, and blue [cf. Fig. 1(f)] (Kido, Kimura, and Nagai, 1995; Chao and Chen, 1998; Schwartz *et al.*, 2006; Sun and Forrest, 2007; Reineke, Lindner *et al.*, 2009). All concepts are discussed in detail in Secs. II and III.

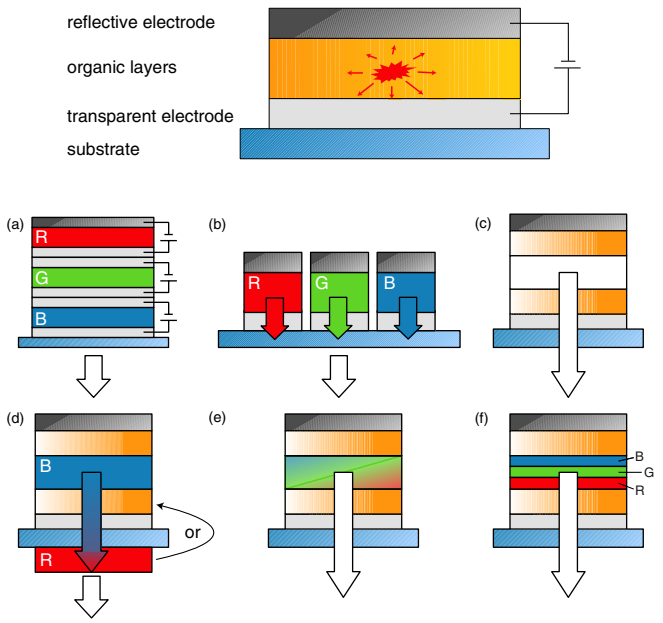

FIG. 1 (color online). Top: Schematic cross section of a bottom-emitting OLED. Bottom: Various device layouts to realize white light emission. (a) Vertically stacked OLEDs, (b) pixelated monochrome OLEDs, (c) single-emitter-based white OLEDs, (d) blue OLEDs with downconversion layers, (e) multiple-doped emission layers (EMLs), and (f) single OLEDs with a sublayer EML design. (c)–(f) Shaded layers represent optional functional layers, e.g., transport layers [not shown for (a) and (b) for better visibility]. R, G, and B stand for red, green, and blue, respectively.

2. Functional layers

Electroluminescence occurs as a consequence of charges, i.e., electrons and holes, being injected into a semiconductor material where they meet and recombine under the emission of photons. Originally observed in anthracene crystals (Helfrich and Schneider, 1965), efficient EL has been reported by Tang and VanSlyke (1987) [later by Burroughes *et al.* (1990) for polymers]. Since then, highly efficient OLEDs have become complex multilayer systems, where various functions such as charge transport, recombination, etc., are separated to reach maximum device efficiency. Figure 2 illustrates a multilayer OLED sequence with its functional layers.

The emission layer is located in the center of the device, where charges meet to form excited molecular states, the so-called excitons. In order to reach the EML, holes are injected from a high-work-function metal [in the bottom-emission layout mostly the transparent conductor indium tin oxide (ITO)] into the highest occupied molecular orbital (HOMO) of an organic semiconductor [the hole-transport layer (HTL)], itself having a comparably high hole mobility. Injection can

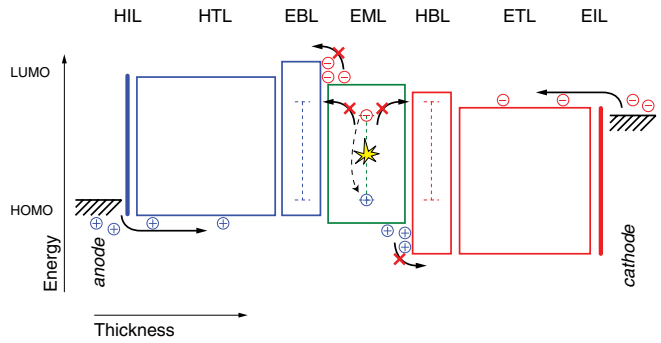

FIG. 2 (color online). Energy diagram of a typical multilayer OLED. Note that in many devices some of the layers depicted are redundant, because different functions may be combined in one layer. From anode to cathode there are the hole-injection layer (HIL), the hole-transport layer (HTL), the electron-blocking layer (EBL), the emission layer (EML), the hole-blocking layer (HBL), the electron-transport layer (ETL), and the electron-injection layer (EIL). Boxes indicate the highest occupied (HOMO) and lowest unoccupied (LUMO) molecular orbital levels of the materials. The dashed lines in the EBL, EML, and HBL are the desired triplet energies of the materials in the case of phosphorescent OLEDs.

be improved by an ultrathin hole-injection layer (HIL), which works for both small-molecule (Koch *et al.*, 2005) and polymer (Guo *et al.*, 2006) devices. The interested reader is referred to reviews of Kahn *et al.* (2001) and Koch (2012), discussing the details of interface physics between both metal and organic materials as well as at organic-organic interfaces. A similar effect can be achieved using metal oxides (such as tungsten, vanadium, or molybdenum oxide), enabling Ohmic injection into a wide variety of organic semiconductors (Greiner *et al.*, 2012). These oxides provide good injection properties with a high degree of flexibility, especially because the actual oxide can be easily exchanged to meet specific needs. Electrical doping of the HTL can be applied to simultaneously improve injection and transport [small molecules (Blochwitz *et al.*, 1998; Walzer *et al.*, 2007), polymers (Yamamori *et al.*, 1998)]. Before the holes reach the EML, they have to pass another (optional) layer, the electron-blocking layer (EBL). This blocking layer is often important to reach high efficiencies and has three key functions (cf. Fig. 2): (i) to prevent leakage of the opposite charge carrier type (here the electrons) from the EML into the HTL making use of a large step in the lowest unoccupied molecular orbital (LUMO) levels forming an energy barrier, (ii) to spatially separate the excitons from the HTL in the case of doping (because the dopants are effective luminescence quenchers) (Zhou *et al.*, 2001), and (iii) to realize exciton confinement. The latter function is especially important in the case of phosphorescent emitters, because their long excited-state lifetimes enhance their migration within the film. Here the requirement is to use blocker materials having a higher triplet level than the emitter molecule to suppress energy transfer (D'Andrade and Forrest, 2003; Goushi *et al.*, 2004; Chin and Lee, 2007). The injection and transport of electrons to the EML follows the same principles (cf. Fig. 2), with the only difference being that they migrate on the LUMO levels of the respective materials. As cathode materials, low-work-function materials such as aluminum, silver, and magnesium are typically used (Tang and VanSlyke, 1987; Adachi, Baldo, Forrest *et al.*, 2001; He, Schneider *et al.*, 2004; Reineke, Lindner *et al.*, 2009).

In polymer OLEDs, the device architecture is less complex with respect to the number of layers used, which is a consequence of solvents involved in the preparation process (Forrest, 2004). Often polymer OLEDs consist only of a single active layer sandwiched between the electrodes, where various materials are blended having different functionality (e.g., host and transport materials, chromophores, and even small-molecule emitter materials) (Tasch *et al.*, 1997; Anthopoulos *et al.*, 2003; Gong *et al.*, 2004; Kim *et al.*, 2004, 2006; Tu *et al.*, 2004, 2006; Xu *et al.*, 2004; Lee *et al.*, 2005; Huang, Hou *et al.*, 2006; Huang, Li *et al.*, 2006; Liu *et al.*, 2006; Wu, Lee, and Chen, 2006; Chuang *et al.*, 2007; Liu, Guo *et al.*, 2007; Liu, Xie *et al.*, 2007; Luo *et al.*, 2007; Wu *et al.*, 2008). It is worth noting that devices are still seen as single-layer diodes despite having electrodes [both anode and cathode (Huang, Hou *et al.*, 2006)] that comprise a multilayer design mainly to improve charge injection. Well known is the combination of poly(3,4-ethylene dioxythiophene):poly(styrene sulfonic acid) (PEDOT:PSS) on top of the transparent ITO anode (Kawamura, Yanagida, and Forrest, 2002; Gong *et al.*, 2005; Xu *et al.*, 2005; Niu *et al.*, 2006, 2007; Huang *et al.*, 2009), which is widely used as a heterolayer anode in polymer OLEDs. State-of-the-art wet-processing techniques allow a higher degree of complexity, for instance, by carefully choosing orthogonal solvents for subsequent layers (Granstrom and Inganas, 1996; Pschenitzka and Sturm, 1999; Chen *et al.*, 2002; Hu and Karasz, 2003; Noh *et al.*, 2003; Niu *et al.*, 2004, 2006, 2007; Gong *et al.*, 2005; Xu *et al.*, 2005; Huang *et al.*, 2009). Cross-linking polymer networks introduce an additional route to designing multilayer polymer systems (Rehmann *et al.*, 2008; Köhnen *et al.*, 2010). A compromise is often found in the combination of solution processes and thermal evaporation to achieve multilayer OLEDs that partially consist of layers comprising solely small molecules (Granstrom and Inganas, 1996; Wang *et al.*, 1999; Kawamura, Yanagida, and Forrest, 2002; Noh *et al.*, 2003; Niu *et al.*, 2004, 2006, 2007; Kim *et al.*, 2006). Finally, similar to small molecule OLEDs, the preparation of the highly reflective cathode requires thermal evaporation in high vacuum.

3. Fluorescent and phosphorescent electroluminescence

The majority of organic semiconductors form (in contrast to their inorganic counterparts) amorphous, disordered films (Pope, 1999), where van der Waals forces determine the structure on the nanoscale. As a consequence, charges are injected statistically with respect to their electron spin, finally determining the formation of singlet and triplet excited states. Because the triplet state has a multiplicity of 3 (Pope, 1999), on average 75% of the excitons formed are triplet states, with the remaining 25% being singlets. Segal *et al.* (2003) showed slightly smaller values for the singlet fraction in both small-molecule and polymeric systems [$\chi_S = (20 \pm 1)\%$ and $(20 \pm 4)\%$, respectively], which are in rather good agreement with this simple statistical picture [for further details see also Baldo *et al.* (1999)]. The low singlet fraction causes OLEDs

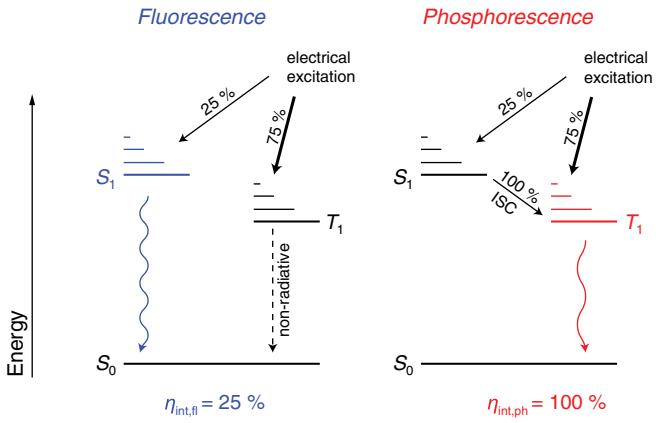

FIG. 3 (color online). Population scheme of singlet and triplet levels of organic molecules under electrical excitation. For phosphorescent emitter materials, the singlet excitons created are efficiently transferred to the triplet state via intersystem crossing (ISC). Additionally given are the theoretical limits for the internal quantum efficiency η_{int}.

based on fluorescent emitter molecules to be rather inefficient with an upper limit of the internal quantum efficiency of $\eta_{int,fl} = 25\%$, because emission solely occurs in its singlet manifold as shown in Fig. 3.

The efficiency of OLEDs was drastically improved with the introduction of phosphorescent emitter molecules (Baldo *et al.*, 1998; Ma *et al.*, 1998; Reineke and Baldo, 2012). These materials are organometallic complexes comprising a heavy-metal atom such as iridium, platinum, palladium, etc., in the molecular core. Making use of this heavy-metal effect, the spin-orbit coupling is strongly enhanced, ultimately weakening the selection rules for previously forbidden, radiative transitions in the triplet manifold of the molecule (Yersin *et al.*, 2002; Yersin, 2004; Thompson, 2007). Along with realizing a highly efficient emissive triplet state in a molecule, the heavy-metal effect strongly enhances the intersystem crossing (ISC) rates between the singlet and triplet manifolds (Yersin *et al.*, 2002; Yersin, 2004). Thus, the fractions of singlet excitons that are created under electrical excitation are efficiently converted into triplet states before they can recombine radiatively. The ISC rate is close to unity in various phosphorescent systems (Kawamura *et al.*, 2005, 2006). Therefore, phosphorescent materials in OLEDs can lead to internal EL efficiencies of $\eta_{int,ph} = 100\%$ (cf. Fig. 3). Furthermore, state-of-the-art emitters are especially optimized for having short excited-state lifetimes (typical values are on the order of microseconds) in order to reduce bimolecular quenching processes limiting the photoluminescence quantum yield at high excitation levels (Baldo, Adachi, and Forrest, 2000; Reineke, Walzer, and Leo, 2007). Furthermore, the emitter lifetimes need to be compatible with the *RC* time of the OLED to avoid emitter saturation effects (Thompson, 2007). In contrast to fluorescence, where emission originates from the lowest excited singlet state, phosphorescent EL induces thermalization losses on the order of the singlet-triplet splitting (Schwartz *et al.*, 2009) for every exciton that is captured by it via energy transfer from host materials or ISC (Sun *et al.*, 2006). The loss might be circumvented if the excitons are resonantly generated on the emitter dopant.

4. Exotic types of electroluminescence

Much research effort is spent on finding alternative concepts to phosphorescence that surpass the limit of $\eta_{int,fl} = 25\%$ in the case of fluorescence, because phosphorescence is accompanied with a serious efficiency decrease at high excitation levels (Baldo, Adachi, and Forrest, 2000; Reineke, Walzer, and Leo, 2007; Staroske *et al.*, 2007; Reineke, Schwartz, Walzer, Falke, and Leo, 2009) (for more details see Sec. I.A.7).

As mentioned in Sec. I.A.3, the vast majority of excitons is created as triplets where, in case of fluorescence, the excited triplet state is long lived (Pope, 1999). Thus, the triplet exciton density in fluorescent OLEDs will be comparably high. A concept to improve the internal quantum efficiency of fluorescent EL makes use of this high density via *delayed fluorescence* (Pope, 1999). Here the interaction of two triplet states (called *triplet-triplet annihilation*) will create delayed singlet excitons: $T_1 + T_1 \rightarrow S_0 + S_n$ (Kepler *et al.*, 1963). Based on this nonlinear process, an internal electron-photon conversion efficiency of unity cannot be reached. The device data of Okumoto *et al.* (2006) showing a twofold improvement to the $\eta_{int,fl} = 25\%$ limit [nearly 10% external quantum efficiency (EQE)] suggest that this process takes place. Kondakov (2007) gave experimental evidence that delayed fluorescence substantially contributes to the internal efficiency of fluorescent OLEDs; however, he suggested that this process cannot be the only reason for the very high efficiency of Okumoto *et al.* (2006).

Endo *et al.* (2009) suggested an alternative concept [thermally activated delayed fluorescence (TADF)] to feed the singlet state of a molecule with its triplet excitons. By tailoring molecules with a small singlet-triplet splitting, reverse intersystem crossing (RISC) will occur with an increased probability, because this process is thermally activated: $T_1 + E[\sim k_B T] \rightarrow S_1$ [see also Endo *et al.* (2011)]. Deaton *et al.* (2010) reported on very high-efficiency devices based on TADF, reaching 16% EQE. Based on this general idea, Goushi *et al.* (2012) reported on efficient triplet-to-singlet backconversion in OLEDs where the emissive state is an interfacial exciplex formed between two organic layers. Devices based on this concept showed a very high RISC efficiency of 86.5% and an external quantum efficiency beyond the fluorescence limit of 5%. Recently, Uoyama *et al.* (2012) reported promising OLED performance data based on this TADF concept. With a specially designed novel class of organic materials, the exchange splitting could be reduced to approximately 80 meV, giving rise to an effective reverse intersystem crossing. These materials possess a very high rate of delayed fluorescence on the order of 10^{-6} s, which is comparable to the radiative rates of phosphorescent emitters (Thompson, 2007). In their report, OLEDs are discussed reaching 19% EQE, which is on a par with the currently used phosphorescent emitter technology. It will be interesting to see how this concept develops in the future. For the first time, a promising, general concept has matured to a serious alternative to the phosphorescence based on heavy-metal complexes.

Finally, *extrafluorescence* was introduced by Segal *et al.* (2007). This concept makes use of an anomaly on the energetic order of singlet and triplet charge-transfer (CT) states

[the precursor states in the exciton formation process (Pope, 1999; Segal *et al.*, 2003)] of a molecule. By having a higher-lying triplet CT state, the rates of singlet exciton formation can be significantly increased, leading to a singlet fraction as high as $\chi_S = 0.84 \pm 0.03$ (Segal *et al.*, 2007).

It is worth mentioning that neither of these concepts finds application in white OLED concepts to date, mainly owing to the fact that the underlying working principles are not yet fully understood.

Even though LEDs based on colloidal quantum dots (QDs) have inorganic lumophores, these QD-LEDs share to a large extent the general device layout of OLEDs. Coe *et al.* (2002) showed that a single monolayer of QDs can be incorporated into an OLED architecture solely acting as a luminescent center of the device. It also has been shown that by incorporating differently emitting QDs into the monolayer, multicolor and white QD-LEDs can be fabricated (Anikeeva *et al.*, 2007). One important difference from OLEDs is the comparably small FWHM [< 40 nm (Anikeeva *et al.*, 2007)] of the QD's luminescence, directly affecting the color rendition properties of white QD-LEDs. Another important distinction from organic lumophors is the fact that QDs are not affected by the spin statistics as observed in OLEDs. QDs are quantum systems, where spin-singlet and spin-triplet character states are mixed very effectively (Coe *et al.*, 2002). However, QDs also have "bright" and "dark" excitonic band edge states that are spin allowed and forbidden, respectively (Shirasaki *et al.*, 2013). In very efficient QDs, their energetic splitting can be as small as 25 meV; thus, the dark states are effectively thermally activated to the bright states [state-of-the-art CdSe QDs can harness virtually 100% of the excitation in the bright state (Shirasaki *et al.*, 2013)]. It is worth noting that much effort is spent to replace the organic functional layers in a QD-LED by inorganic ones to benefit from the robustness of the latter (Caruge *et al.*, 2008).

5. Intermolecular energy transfer

White OLEDs are highly complex, multicomponent luminescent systems which greatly rely on various energy transfer mechanisms. These in turn lead to the distribution of the excitation to the desired emitter molecules. Thus, it is necessary to briefly review the possible energy transfers that can happen between different molecular species, which are referred to as *donor* (D) or *acceptor* (A) whenever they yield or accept energy, respectively. Furthermore, their multiplicities are denoted with preceding superscripts, i.e., 1 or 3 for singlets and triplets, respectively. Furthermore, asterisks mark excited states and double asterisk levels higher than the lowest possible electronic excitation.

Trivially, energy can be transferred as a two-step process (radiative energy transfer) that involves the emission and absorption of a photon $h\nu$ having a frequency ν:

$$D^* \rightarrow D + h\nu, \tag{1}$$

$$h\nu + A \rightarrow A^*. \tag{2}$$

This energy exchange is often referred to as reabsorption. Because the two steps are completely decoupled and solely depend on the specific properties of D and A, it is not necessary to distinguish between singlets and triplets. Reabsorption in OLEDs plays only a minor role, because most organic materials possess a significant Stokes shift between absorption and emission bands so that devices become transparent for the emitted wavelength, which is a great advantage of OLEDs compared to inorganic LEDs. However, reabsorbing photons is of importance in white OLED concepts that make use of an external downconversion layer [cf. Fig. 1(d)]. In contrast to the following energy transfer types, reabsorption can overcome macroscopic distances between D and A states.

Nonradiative energy transfers are of central importance in OLEDs. Such transfers conserve the initial donor energy and are proportional to the number of transitions in the emission band of the donor $I_D(\nu)$ and in the absorption band of the acceptor $\varepsilon_A(\nu)$ that are equal in energy (Klessinger and Michl, 1989). This is quantified in the spectral overlap integral J which reads

$$J = \int_0^\infty \bar{I}_D(\nu)\bar{\varepsilon}_A(\nu)d\nu, \tag{3}$$

where $\bar{I}_D$ and $\bar{\varepsilon}_A$ represent normalized intensities with respect to the integrated band. Without going further into detail, there are two distinctive energy transfer mechanisms, introduced by and named after Förster (1948) and Dexter (1953), which can be ascribed to Coulomb and exchange interactions, respectively [for more details on the quantum mechanical description, see Klessinger and Michl (1989) or equivalents].

In the Förster framework (Förster, 1948), the rate constant for the dominating dipole-dipole interaction can be written as (Braslavsky *et al.*, 2008)

$$k_F = k_{\not A}\frac{9(\ln 10)\kappa^2\Phi_D}{128\pi^5 N_A n^4} J \frac{1}{R_{DA}^6} = k_{\not A}\left[\frac{R_0}{R_{DA}}\right]^6, \tag{4}$$

for distances exceeding orbital overlap interactions. Here $k_{\not A}$ is the rate constant of the excited donor in the absence of an acceptor, κ is an orientation factor, n is the refractive index of the medium in the range of spectral overlap, N_A is the Avogadro constant, Φ_D is the luminescence quantum yield of the donor emission, and R_{DA} is the intermolecular distance between donor and acceptor. Here the various parameters merge to become the Förster radius R_0. This transfer can occur only if both D and A transitions are allowed (Klessinger and Michl, 1989), which leads to the following allowed energy transfer reactions:

$$^1D^* + {}^1A \rightarrow {}^1D + {}^1A^*, \tag{5}$$

$$^1D^* + {}^3A \rightarrow {}^1D + {}^3A^*. \tag{6}$$

Note that there are examples of molecules having a triplet ground-state configuration (Reinhold, 2004; Tanaka *et al.*, 2006), giving rise to ^3A on the left side of Eq. (6). A transfer of a triplet to a singlet state, i.e., $^3D^* + {}^1A \rightarrow {}^1D + {}^3A^*$, is strictly forbidden in the Förster theory as it would require two simultaneous intersystem crossing steps. This picture changes if a phosphorescent donor is incorporated. Here the recombination in the triplet manifold is enhanced due to spin-orbit coupling. The following additional transfers are thus possible (Klessinger and Michl, 1989; Reinhold, 2004):

$$^3D^* + {}^1A \rightarrow {}^1D + {}^1A^*, \tag{7}$$

$$^3D^* + {}^3A \rightarrow {}^1D + {}^3A^*. \quad (8)$$

Even though the transition from $^3D^*$ to ^1D requires intersystem crossing and thus has a lower rate than starting from $^1D^*$, they may have a similar probability, because the lifetime of the triplets is correspondingly longer. Note that for the process in Eq. (7), two different types of molecules have to be involved in order to excite the energetically higher singlet state of A with the triplet D-state energy. The Förster energy transfer can efficiently overcome distances of up to 10 nm, which is much larger than typical molecular dimensions (Pope, 1999).

Dexter energy transfer in contrast is mediated by exchange interactions, which requires orbital overlap of D and A, resulting in a decrease of this interaction with increasing intermolecular distance (Dexter, 1953). Dexter-type energy exchange obeys the Wigner-Witmer spin conservation rules, requiring the total spin of the configuration to be conserved throughout the reaction (Wigner and Witmer, 1928). The resulting energy transfer reactions read

$$^1D^* + {}^1A \rightarrow {}^1D + {}^1A^*, \quad (9)$$

$$^3D^* + {}^1A \rightarrow {}^1D + {}^3A^*, \quad (10)$$

and

$$^3D^* + {}^3A^* \rightarrow {}^1D + {}^{1,3,5}A^*, \quad (11)$$

for triplet-triplet annihilation (Kepler *et al.*, 1963; Suna, 1970). In the latter equation, A can be in its singlet, triplet, or quintet configuration (Klessinger and Michl, 1989). Since the singlet-singlet interaction is an efficient Förster-type transfer [cf. Eq. (5)], it is rarely observed based on exchange interactions. In contrast, the triplet-triplet energy transfer is of great importance as it provides the basis for efficient triplet excited-state migration in organic materials. The corresponding rate constant reads (Dexter, 1953)

$$k_D = \frac{2\pi}{\hbar} K^2 J e^{-2R_{DA}/L}, \quad (12)$$

where K is a constant in units of energy (Murphy *et al.*, 2004). The exponential dependence on the intermolecular distance R_{DA} accounts for the necessity of molecular orbital overlap. Accordingly, Dexter transfers are short-distance interactions, typically reaching up to 1 nm (cf. up to 10 nm for Förster-type energy exchange).

Both Förster- and Dexter-type energy transfers enable excitons to migrate throughout organic solids. Here the net charge carried is zero. The driving force of this exciton motion is a gradient in the exciton concentration $\nabla n(\vec{r}, t)$ leading to a series of uncorrelated hopping steps from molecule to molecule (a *random walk*). Particle diffusion is described by Fick's second law (Fick, 1995). Neglecting higher-order processes and applying it to excitons, it reads

$$\frac{\partial n(\vec{r}, t)}{\partial t} = G(\vec{r}, t) - \frac{n(\vec{r}, t)}{\tau} + D\nabla^2 n(\vec{r}, t). \quad (13)$$

$G(\vec{r}, t)$ is the exciton generation, D is the diffusion constant, and τ is the excited-state lifetime.

Exciton diffusion plays a key role in the working principle of OLEDs, especially in white OLEDs that need to distribute excitons to different emitters. Under electrical excitation, excitons are often formed close to an interface between different materials, usually with a generation width small compared to the total layer thickness (Sun *et al.*, 2006; Reineke, Walzer, and Leo, 2007; Rosenow *et al.*, 2010; Wünsche *et al.*, 2010). Thus, it is often adequate to model the exciton generation as a delta function in space, i.e., $G(x, t) = G\delta(x = x_0, t)$. This solves to the steady-state ($\partial n/\partial t = 0$) solution of Fick's second law (Baldo and Forrest, 2000; Giebink, Sun, and Forrest, 2006; Zhou *et al.*, 2007; Wünsche *et al.*, 2010):

$$n(x) = n_0 e^{-x/L_x} \quad \text{with} \quad L_x = \sqrt{D\tau}, \quad (14)$$

where L_x is the diffusion length and n_0 is the exciton density at the interface.[4]

6. Where the light goes

After discussing the fundamentals of light generation and exciton transfer in the previous sections, we now briefly discuss, where the photons (created in the emission layer) propagate to with respect to the important question: What fraction of photons is able to escape to air (here the far field, defined as the photons that leave the device to the forward hemisphere)?

Figure 4 shows a cross section of a conventional bottom-emission OLED, additionally indicating various light propagation modes. They are mainly determined by the thin-film structure of the device and the respective optical properties (i.e., refractive indices and absorption coefficients) (Greiner, 2007). Organic materials and ITO (the latter depending on its composition) typically have refractive indices in the range of $n \sim 1.7$–1.9 and conventional glass substrates of $n = 1.51$. Thus, in first approximation,[5] two optical interfaces, i.e., the organic/substrate and the substrate/air interfaces, are formed, where total internal reflection may occur (Krummacher *et al.*, 2009; Mladenovski *et al.*, 2009; Reineke, Lindner *et al.*, 2009). The refractive index difference at the organic/substrate interface causes a large fraction of light to be trapped inside the organic layer stack, forming the so-called organic or waveguide (wg) modes (cf. Fig. 4). Based on similar considerations, only a fraction of the light that is originally coupled to the substrate can escape the device (the so-called far-field, air, or outcoupled modes). Additionally, the emitting molecules can directly couple to surface plasmons of the highly reflective electrode (here cathode)—a process that is very efficient for short distances between EML and cathode and strongly decreases with increasing spacing (Lin *et al.*, 2006; Krummacher *et al.*, 2009; Mladenovski *et al.*, 2009; Reineke, Lindner *et al.*, 2009).

[4]Because exciton motion is typically isotropic and the systems are planar structures, diffusion can be reduced to one dimension in space, e.g., L_x.

[5]Because (i) the organic materials all show different, distinct wavelength dependencies, and (ii) slight changes in n are observable for every two organic materials compared.

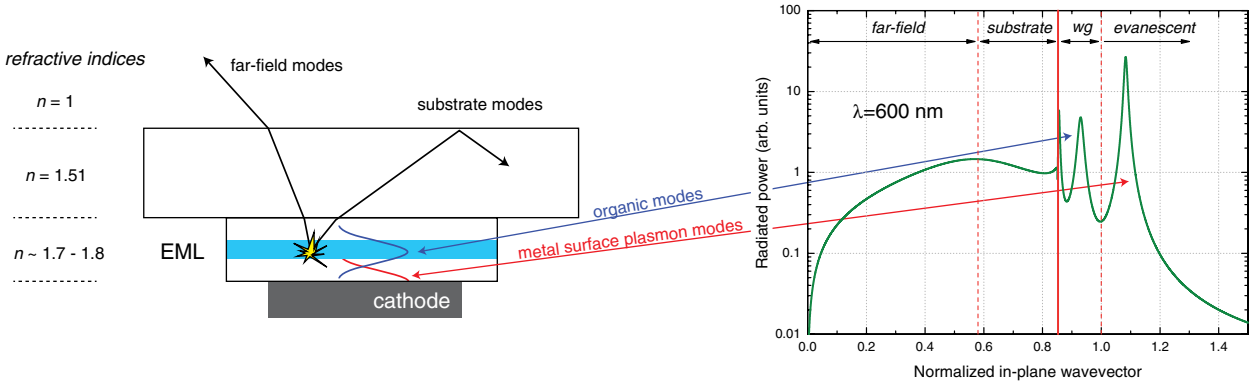

FIG. 4 (color online). Left: Cross section of an OLED with indication of different light modes. Right: Typical power spectrum of the internally generated light shown as a function of the in-plane wave vector. Vertical lines separate the various possible light modes. Neither waveguide (wg) nor evanescent modes (thick line) can be accessed with external light-outcoupling techniques; thus they dissipate within the layer structure. Model calculation (Furno *et al.*, 2012) for a bottom-emitting device similar to devices discussed by Meerheim *et al.* (2008b).

Figure 4 additionally shows a power spectrum, obtained from model calculations (Furno *et al.*, 2012), of a conventional monochrome bottom-emitting OLED (cf. Meerheim *et al.*, 2008b, 2010), plotted as a function of the in-plane wave vector (Furno *et al.*, 2010, 2012; Meerheim *et al.*, 2010). In such a power spectrum, the modes discussed above can easily be attributed to different ranges of the in-plane wave vector, indicated by the vertical lines in Fig. 4. Here the fraction of photons that directly leaves the device (far field) typically is in the range of only 20% (Adachi, Baldo, Thompson, and Forrest, 2001; Gärtner and Greiner, 2008; Krummacher *et al.*, 2009; Mladenovski *et al.*, 2009; Furno *et al.*, 2010; Meerheim *et al.*, 2010). More light can be extracted to the far field by applying modifications of the substrate/air interface (e.g., periodic, shaped substrates) by converting substrate into air modes [(Möller and Forrest, 2002; Greiner, 2007; Sun and Forrest, 2008a; Reineke, Lindner *et al.*, 2009); for details see Sec. IV]. On the contrary, as indicated by the thick solid line in Fig. 4, modes with larger in-plane wave vector, i.e., waveguide and evanescent surface plasmon modes, cannot be outcoupled by external techniques.

Concepts for improved light outcoupling, including approaches to reduce waveguide and surface plasmon modes, are discussed in Sec. IV.A. Similarly, top-emitting OLEDs, which have significantly different optical properties compared to bottom-emitting devices that largely influence the outcoupling efficiency, are introduced and analyzed in Sec. IV.B.

7. Efficiency roll-off

Even though state-of-the-art phosphors have excited-state lifetimes down to 1 μs, the lifetime is still about orders of magnitude longer than their fluorescent counterparts, which is the main reason for different electroluminescent properties of fluorescent and phosphorescent emitters (Pope, 1999). The following calculation illustrates the difference in the respective excited-state properties. Representative fluorescent and phosphorescent excited-state lifetimes are set to 10 ns and 1 μs, respectively (Sokolik *et al.*, 1996; Reineke, Walzer, and Leo, 2007). The brightness L of an OLED is proportional to the excited-state density n and inversely proportional to the excited-state lifetime τ (Reineke, Walzer, and Leo, 2007): $L \sim n/\tau$. Considering the spin statistics discussed in Sec. I.A.3, one derives for a fluorescent (fl) and a phosphorescent (ph) system, respectively,

$$L \sim \frac{n_{\mathrm{fl}}}{4\tau_{\mathrm{fl}}} \quad \text{and} \quad L \sim \frac{n_{\mathrm{ph}}}{\tau_{\mathrm{ph}}}, \tag{15}$$

with corresponding subscripts. This leads to an expression for the ratio between the excited-state densities $n_{\mathrm{ph}}/n_{\mathrm{fl}}$:

$$\frac{n_{\mathrm{ph}}}{n_{\mathrm{fl}}} \sim \frac{\tau_{\mathrm{ph}}}{4\tau_{\mathrm{fl}}} = \left[\frac{1\ \mu\mathrm{s}}{4 \times 10\ \mathrm{ns}} = \frac{\mathbf{25}}{\mathbf{1}}\right]. \tag{16}$$

The direct consequence is illustrated in Fig. 5. To reach the same luminance level in fluorescent and phosphorescent systems, the exciton density is typically about 25-fold higher in the case of phosphorescence, which increases the probability of excited state annihilation processes, such as triplet-triplet annihilation, triplet-polaron quenching (Baldo, Adachi, and Forrest, 2000; Reineke, Walzer, and Leo, 2007), and in some cases field-induced exciton dissociation (Kalinowski *et al.*, 2002). These processes cause the quantum efficiency of phosphorescent systems to noticeably drop at

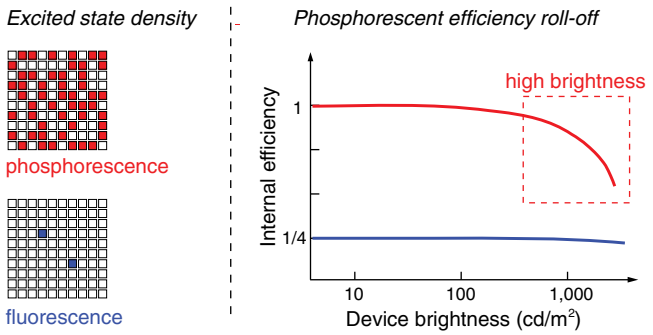

FIG. 5 (color online). Left: The excited-state density in the cases of phosphorescence and fluorescence, respectively. Right: Typical efficiency vs brightness characteristics. In the case of phosphorescence, the efficiency drastically decreases at high brightness as a consequence of quenching processes.

high brightness (efficiency roll-off) as depicted in Fig. 5. For state-of-the-art phosphorescent systems, this roll-off typically starts at around 1000 cd m^{-2} (Baldo, Adachi, and Forrest, 2000; Reineke, Schwartz, Walzer, and Leo, 2007; Reineke, Walzer, and Leo, 2007; Su *et al.*, 2008). Thus, especially for lighting applications, where a few thousand cd m^{-2} are seen as a realistic device brightness (cf. Sec. I.B.3), phosphorescent OLEDs typically work at a decreased internal efficiency [$\eta_{\mathrm{int,ph}}(L_{\mathrm{high}}) < 100\%$].

B. Quantification of light and efficiency

1. Figures of merit

Typically, three device efficiencies are discussed in literature: the current efficiency η_{CE}, the luminous efficacy[6] η_{LE}, and the external quantum efficiency η_{EQE} (Forrest, Bradley, and Thompson, 2003). While the latter is a measure of the number of photons that are extracted to air per injected electrons, the other two efficiencies are photometric quantities that take the sensitivity of the human eye into account.

The current efficiency is calculated from the luminance L_{0°, obtained in the forward direction, and the current density j_{meas} passing through the device:

$$\eta_{\mathrm{CE}} = \frac{L_{0^\circ}}{j_{\mathrm{meas}}} \quad [\mathrm{cd\,A^{-1}}]. \tag{17}$$

The luminous efficacy can be calculated considering the operating voltage at the point of measurement $V(j_{\mathrm{meas}})$. It reads

$$\eta_{\mathrm{LE}} = \eta_{\mathrm{CE}} \frac{f_D \pi}{V(j_{\mathrm{meas}})} [\mathrm{lm\,W^{-1}}], \tag{18}$$

with

$$f_D = \frac{1}{\pi I_0} \int_0^{\pi/2} \int_{-\pi}^{+\pi} I(\theta, \phi) \sin\theta d\phi d\theta. \tag{19}$$

Here f_D accounts for the angular distribution of the emitted light intensity $I(\theta, \phi)$ in the forward hemisphere which is a function of two angles [azimuth (θ) and polar (ϕ)]. Furthermore, I_0 represents the light intensity measured in the forward direction. For OLEDs with changing spectral distribution as a function of the observation angle, i.e., $I(\theta, \phi, \lambda)$, the spectral changes also need to be considered (Meerheim, Nitsche, and Leo, 2008).

Finally, the radiometric external quantum efficiency can be calculated with

$$\eta_{\mathrm{EQE}} = \eta_{\mathrm{CE}} \frac{f_D \pi e}{K_r E_{\mathrm{ph}}} \left[\frac{\%}{100}\right], \tag{20}$$

where E_{ph} is the average photon energy of the emitted device spectrum. Apparently, the integrated quantities η_{LE} and η_{EQE} are only correctly determined if the angular distribution f_D is taken into account. This is possible using an integrating sphere or a goniometer setup (Meerheim, Nitsche, and Leo, 2008; Hofmann *et al.*, 2010). For a long time, it has been common sense that these quantities can be calculated assuming a Lambertian emission pattern of the emitted light, i.e., $I(\theta, \phi) = I_0 \cos\theta$. However, recent publications show that this assumption is not valid (Meerheim, Nitsche, and Leo, 2008; Mladenovski *et al.*, 2009; Freitag *et al.*, 2010), calling for precise methods of efficiency determination.

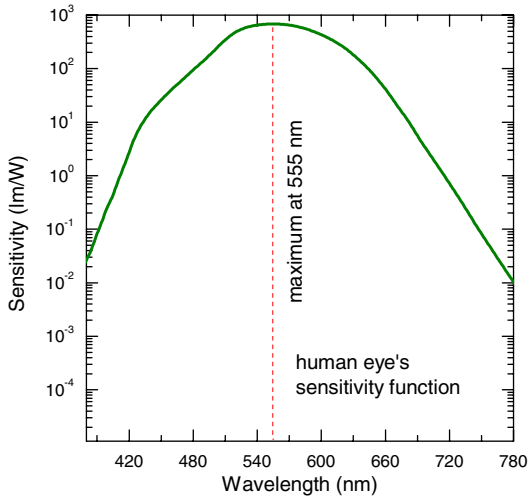

FIG. 6 (color online). Commission Internationale de l'Éclairage (CIE) photopic (daylight) spectral sensitivity function $V(\lambda)$. Its maximum at a wavelength of 555 nm corresponds to 683 lm W^{-1}.

Photometric quantities are converted into radiometric ones and vice versa by the introduction of the luminous efficacy of radiation K_r that is calculated by

$$K_r = \frac{\int_{380\ \mathrm{nm}}^{780\ \mathrm{nm}} \Phi_r(\lambda) V(\lambda) d\lambda}{\int_0^\infty \Phi_r(\lambda) d\lambda} [\mathrm{lm\,W^{-1}}], \tag{21}$$

where Φ_r is the radiant flux and $V(\lambda)$ is the weighting function that takes the sensitivity of the human eye into account (cf. Fig. 6). In other words, the luminous efficacy of radiation K_r quantifies how many lumen a given spectrum can produce per watt. Thus, it marks the theoretical limit for the luminous efficacy η_{LE} of any OLED spectrum, neglecting electrical and optical losses.

2. Color rendering and quality

To become a future light source, white OLEDs require besides high luminous efficacies also a high level of color quality to be widely accepted. Typical reference light sources are *Planckian radiators* which can fully be defined by their color temperature T_C. Thus, their chromaticity changes under a variation of T_C, as shown in Fig. 7, resulting in the so-called *Planckian locus*. A light source used for illumination should emit a spectrum with a color point close to this locus to be regarded as a true white light source. However, keep in mind that having a color point on the Planckian curve does not necessarily mean that the light source has a good color rendering (see below), which is a consequence of the specific spectral sensitivity of the receptors in the human eye. If a spectrum is off the Planckian locus, its chromaticity can be

[6]Note that the luminous efficacy is often referred to as *power efficiency* in the literature. However, strictly speaking, an efficiency should be dimensionless, which is not the case for the quantity discussed (cf. lm W^{-1}).

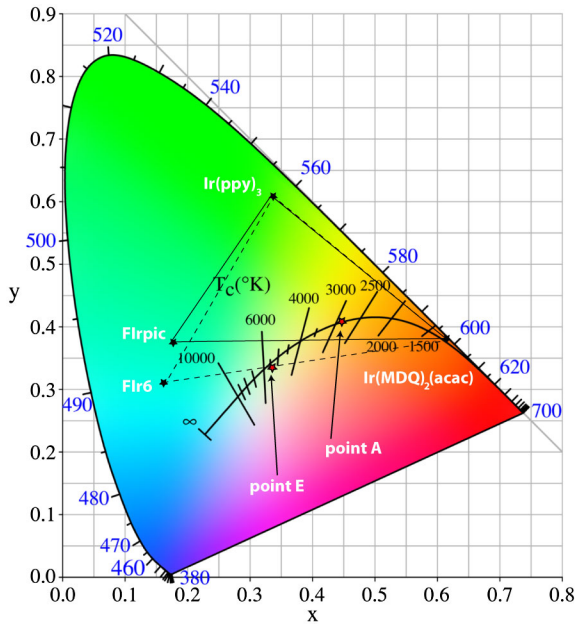

FIG. 7 (color online). CIE 1931 chromaticity diagram. Monochrome colors are located on the edges of this color space (values are in nm). Additive mixing of any monochrome colors leads to a color within the horseshoe. The black line indicates the Planckian locus and the corresponding correlated color temperatures (CCTs). Stars indicate the important standard illuminants *E* and *A*. CIE coordinates are plotted for commonly used phosphorescent emitters together with the color space they make possible with three-color mixing.

described by the correlated color temperature (CCT). [For more details, see, for instance, Ohta and Robertson (2005).]

Two important Commission Internationale de l'Éclairage (CIE) standard illuminants are the color points *E* and *A*, indicated in the CIE 1931 color space in Fig. 7 (Hunt, 1995). Point *E* slightly below the Planckian locus is also referred to as a point of equal energy, corresponding to CIE coordinates of (0.33, 0.33). It is perceived as "colorless" white light. On the contrary, the CIE standard illuminant *A* [CIE coordinates of (0.448, 0.408)], also called the warm white point with $T_C = 2856$ K, marks the chromaticity of tungsten incandescent lamps, which are widely accepted as being the most comfortable artificial light sources to date. Many electroluminescence spectra reported in the literature are displaced with respect to the Planckian locus. In order to discuss such a distance in this review, we introduce a dimensionless measure α_{CIE} that describes the shortest distance of the measured CIE coordinates to coordinates $(x_{\mathrm{locus}}, y_{\mathrm{locus}})$ on the Planckian locus (this is the orthogonal connection). It reads

$$\alpha_{\mathrm{CIE}} = \sqrt{(x - x_{\mathrm{locus}})^2 + (y - y_{\mathrm{locus}})^2}. \tag{22}$$

Further we define this value to have a positive sign (+) when the CIE coordinates are above the Planckian locus and a negative sign (−) when located below. Thus, in this definition, a light source with $\alpha_{\mathrm{CIE}} = 0$ is a Planckian radiator. This value is seen as help for the reader to easily access the quality of any white device.

Equally important as its chromaticity is the ability of a light source to reproduce the color of objects. In order to quantify the color rendering properties of artificial light sources, the Commission Internationale de l'Éclairage introduced the color rendering index (CRI) in 1965 [for the updated version see Azuma *et al.* (1995)]. It is a dimensionless measure ranging from 0 to 100, calculated as the average of the special color rendering indices $R_i = 100 - 4.6d_i$. These are determined by illuminating eight defined color cards with both a light source of interest and a reference (i.e., either a Planckian radiator or a daylight spectrum for high CCTs above 5000 K). Here d_i is the distance between both rendered spectra in the CIE 1964 $U^*V^*W^*$ color space (Ohta and Robertson, 2005). It is important to note that the CRI is defined only in the proximity of the Planckian locus. A lower limit for a good light source is a CRI of 80.

As an example, the CRI is calculated for two different spectra composed of photoluminescence emission of three phosphorescent emitters [different blue, $\mathrm{Ir(ppy)_3}$ for green, and $\mathrm{Ir(MDQ)_2(acac)}$ for red], realizing emission at color point *A* (see Fig. 8). The first calculated spectrum is based on the light-blue emitter FIrpic (Fig. 8, top). Here, in order to reach color point *A*, the relative intensity of the green emitter $\mathrm{Ir(ppy)_3}$ is only 1%, revealing a noticeable dip in

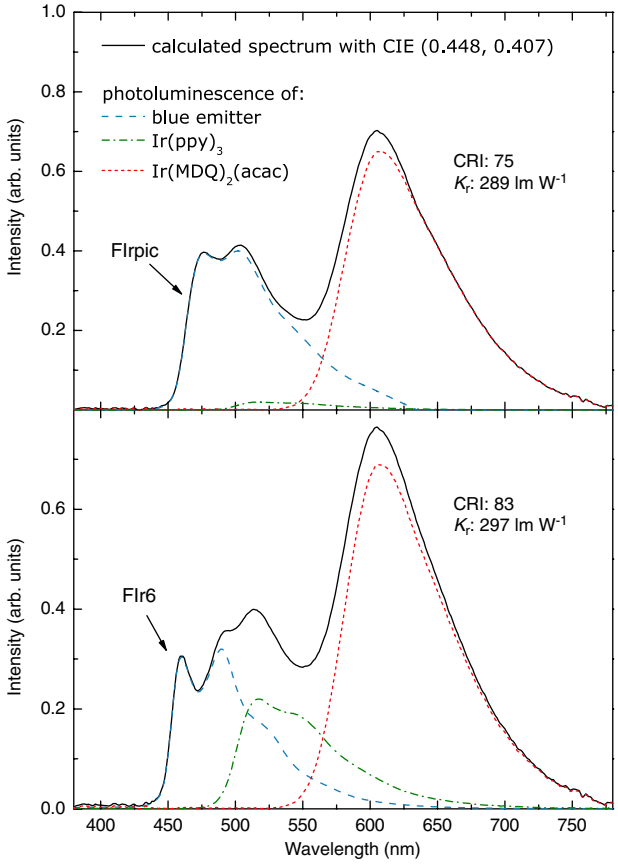

FIG. 8 (color online). Under a variation of the blue emitter with different spectral positions (top: FIrpic, bottom: FIr6), a spectrum is calculated based on three emitters to realize color coordinates at color point *A* within the CIE chromaticity diagram (see Fig. 7). Additionally given are the color rendering index (CRI) and the luminous efficacy of radiation K_r.

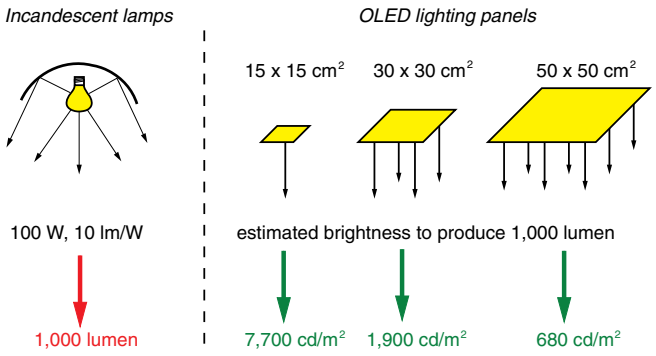

FIG. 9 (color online). Idealized comparison of incandescent lamps and OLED lighting panels to estimate the panel size needed to achieve similar luminous flux outputs (here 1000 lm). Calculations for the OLEDs are based on the luminous efficacy η_{LE} data obtained from Reineke, Lindner *et al.* (2009) (device LI).

the spectrum at 550 nm—the part of the spectrum with highest eye sensitivity (cf. Fig. 6). The CRI of this simulated spectrum is only 75, and the corresponding luminous efficacy of radiation is 289 lm W^{-1}. Exchanging FIrpic with the deeper-blue emitter FIr6 improves the color quality (Fig. 8, bottom). Here the CRI is increased to 83 because more green emission is necessary (17%), resulting in a more balanced spectrum. Furthermore, due to the higher intensity in the green part of the spectrum, K_r increases to 297 lm W^{-1}.

3. Device brightness

As mentioned at the beginning of Sec. I.B, OLEDs are, in contrast to their inorganic counterparts, ultrathin area light sources. Obviously two device parameters can be adjusted to realize a desired luminous flux: the device area and its operating brightness. Figure 9 compares OLED panel sizes and luminance levels to achieve a luminous flux that matches the output of a 100 W incandescent bulb. Interestingly, even large OLED areas of 50×50 cm^2 need a luminance of 680 cd m^{-2} (about a factor of 2–3 brighter than a typical computer display) to reach the flux of the light bulb. The discussion of Sec. I.A.7 shows that the high brightness operation of OLEDs is accompanied with a decrease in device efficiency as a consequence of excited-state annihilation processes (Baldo, Adachi, and Forrest, 2000; Kalinowski *et al.*, 2002; Reineke, Walzer, and Leo, 2007). Furthermore, the device long-term stability is inversely proportional to its operating brightness (Zhang *et al.*, 2001; Meerheim *et al.*, 2006; Tsai and Jou, 2006; Meerheim, Nitsche, and Leo, 2008). On the other hand, the production costs of an OLED panel and therefore the costs per lumen increase roughly linearly with the panel area.

Independent of what future lighting solutions will look like in detail, it is apparent that a certain level of brightness is necessary for general lighting applications. Initially, 1000 cd m^{-2} was established in the literature as a level to ensure best device comparability.[7] However, in the last few years 3000 cd m^{-2} was increasingly quoted as the standard level for OLED lighting applications. It can be expected that this level will not be significantly exceeded because higher intensities generate glare, which removes one of the key advantages of area sources such as the OLED.

[7]As discussed in Sec. I.A.7, the device efficiency will drastically decrease from low luminance (where typically the maximum luminous efficacy is obtained) to illumination relevant levels.

II. WHITE POLYMER OLEDs

In this section, we discuss various concepts aimed at producing white light emission from polymer materials. It is worth noting, as mentioned in Sec. I.A.2, that often small molecules are incorporated into devices that are referred to as polymer OLEDs. We follow this common terminology and also review such hybrid devices here.

Figure 10 summarizes the key concepts that enable emission of white electroluminescence. First reports on white OLEDs use polymer materials to function solely as host material and in part as charge carrier transport materials, while the emission originates from small molecular dyes dispersed into the polymeric matrix [see Fig. 10(a)]. On the other hand, light-emitting polymers themselves can be combined, each covering a different spectral range, to achieve a broadband emission. Here, white light can be realized either by blending the polymers in one single emission layer [see Fig. 10(b)] or in a heterolayer design [see Fig. 10(c)]. Of course, these concepts can generally be combined in virtually any form. Finally, concepts have been proposed to realize white emission from a single compound polymer [see Fig. 10(d)]. This is commonly realized by synthesizing multifunctional copolymers.

A. Small-molecule-doped polymer films

1. Fluorescence-emitting dopants

We start by reviewing the concept of small-molecule-doped polymer systems, as illustrated in Fig. 10(a), because the first reports about white polymer OLEDs by Kido *et al.* (1994) and Kido, Shionoya, and Nagai (1995) are based on this approach. In their early work they used

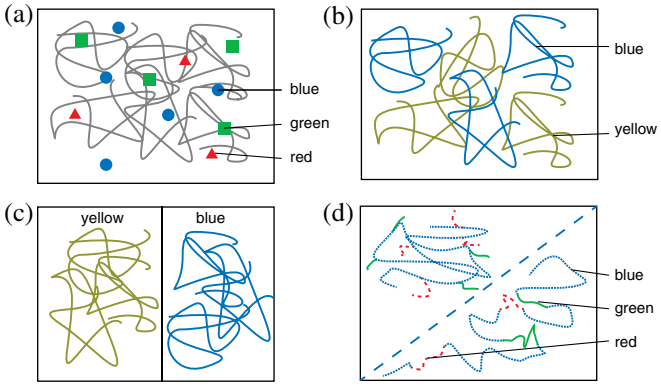

FIG. 10 (color online). The main concepts for white light emission shown from polymer OLEDs. (a) Polymer host materials (gray) doped with small molecule fluorescent or phosphorescent emitter molecules (filled symbols), (b) two or more light-emitting polymers blended in a single layer, (c) light-emitting polymers in a heterolayer architecture, and (d) single component, multicolor emitting copolymers.

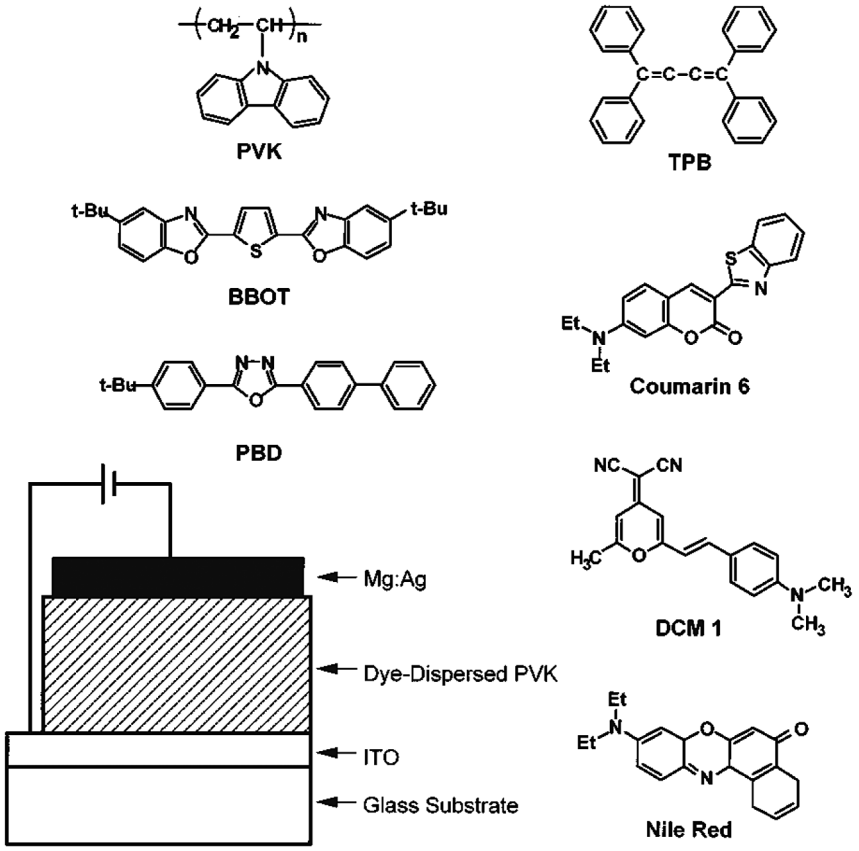

FIG. 11. Device structure and materials used in the first polymer-based white OLED reported by Kido, Shionoya, and Nagai (1995). BBOT and PBD are electron-transporting materials that are added to the hole-transporting PVK matrix to improve carrier balance. From Kido, Shionoya, and Nagai, 1995.

poly(*N*-vinylcarbazole) (PVK) as host material for various fluorescent dyes (see Fig. 11).

In Fig. 12, the EL spectra of different devices from Kido, Shionoya, and Nagai (1995) are displayed, already showing one promising property of organic LEDs, the easy variation of the emitted color in a broad range. Here device *D* completely spans the spectral range from 400 to 700 nm, which covers almost the complete visible spectrum (380–780 nm). Their device reached a maximum brightness of 4100 cd m^{-2} (they did not report on device efficiency). Kido, Shionoya, and Nagai (1995) concluded that the emitter dopant excitation must follow competing pathways, being resonant energy transfer from host to emitter molecules and direct charge trapping at dopant sites. Furthermore, energy transfer between different species of emitter molecules is generally possible.

Much effort was spent to improve the device efficiency in the following years. Huang, Hou *et al.* (2006) reported a device structure with improved luminous efficiency based on a polyfluorene (PF) host polymer material. For orange emission they added the laser dye rubrene, dispersed into the host material with a low concentration of 0.2%. The reason for this low concentration is twofold: (i) The very high photoluminescence quantum yield (PLQY) of rubrene approaching 100% (Mattoussi *et al.*, 1999) is realized only at low concentrations. At higher concentrations, strong concentration quenching reduces the emission efficiency. (ii) In their devices, Huang *et al.* made use of an incomplete energy transfer from the host material PF to rubrene, so that PF itself covers the blue part of the spectrum (see the inset of Fig. 13). Additionally, in order to improve the electron transport within the light-emitting polymer (LEP) film, an electron-transporting material PBD was incorporated with various concentration (0–8 wt %). Figure 13 plots η_{CE} and η_{LE} of these devices as functions of brightness. At a brightness of 3000 cd m^{-2}, the device with 5% PBD content, having the best color quality [CIE color coordinates of (0.33, 0.43)], reaches 12.6 lm W^{-1}. This is a very high efficiency considering that only fluorescent materials were used, which allows internal quantum efficiencies of only roughly 25% (cf. Sec. I.A.3). The fluorescent emitters make it possible for the current efficiency of these devices to remain constantly high over a wide range of luminance [see Fig. 13(a)]. It is necessary to mention that the CIE coordinates with $\alpha_{CIE} = +0.07$ are relatively far apart from the Planckian locus, which artificially enhances the luminous efficacy of radiation K_r.

2. Phosphorescent emitters

In order to reduce the losses in the triplet manifold of the materials (cf. Sec. I.A.3), phosphorescent dopants, which proved to be successful for high-efficiency small-molecule-based devices (Baldo *et al.*, 1998; D'Andrade, Holmes, and

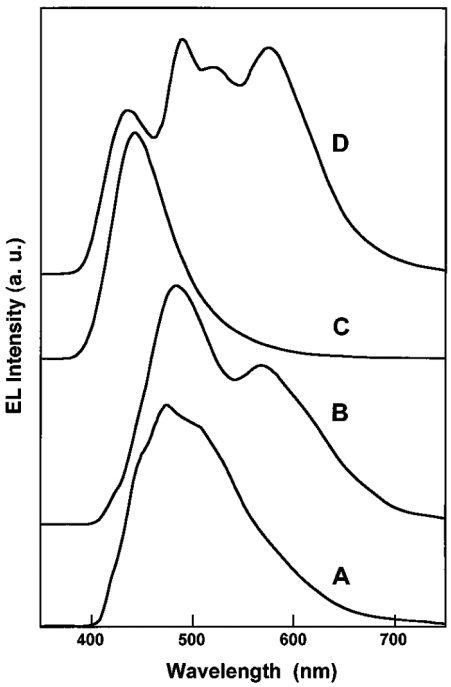

FIG. 12. EL of ITO or dye-dispersed PVK (100 nm)/Mg:Ag devices. PVK is molecularly dispersed with (spectrum A) 30 wt % BBOT, (spectrum B) 30 wt % BBOT, and 0.007 mol % Nile red, (spectrum C) 30 wt % PBD and 3 mol % TPB, (spectrum D) 3 mol % TPB, 30 wt % PBD, 0.04 mol % Coumarin 6, 0.02 mol % DCM 1, and 0.015 mol % Nile red. From Kido, Shionoya, and Nagai, 1995.

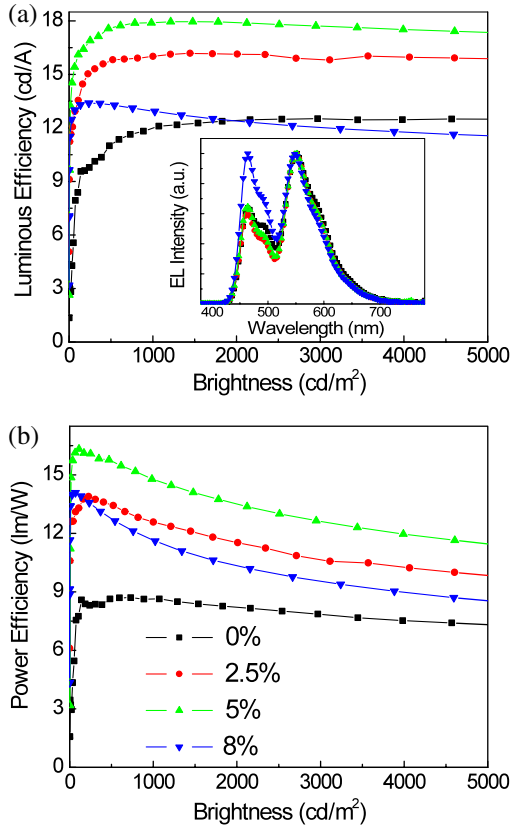

FIG. 13 (color online). (a) Current efficiency (cd A^{-1}) of devices comprising different amounts of 2-(4-biphenylyl)-5-(4-tert-butylphenyl)-1,3,4-oxadiazole (PBD). Inset: EL spectra of the corresponding devices. (b) Luminous efficacy (lm W^{-1}). From Huang, Hou *et al.*, 2006.

Forrest, 2004), were similarly introduced to polymeric systems.

Kawamura, Yanagida, and Forrest (2002) reported on the use of multiple-doped PVK emission layers to achieve white emission. PVK with its triplet energy level at roughly 2.5 eV (496 nm)[8] is suitable as host material for most of the phosphorescent emitters. By varying the emission wavelength of the phosphor [474, 517, 565, and 623 nm for FIrpic, $Ir(ppy)_3$, $Bt_2Ir(acac)$, and $Btp_2Ir(acac)$, respectively], they observe the lowest efficiency for single emitter devices comprised of FIrpic, because the triplet energy of FIrpic is higher than that of PVK, resulting in endothermic energy transfer (Adachi, Kwong *et al.*, 2001). A triple-doped device comprised of FIrpic, $Bt_2Ir(acac)$, and $Btp_2Ir(acac)$ in a 10:0.25:0.25 mixing ratio yields a maximum EQE of 2.1% and 1.4 lm W^{-1} [CIE (0.33, 0.41); $\alpha_{CIE} = +0.06$]. Achieving a balanced white emission requests the lower-wavelength components to be highly diluted into the EML so that the energy transfer from the host material and blue emitter is not complete (Kawamura, Yanagida, and Forrest, 2002).

Niu *et al.* (2007) used three phosphorescent emitters [FIrpic, Ir(ppy), and Os-R1 (an osmium-based organometallic complex)] in a multilayer device, where the HTL (VB-TCTA) is formed by cross-linking and the electron-transport layer (ETL) (TPBi) is prepared by thermal evaporation. With an optimized VB-TCTA thickness of 25 nm, they reach a maximum EQE of 6.15%. At 800 cd m^{-2}, the luminous efficacy is 5.59 lm W^{-1} ($\alpha_{CIE} < +0.01$). Further efficiency improvements were reported by Wu *et al.* (2008) and Huang *et al.* (2009), who reported efficiencies of 12.9% EQE and 8.2 lm W^{-1} (maximum values, $\alpha_{CIE} = +0.08$) and 12.6% EQE and 18.5 lm W^{-1} (at 100 cd m^{-2}, $\alpha_{CIE} = 0$), respectively. In both reports, the electron-transporting material OXD-7 was added to the EML to improve the electron transport (Hamada *et al.*, 1992). The very high efficiencies of Huang *et al.* (2009) are in part a consequence of the improved electron injection and transport which is realized by the incorporation of an *n*-doped electron-transport material. They used Li_2Co_3 salt to dope the ETL made of poly[9,9-bis(2-(2-(2-diethanolamino ethoxy)ethoxy)ethyl) fluorene] (PF-OH). Compared to undoped PF-OH, a device with 15 wt % doped ETL shows a 1.58-fold improvement in the luminous efficacy.

Recently, Cheng *et al.* (2010) discussed devices that comprise two phosphorescent emitters, i.e., FIrpic and Ir(SBFP)2 (acac) for light blue and orange, respectively, dispersed into a silane-based [cf. Holmes *et al.* (2003)], wide-band-gap polymer P36HCTPSi. By adjusting the concentration of $Ir(SBFP)_2(acac)$ to 4 wt %, these devices, including an additional ETL prepared by means of thermal evaporation, reach 14.1% EQE and 25.6 lm W^{-1} at 1000 cd m^{-2}. However, the color quality with a CRI of 42 and CIE coordinates far apart from the Planckian locus (0.41, 0.49) call for strategies to improve the emitted color.

[8]Note that other publications [see, e.g., Wu *et al.* (2008)] state a much higher triplet energy of PVK of 3.0 eV.

3. Hybrid fluorescent blue, phosphorescent green, and red systems

An alternative approach to realize white light is to utilize blue fluorescence which is complemented by the emission of lower-wavelength phosphorescent emitters. Commonly, the polymer host material simultaneously serves both as a matrix for the phosphors and as a blue emitter. In general, this concept can be optimized to enable triplet harvesting as reported by Schwartz *et al.* (2007) for small-molecule OLEDs (details are given in Sec. III.B.3), where singlet excitons will be used for blue fluorescence and the remaining triplets channeled to phosphorescent emitters, where they emit at potentially 100%. However, this concept has strict requirements on the energy levels of the materials and the exciton distribution within the device. To our knowledge, triplet harvesting has not been reported for polymeric white OLEDs to date [see, e.g., Gather, Köhnen, and Meerholz (2011)].

Polyhedral oligomeric silsesquioxane-terminated poly(9,9-dioctylfuorene) (PFO-poss) is used by Xu *et al.* (2005) as a blue-emitting polymer that additionally hosts two phosphorescent emitters for green [$Ir(Bu\text{-}ppy)_3$] and red [$(Piq)_2Ir(acaF)$]. A device with 0.14 wt % for each emitter dopant emits white light at the point of equal energy [(0.33, 0.33)] with a maximum luminous efficacy of 5.5 $\mathrm{lm\,W^{-1}}$ at 5.6 V (no EQE reported). Based on another blue-emitting polymer (BlueJ) and two phosphors, Kim *et al.* (2006) achieved 3.2% EQE at a brightness of 905 $\mathrm{cd\,m^{-2}}$ (12.5 $\mathrm{cd\,A^{-1}}$, no η_{LE}) with emission at (0.33, 0.33). In contrast to Xu *et al.* (2005), they added 25% of PVK to the EML to improve the charge carrier balance.

Gong *et al.* (2004, 2005) used a PFO-based polymer as a blue emitter and host material for the red-phosphorescence-emitting $Ir(HFP)_3$. In their later report (Gong *et al.*, 2005), they built this EML into a multilayer OLED architecture to improve the device efficiency. The optimized device has a luminous efficacy of 3 $\mathrm{lm\,W^{-1}}$ at approximately 2400 $\mathrm{cd\,m^{-2}}$ with CIE coordinates of (0.33, 0.33). The moderate contribution of the red emitter $Ir(HFP)_3$ to the overall emission spectrum suggests either that only a limited number of excitons reach the molecule or that additional quenching sites in the complex structure are present, suppressing the red emission.

Niu *et al.* (2006) followed another concept. Mainly to improve the CRI of the device, they combined a single-component white-emitting polymer (WPF03) (Tu *et al.*, 2006) (cf. Sec. II.C) with a red-emitting phosphorescent molecule [$(Ppq)_2Ir(acac)$]. By further making use of weak emission from an admixture of the electron-transporting material PBD [see Kido, Shionoya, and Nagai (1995)], they realized a broadband emission from 400 to 750 nm with a very high CRI of 92 [CIE coordinates (0.34, 0.35), $\alpha_{CIE} < -0.01$]. However, the overall device efficiency of 5.3 $\mathrm{cd\,A^{-1}}$ (no η_{EQE} and η_{LE}) is comparably low. This is most likely due to small energetic displacement of the emission peaks of the red fluorescent chromophore in WPF03 and $(Ppq)_2Ir(acac)$ of only 50 nm or 188 meV. Thus, the triplet level of the red chromophore is expected to be below that of $(Ppq)_2Ir(acac)$, inducing noticeable emission quenching.

B. White emission from multiple light-emitting polymers

1. Blended polymeric systems

Although they did not mention the application for white light sources, Berggren *et al.* (1994) reported on color-tunable LEDs made from polymer blends [see Fig. 10(b)]. By altering the operating voltage and/or the stoichiometry of the polymer blends, they were able to "shift the emission from blue to near-infrared, with green, orange and red as intermediate steps ...." Their devices had efficiencies ranging from 0.1% to 1% EQE.

The first white polymer OLEDs based on polymer blends were discussed by Tasch *et al.* (1997). By highly diluting a red-emitting polymer poly(perylene-co-diethynylbenzene) into a blue ladder-type polymer polyparaphenylene with a concentration of 0.05%, white emission is realized. Here the red emitter is excited via exciton energy transfer and charge transfer and trapping. With an addition of 10 wt % PMMA to the mixed layer, CIE coordinates of (0.31, 0.33) ($\alpha_{CIE} = +0.01$) were reached with a maximum external quantum efficiency of 1.2%. The concept of incorporation of insulating materials such as PMMA into the polymer blend to control the intermolecular energy transfer and emission spectrum was further discussed by Granstrom and Inganas (1996).

Hu and Karasz (2003) realized white light emission by blending two copolymers (for blue and green) together with an additional small molecular dye (MPD) for red emission. An optimized device with admixtures of charge transport moieties reached a maximum photon per electron efficiency of 2.6% with CIE coordinates of (0.36, 0.35) ($\alpha_{CIE} < +0.01$).

Huang, Li *et al.* (2006) reported on a simple two-polymer-blend white device with a greatly improved device efficiency. The working principle is illustrated in Fig. 14. They introduced a Cs_2CO_3 interfacial layer between the LEP layer and cathode to enhance the injection of the minority charge carriers. Furthermore, the dopant's (MEH-PPV) energy levels are within the band gap of the host material (PFO), so that the excitation of the dopant can occur via energy transfer and charge trapping [see Tasch *et al.* (1997)], the latter leading to a charge confinement effect. The combination of improved carrier injection and charge confinement yields very high efficiencies of 6% EQE and 16 $\mathrm{lm\,W^{-1}}$ [peak values, CIE (0.36, 0.40) $\alpha_{CIE} = +0.03$]. Even at 1000 $\mathrm{cd\,m^{-2}}$, the

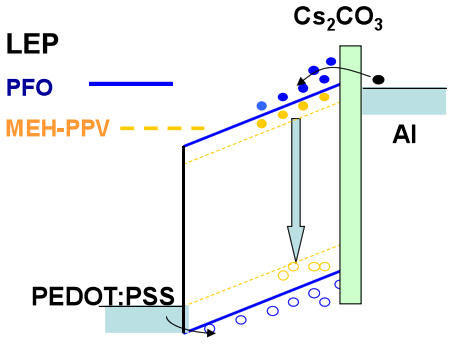

FIG. 14 (color online). Band diagram illustrating the working principle of the polymer blend white OLED. The Cs_2CO_3 interfacial layer (EIL) improves the electron injection. Adapted from Huang, Li *et al.*, 2006.

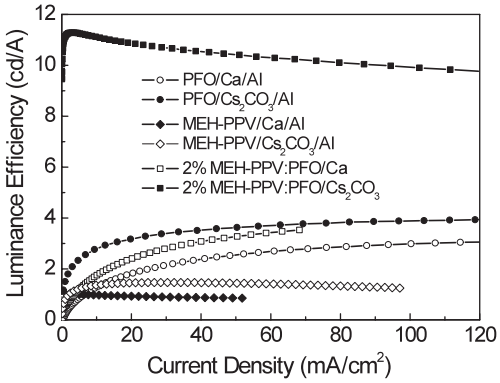

FIG. 15. Current efficiency of three sets of devices. The composition of the EML and the interfacial electron injection layer are varied. (To our knowledge, the labels of the last two devices are incomplete. They should both contain an "/Al" cathode.) From Huang, Li *et al.*, 2006.

luminous efficacy remains at a high value of 12.6 lm W^{-1}. Figure 15 illustrates the improvement in device efficiency compared to reference devices (three sets of devices). Open versus solid symbols compare the interfacial injection layer (Cs_2CO_3 versus Ca reference). The different device sets compare the EML comprising either each LEP or the mixture of 2% MEH-PPV in PFO. There the device with Cs_2CO_3 and charge confinement structure shows a twofold to threefold improvement in efficiency compared to the other devices.

2. White light from polymer heterolayers

Another concept apart from blending emitting polymers in a single layer is to create a heterointerface between two differently emitting polymers [cf. Fig. 10(c)]. Here it is necessary to engineer the recombination zone, typically only a few nanometers wide, to be close to the heterointerface in order to realize emission from both material species. In contrast to the concept of polymer blending, the preparation of multilayer polymer devices is more complicated because the solvents used in wet-processing techniques may harm the underlying layers (cf. Sec. I.A.2).

In the early report of Chao and Chen (1998), white light is created at a PVK/C12O-PPP interface. However, instead of utilizing the emission of both polymers, the spectrum is composed of the blue fluorescence of C12O-PPP and an exciplex emission formed between the PVK HOMO and the C12O-PPP LUMO levels. Further work on this topic was by Thompson *et al.* (2001), where different heterointerfaces were investigated, all showing a broad emission that is a mixture of blue exciton and longer-wavelength exciplex emission. However, it is still questionable whether exciplex emission can be utilized for efficient luminescence. For instance, Castellani and Berner (2007) reported on the competition of exciton and exciplex emission in multilayered organic LEDs. They concluded that the emission efficiency is noticeably reduced if an exciplex emission is incorporated.

One way to overcome the problems in preparation of multilayer polymer systems is the technique of cross-linking [see, e.g., Niu *et al.* (2007)], where the polymerization of the material is realized after layer deposition by either annealing or photochemical means. Köhnen *et al.* (2010) reported on a fully wet-processed bilayer polymer system consisting of two fluorescent emitters with complementary emission colors (a PPV derivative for yellow and a polyfluorene for blue). In their work, the yellow-emitting PPV derivative (SY) was thermally cross-linked. An optimized device emits white light with CIE coordinates (0.323, 0.345) very close to color point *E*. The maximum efficiency of the device is 6.1 cd A^{-1} ($\alpha_{CIE} < +0.01$, no η_{EQE} and η_{LE} stated). At 2400 cd m^{-2}, the device efficiency is still as high as ~5.6 cd A^{-1}. One important advantage of this device design is the low color shift as a function of current density [from 100 to 10 000 cd m^{-2}, the CIE coordinate shift is ($\Delta x = 0.009$, $\Delta y = 0.006$)]. Furthermore, even though the spectrum consists only of contributions from two emitters, the CRI = 84 is very high.

C. Single-component polymer systems

In Fig. 10(d), an alternative but very promising concept for white OLEDs based on polymers is illustrated. The key idea is to realize a single copolymer that contains all the different emitting chromophores needed to cover the visible spectrum. Clearly the advantages of this approach are the simple fabrication, the isotropic, yet statistical distribution of the chromophores within the film (Gather, Alle *et al.*, 2007), the control of the interspecies energy transfer by the molecular design, and the low probability of phase separation within the film (Berggren *et al.*, 1994; Forrest, 2004; Gather, Köhnen, and Meerholz, 2011).

With respect to the molecular design, one has to distinguish between two concepts [cf. Fig. 10(d)]: (i) The main polymer (host) and all chromophores form the copolymer main chain in a stoichiometric manner, where conjugation occurs. (ii) The chromophores are attached to the polymer main chain as sidegroups, where the conjugation is lost. In the latter approach, the chromophores can be seen as isolated molecules dispersed in a host polymer.

1. Conjugated copolymers comprising main-chain chromophores

Tu *et al.* (2004) reported on an efficient white light-emitting polymer by admixing moieties of an orange fluorophore (1,8-naphthalimide) into the blue PFO main polymer. Used as a single EML device, a chromphore concentration of 0.05% in the PFO main chain yields a device efficiency of 5.3 cd A^{-1} and 2.8 lm W^{-1} at 6 V [CIE (0.26, 0.36), $\alpha_{CIE} = +0.06$]. Later they showed that the device efficiency could be easily altered by changing the molecular integration of the red chromophore in the polyfluorene backbone (Tu *et al.*, 2006). By changing the orange chromophore to TPABT, Wang and co-workers improved the device efficiency to 8.99 cd A^{-1}, 5.75 lm W^{-1}, and 3.8% EQE even with improved color quality [CIE (0.35, 0.34), $\alpha_{CIE} = -0.01$] (Liu *et al.*, 2006). This improvement can be attributed to a higher PLQY of TPABT (76%) compared to 1,8-naphthalimide (25%), as measured in a model compound configuration.

Lee *et al.* (2005) were the first to report on a main-chain copolymer containing emitting units for the three basic colors of blue (PDHF), green (DTPA), and red (TPDCM). The

overall content of green and red chromophores makes up less than 3% in total. Despite the broad spectrum realized with CIE coordinates (0.34, 0.35), the device efficiency was very low with a maximum current efficiency of 0.04 cd A^{-1} ($\eta_{EQE} \approx 0.025\%$). Improvements of this concept (based on different chromophores) were given by Chuang *et al.* (2007) and Luo *et al.* (2007). Similarly to Liu *et al.* (2006), both groups used highly efficient fluorescent benzothiadiazole derivatives for green and red chromophores. Chuang *et al.* (2007) reached maximum efficiencies of $\eta_{EQE} = 2.22\%$ with CIE coordinates of (0.37, 0.36) ($\alpha_{CIE} < +0.01$). Luo *et al.* (2007) even reached a maximum EQE of 3.84%, corresponding to a current efficiency of 6.20 cd A^{-1} [CIE (0.35, 0.34), $\alpha_{CIE} = -0.01$].

2. Copolymers with side-chain chromophores

Instead of attaching the chromophores directly to the backbone of the copolymer, Wang and co-workers also studied the concept of attaching the emitting units to the main chain via alkyl chains (Liu *et al.*, 2005; Liu, Guo *et al.*, 2007; Liu, Xie *et al.*, 2007).

In their first report on this concept (Liu *et al.*, 2005), they included a benzothiadiazole derivative (TPATBT, $\eta_{PL} = 0.37$ in PMMA[9]) in the polyfluorene main chain for red emission and additionally a naphthalimide derivative (DPAN, $\eta_{PL} = 0.91$ in PMMA) as a pendant chain. This configuration reached maximum values of 0.83 lm W^{-1} and 1.59 cd A^{-1} [CIE (0.31, 0.34), $\alpha_{CIE} = +0.01$]. Using a more efficient red chromophore (MB-BT-ThTPA, $\eta_{PL} = 0.51$ in PMMA), they compared the influence of the position of the red emitter in the copolymer, i.e., either in the main chain or as a side chain attached by an alkyl bridge (Liu, Xie *et al.*, 2007). This concept is illustrated in Fig. 16. By repositioning the MB-BT-ThTPA from the main to the side chain, the device efficiency is more than doubled [from 1.99 lm W^{-1} and 3.80 cd A^{-1} to 4.17 lm W^{-1} and 7.30 cd A^{-1} (both with $\alpha_{CIE} = 0$ close to color point *E*)]. This improvement is attributed to the more effective molecular design forming an intramolecular dopant or host system without affecting the electronic properties of the host material (polymer backbone—polyfluorene). Similar to these findings, they reported on an improvement (factor of 1.5–1.8) in device efficiency for a two-color single-component copolymer, when the orange chromophore is attached as a side chain rather than incorporated into the polymer backbone (Liu, Guo *et al.*, 2007).

Recently, Zhang *et al.* (2010) reported on a highly efficient single-component polymer system containing three chromophores that are covalently attached to the polymer backbone. With a correlated color temperature of approximately 4500 K [CIE coordinates (0.37, 0.42), $\alpha_{CIE} = +0.04$], the best device reaches 6.2% EQE and a luminous efficacy of 10.4 lm W^{-1} measured at 500 cd m^{-2}.

The color shift as a function of operating voltage is a widely observed phenomenon, especially for single-component copolymer systems. Gather, Alle *et al.* (2007) focused on the understanding of its origin. In their study, they investigated a statistical copolymer comprising blue, green, and red chromophores embedded in a spiro-polyfluorene polymer. Their data clearly showed that saturation of the red emitter is not the origin of the color shift. They showed that the trapping rate of electrons depends on the electric field within the EML. Therefore, the shift of color is related to the applied field rather than to the current flowing through the device (Gather, Alle *et al.*, 2007). Because the red chromophore inherently has a low band gap and it is present only in very low amounts below the percolation limit, where it can act as a trap, this concept seems to suffer from this general effect.

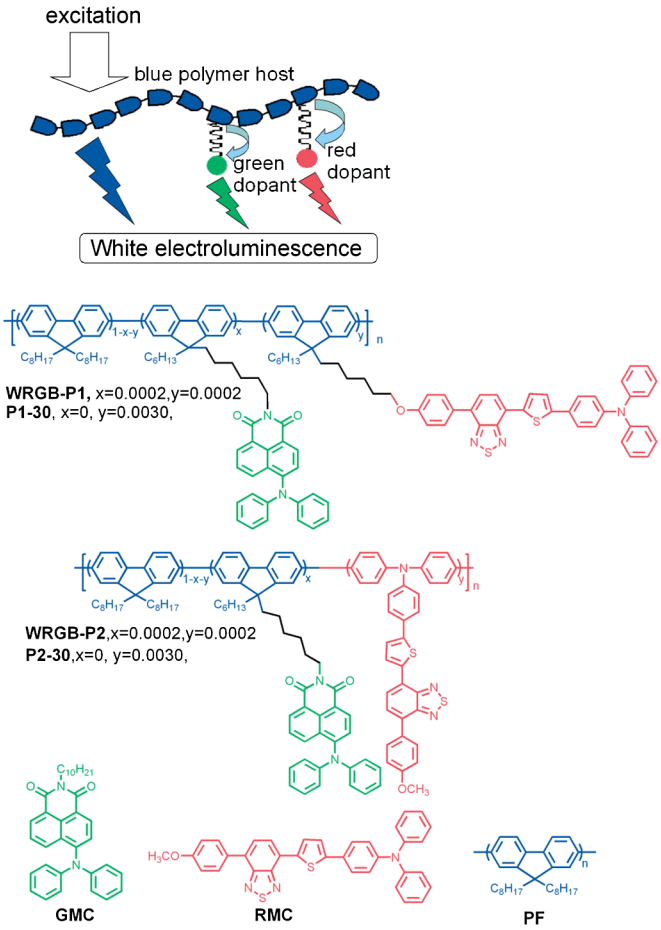

FIG. 16 (color online). Top: Diagram showing the working principle of a blue-emitting polymer backbone with green- and red-emitting side-chain chromophores. Bottom: Molecular structures incorporated to realize this concept. The blue-emitting main chain is a poly(fluorene-co-benzene) (PF), the green model compound (GMC) is DPAN, and the red model compound (RMC) is MB-BT-ThTPA. From Liu, Xie *et al.*, 2007.

3. Copolymers with phosphorescent emitters in side-chain position

All the concepts from above were solely based on fluorescence-emitting materials. However, similar to the general consideration that phosphorescence should enhance the device efficiency, the incorporation of phosphors into a single-component copolymer seems promising. Jiang *et al.* (2006) discussed an approach for a hybrid fluorescent-phosphorescent copolymer. Based on a polyfluorene

[9]'PL' represents photoluminescence.

TABLE I. Summary of selected, high-performance devices based on different device concepts as discussed in Sec. II. Device efficiencies are maximum values; additional values at higher brightness are given in parentheses.

Concept	η_{EQE} (%)	η_{CE} (cd A^{-1})	η_{LE} (lm W^{-1})	CIE (x, y); α_{CIE}	Reference
Small-molecule-doped polymers					
Fluorescent emitters	...	17.9 (17.7)[a]	16.3 (12.6)[a]	(0.33, 0.43); +0.07	Huang, Hou *et al.* (2006)
Phosphorescent emitters	14.2 (12.6)[b]	...	23.4 (18.5)[b]	(0.38, 0.38); $<+0.01$	Huang *et al.* (2009)
Fluorescent blue or phosphorescent	...	(10.4)[c]	(3)[c]	(0.33, 0.33); <-0.01	Gong *et al.* (2005)
Multiple light-emitting polymers					
Polymer blends	6	11.2	16 (12.6)[d]	(0.36, 0.40); +0.03	Huang, Li *et al.* (2006)
Polymer heterolayers	...	6.1 (5.6)[c]	...	(0.323, 0.345); $<+0.01$	Köhnen *et al.* (2010)
Single-component copolymers					
Fluorescent main-chain chromophores	(3.84)[e]	(6.20)[e]	...	(0.35, 0.34); −0.01	Luo *et al.* (2007)
Fluorescent side-chain chromophores	6.7 (6.2)[f]	15.4 (14.2)[f]	11.4 (10.4)[f]	(0.37, 0.42); +0.04	Zhang *et al.* (2010)
Phosphorescent side-chain chromophores	...	5.6	...	(0.44, 0.38); −0.02	Jiang *et al.* (2006)

[a]At 3000 cd m^{-2}.
[b]At 100 cd m^{-2}.
[c]At 2400 cd m^{-2}.
[d]At 1000 cd m^{-2}.
[e]At 654 cd m^{-2}.
[f]At 500 cd m^{-2}.

backbone, they added a benzothiadiazole chromophore for green emission to the polymer backbone and attached a phosphorescent emitter (2-phenylquinoline iridium complex) via an alkyl bridge. In the emission spectra, the benzothiadiazole peaks at 520 nm, the iridium complex at 580 nm, resulting in a energetic difference of roughly 250 meV. This possibly explains the relatively low device efficiencies of 5.6 cd A^{-1}, despite the fact that the emission is close to warm white color point A, with CIE coordinates of (0.44, 0.38, $\alpha_{CIE} = -0.02$). Because the singlet-triplet splitting (cf. Secs. II.A.3 and III.B.3) of the benzothiadiazole green chromophore is expected to be larger than this energy difference of green and red peak energies, the triplet energy of the green unit will act as an efficient quenching site for the red phosphorescence.

D. Summary

Table I summarizes the efficiency and color coordinates of devices with the highest efficiency for all concepts discussed in Sec. II. Interestingly, the focus in the field of polymer OLEDs seems to be on emission close to color point E, i.e., white light sources with a high color temperature in the range of 6000 K [exceptions are the reports by Jiang *et al.* (2006), Huang *et al.* (2009), and Zhang *et al.* (2010) with (correlated) color temperatures ranging between 3000 and 5000 K]. This is in contrast to the following discussion, where it is shown that emission close to the warm white point A ($T_C = 2856$ K) is desired in the field of small-molecule-based white OLEDs. An obvious reason is the potentially higher luminous efficacy that can be reached at standard illuminant A. From a scientific point of view it is interesting whether the concepts presented above are favorable for equally intense emission bands from the emitters or not.[10] This question arises as sometimes the maximum quantum efficiency of a multiemitter system is obtained only for a specific intensity ratio of the different emitters [see, e.g., Schwartz *et al.* (2009) and Rosenow *et al.* (2010)].

Unfortunately, the reports about device parameters are often sparse (see Table I), making it hard to compare the different concepts. Still, to date the concepts based on small molecules used as emitters in a polymer matrix seem to be superior to fully polymeric approaches. For instance, the devices reported by Huang *et al.* (2009) comprising phosphorescent emitters already reach very high external quantum efficiencies approaching the "rule-of-thumb" limit of 20% EQE (cf. Sec. I.A.3) for flat devices without any outcoupling improvement techniques. However, we believe that its comparably high efficiency is mainly due to the fact that it is easier to achieve, because researchers can easily make use of a great variety of high-efficiency small molecular weight emitter molecules (cf. Sec. III). One key disadvantage of mixing different emitters in a polymer or even polymer blend is the poor control over the actual morphology on the nanoscale, which is of key importance for color control and high efficiency. Especially device optimization and development are often complex and unpredictable, because each component as well as the actual processing conditions affects the overall composition of these multicomponent systems.

Despite their currently still poor performance, the concepts solely comprised of polymers (cf. Secs. II.B and II.C) should be favorable because they inherently fit better to the wet-processing techniques, promising ease of fabrication. From the technological point of view, the greatest promise lies in concepts based on single-polymer approaches as discussed in Sec. II.C. Here the hope is that by sophisticated engineering, color control and charge transport can be met in a single polymer, ultimately providing an easy-to-process, low-cost solution. A key advantage is the promise of easily maintaining color control by making use of the stoichiometric composition of the individual chromophores. The realization of such a single-component polymer, however, will need much more future work. Here phosphorescent emitters need to be incorporated into the system to realize maximum efficiency. This in turn calls for careful design of the overall copolymer,

[10]To reach color point E, the intensities of the emission bands are similar for all incorporated emitters while the shape of a multiemitter spectrum at color point A looks more like a staircase (cf. Fig. 8).

because it should be engineered to be free of quenching centers for the chromophores incorporated. By a careful design, single copolymers are likely able to mimic the triplet-harvesting concepts shown with small molecules (cf. Sec. III.B.3), comprising a blue fluorescent chromophore and together with phosphorescent green and red chromophores with potentially 100% internal quantum efficiency. In addition, single-component polymer systems may be very effective in suppressing effects like phase separation [see, e.g., Berggren *et al.* (1994)].

The key difference of small-molecule-doped polymers (cf. Sec. II.A) and single-component polymer systems (cf. Sec. II.C) from a device point of view is the transition from engineering the color through adjusting it during fabrication to defining the ultimately emitted color during the polymer synthesis. The latter is more systematic and desirable.

As is obvious from the data for white small-molecule OLEDs, the field of white polymer OLEDs has fallen considerably behind. All first commercial applications of OLEDs are based on small-molecule devices, which has stimulated the research on these materials and devices. It remains to be seen whether white OLEDs based on polymers can close this performance gap and profit from their advantages, the simpler structure, and the possibility of depositing them by efficient wet-coating technologies.

III. WHITE OLEDs BASED ON SMALL MOLECULES

In contrast to solution processing, thermal evaporation allows a much higher degree of layer complexity, composition control, and thickness accuracy. In many cases, the complete device consists of more than ten subsequently evaporated thin films which are designed to meet a specific function within the device (see Fig. 2). On the other hand, the preparation by thermal evaporation also allows subnanometer control of the deposited layers, opening more design freedom, which enables better device engineering and optimization.

This section contains three major parts that cover fully fluorescent devices (Sec. III.A), hybrid structures with fluorescent blue emitters where the residual spectral range is complemented by phosphorescent emitters (Sec. III.B), and finally fully phosphorescent devices (Sec. III.C). One may notice that we are more selective in this section compared to the discussion of the polymer-based white OLEDs (cf. Sec. II). This is simply due to the fact that the reports discussing white OLEDs based on small molecules by far exceed the number of papers on polymer devices. Stacked OLEDs based on any concepts from above will be discussed in Sec. IV.

It is worth noting that all concepts apart from fluorescent devices, which are limited in internal efficiency because of the spin statistics of the excitons (cf. Sec. I.A.3), bear the potential to reach $\eta_{\text{int}} = 1$. In many cases, impressive work has been done that confirms this potential.

A. Fluorescent devices

Fluorescent emitters can be used in three different emission layer concepts: (i) bulk layers for emission (Choukri *et al.*, 2006; Duan *et al.*, 2008); (ii) host-guest systems, where the fluorophore is dispersed into a wide-band-gap material (Xie *et al.*, 1999; Huang *et al.*, 2002; Kim and Shinar, 2002; Wu *et al.*, 2005; Tsai and Jou, 2006); and (iii) hybrid configurations, where the fluorophore itself is used as an emitter and in addition as a host for a longer-wavelength dye (Chuen and Tao, 2002; Jou *et al.*, 2006; Yang *et al.*, 2011). The latter concept makes use of an incomplete energy transfer from host to guest molecules. Many fluorescent emitters undergo strong concentration quenching [see, for instance, Swanson *et al.* (2003) and Xie, Liu, and Zhao (2003)] so that the designated use of a material (as a pure film or dispersed in a matrix) is often determined by its photophysical properties. In addition to the above concepts, nonemitting interlayers are often introduced to the device structure, mainly to achieve charge carrier confinement either at interfaces (Wu *et al.*, 2005) or in quantum-well-like structures (Xie *et al.*, 1999). This is realized by adjusting the energy levels (HOMO and LUMO) of the respective materials to artificially form energy barriers.

In contrast to devices comprising phosphorescent materials where the triplet manifold of the materials used becomes important, the nonradiative triplet levels of the fluorescent materials do not play an important role in the device design. This is mainly caused by the fact that the energy transfers of singlet excitons of fluorophores to triplet states of fluorescent materials are quantum mechanically forbidden (Pope, 1999; Baldo, Thompson, and Forrest, 2000) and thus do not represent a prominent quenching channel. Later discussion will show that this picture strongly changes when using phosphors in the device (cf. Secs. III.B and III.C).

The very first reports on white OLEDs solely comprising small molecules by Hamada *et al.* (1996), Jordan *et al.* (1996), and Strukelj, Jordan, and Dodabalapur (1996) will be mentioned only for completeness. None show improvements to the devices discussed by Kido *et al.* (1994) and Kido, Shionoya, and Nagai (1995) with respect to their color quality and/or efficiency. Furthermore, the incorporation of exciplex formation and emission may generally be used for the realization of white OLEDs (Feng *et al.*, 2001; Mazzeo *et al.*, 2003); however, the overall efficiency of such devices seems to be rather limited. The only exception so far is the report by Tong *et al.* (2007), discussing white OLEDs based on a single emissive material TPyPA, where the emission originates from its singlet and exciplex state (formed at the interface to the well-known electron-transporting material BPhen). These devices reach a maximum luminous efficacy of 9.0 lm W^{-1} with CIE coordinates of (0.31, 0.36; $\alpha_{\text{CIE}} = +0.02$).

Tsai and Jou (2006) reported on highly efficient fluorescent white OLEDs based on a mixed host EML dual doped with two fluorophores. By optimizing the blend of hole-transporting NPB and electron-transporting TBADN to a 1:1 ratio, 4.7% EQE and 6.0 lm W^{-1} ($\eta_{\text{LE,max}} = 11.2\ \text{lm W}^{-1}$) were obtained at 10 mA cm^{-2}. The emission, based on blue DPAVBi and red rubrene emitters, reaches CIE color coordinates of (0.329, 0.353; $\alpha_{\text{CIE}} = +0.02$). No luminance level is given in their report at which the efficiency values stated, however, 10 mA cm^{-2}, are likely to correspond to brightness values of approximately 1000 cd m^{-2} [see Yang *et al.* (2011)].

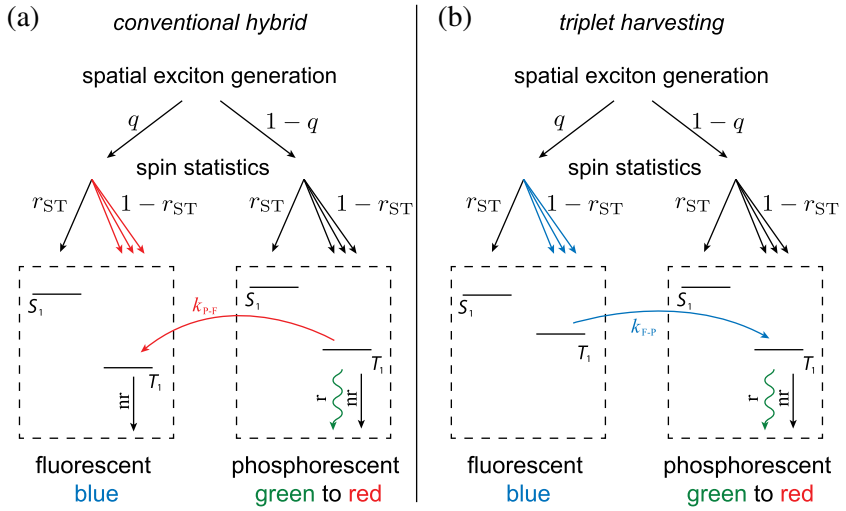

FIG. 17 (color online). Scheme for electrical excitation in (a) conventional hybrid and (b) triplet-harvesting concepts. For simplicity, the exciton generation is assumed to be spread only to two materials, i.e., fluorescent blue and phosphorescent green to red. Here q denotes the fraction of excitons that are created on the blue fluorophore, r_{ST} is the fraction of singlet excitons formed, "r" and "nr" stand for radiative and nonradiative, respectively, and $k_{F\text{-}P}$ and $k_{P\text{-}F}$ are energy transfers from fluorophore to phosphor or vice versa.

Yang *et al.* (2011) recently discussed a hybrid combination of simultaneous host and dopant emission, forming a two-color white device. They highly diluted the red emitter DCM into the blue-emitting host Bepp2 (0.2 wt % for a thin slab of 3 nm followed by 0.5 wt % doping for the remaining 42 nm of the EML) so that the energy transfer from host to guest is incomplete. At 10 mA cm^{-2}, corresponding to roughly 1000 cd m^{-2}, this device reached 5.2% EQE corresponding to 4.8 lm W^{-1} (maximum values 5.6% EQE, 9.2 lm W^{-1}) with color coordinates of (0.332, 0.336) ($\alpha_{CIE} = 0$) and a CRI = 80.

Note that both reports from Tsai and Jou (2006) and Yang *et al.* (2011) with EQE values close to 5% represent rule-of-thumb limits for devices fully based on fluorescence (cf. Sec. I.A.3).

B. Hybrid fluorescent-phosphorescent OLEDs

A large part of the research conducted on white small-molecule OLEDs comprises blue fluorescent emitters together with longer-wavelength phosphorescent emitters to achieve the white spectrum. The reason for this device concept is twofold: (i) blue phosphorescent emitters with long-term stability are hard to find (Su *et al.*, 2008), and devices based on freely available materials often degrade within hours of operation (Reineke, Lindner *et al.*, 2009). Thus, blue fluorescent emitters are commonly used to avoid this stability bottleneck (Schwartz *et al.*, 2006). (ii) Because blue phosphorescent materials call for host materials with even larger band gaps, the operating voltage of devices based on phosphorescent blue emitters will increase (Seidler *et al.*, 2010) with the luminous efficacy decreasing accordingly (Sun *et al.*, 2006; Reineke, Lindner *et al.*, 2009; So and Kondakov, 2010).

1. Conventional architectures

In general, the blue fluorescent emitters used in hybrid white emission layers have triplet levels lower than the respective T_1 states of the phosphorescent materials. For instance, Schwartz *et al.* (2006) reported a triplet level of a highly efficient blue emitter Spiro-DPVBi at 2.0 eV, while its fluorescent peak is at 475 nm (2.6 eV). Thus, the blue triplet level typically represents a prominent quenching channel. This problem is illustrated in Fig. 17(a) for a simplified case where all phosphorescent materials incorporated are treated as one system, which may be more complex in real devices. In order to address all colors in the OLED, the emission layer is designed to realize exciton generation in all sublayers hosting the different emitters. In Fig. 17, excitons are created with a fraction q on the fluorescent emitter, leaving $1 - q$ to be generated in the phosphorescent system. All formed excitons obey the spin statistics known to be present in organic LEDs (cf. Sec. I.A.3), which is represented here by the fraction of created singlets r_{ST}. Note that, in general, r_{ST} may be different for every emitter system (Segal *et al.*, 2003). However, to keep this discussion simple, r_{ST} is used as a fixed value for any emitter system here.[11] Since the triplet level of the fluorescent blue emitter is lower than the respective levels of the phosphorescent materials, efficient transfer from phosphors to the fluorophore can occur, represented by the rate $k_{P\text{-}F}$. Obeying the selection rules for purely organic materials (Sec. I.A.3), this triplet level is nonemissive ("nr" = nonradiative); thus excitons reaching it will be lost for emission.

Overall there are two channels for exciton quenching: (i) The direct formation of triplet excitons on the fluorescent triplet level, which is proportional to $q(1 - r_{ST})$. Since $1 - r_{ST}$ is a property of the specific material and typically on the order of 75% (Segal *et al.*, 2003), the only way to reduce this channel is to reduce q. However, this will decrease

[11] Even more complicated is the fact that the fluorescent blue system can be either a pure film or a host-guest system. In the latter case, one would need to include exciton transfers from host to guest for both singlets and triplets.

the fluorescent intensity at the same time ($\sim qr_{ST}$). (ii) The energy transfer from the phosphorescent system to the fluorescent triplet level $k_{P\text{-}F}$ will reduce the quantum efficiency of the phosphorescent emitter (Kawamura *et al.*, 2006):

$$\eta_P = \frac{k_r}{k_r + k_{nr}} \xrightarrow{T_{1,F}<T_{1,P}} \frac{k_r}{k_r + k_{nr} + k_{P\text{-}F}}. \tag{23}$$

Obviously, the emission efficiency of the phosphorescent system can be greatly reduced if $k_r \approx k_{P\text{-}F}$. Triplet quenching introduced by $k_{P\text{-}F} > 0$ can easily be prevented by introducing a thin interlayer between fluorescent and phosphorescent systems. Because the energy transfer leading to $k_{P\text{-}F}$ is a Dexter type (Sec. I.A.5), requiring orbital overlap, interlayer thicknesses in the range of 2 nm are sufficient (Schwartz *et al.*, 2006).

The first report on hybrid white OLEDs comprising an interlayer was made by Schwartz *et al.* (2006). Their general device structure consists of a hole-transporting phosphorescent multilayer system for red and green and an electron-transporting Spiro-DPVBi layer for blue emission. Thus, excitons are generated at the interface between green phosphorescent and blue fluorescent layers, where a large part of the green excitons can be quenched by the Spiro-DPVBi triplet level at roughly 2.0 eV. In order to suppress exciton transfer, they introduced a composite exciton blocking layer consisting of the hole-transporting material TCTA and the electron-transporting material TPBi (Schwartz *et al.*, 2006). Both have triplet energy levels of 2.83 and 2.59 eV (Reineke, Lindner *et al.*, 2009; Reineke, Schwartz,Walzer, and Leo, 2009) above the Ir(ppy)$_3$ T_1 state that enable efficient blocking of excitons from the green emission layer. At the same time, the mixture of both materials makes it possible to assure that excitons are still created on each side of the EML, being essential to maintain a balanced white spectrum. Figure 18 shows the characteristics of two devices without and with additional composite TCTA:TPBi interlayers. The values best suited for comparison are the EQE values, as they are not additionally affected by spectral changes. Here, by introducing the interlayer, the EQE is almost doubled from 4.5% to 8.0% EQE, as measured at 1000 cd m^{-2}. The corresponding CIE coordinates of the device with interlayer are (0.47, 0.42) ($\alpha_{CIE} = +0.02$), the color rendering index is as high as 85, and the luminous efficacy reaches 13.7 lm W^{-1} at 1000 cd m^{-2} (Schwartz *et al.*, 2006). Comparison of the device efficiency with and without interlayer indicates that the transfer $k_{P\text{-}F}$ can easily reach the same order of magnitude as the radiative rate of the phosphor [cf. Eq. (23); see also Baek and Lee (2008)].

Another advantage of a composite exciton blocking layer is the ability to alter its transport properties with the mixing ratio of the two materials, ultimately enabling one to tune the color of the devices (Schwartz, Ke *et al.*, 2008; Leem *et al.*, 2010). Besides the use of composite spacing layers that contain preferentially hole- and electron-transporting materials, single-material interlayers are also used. Widely used molecules are NPB [hole transporting (Yan *et al.*, 2007; Ho, Wong *et al.*, 2008)], TPBi [electron transporting (Ho, Lin *et al.*, 2008)], and CBP (Seo *et al.*, 2007; Baek and Lee, 2008; Zhang *et al.*, 2008). The latter material, CBP, is often discussed as having ambipolar transport properties. Note that the observed ambipolarity is often a stringent interplay between charge carrier mobility and energy level alignments within the complex layer structure.

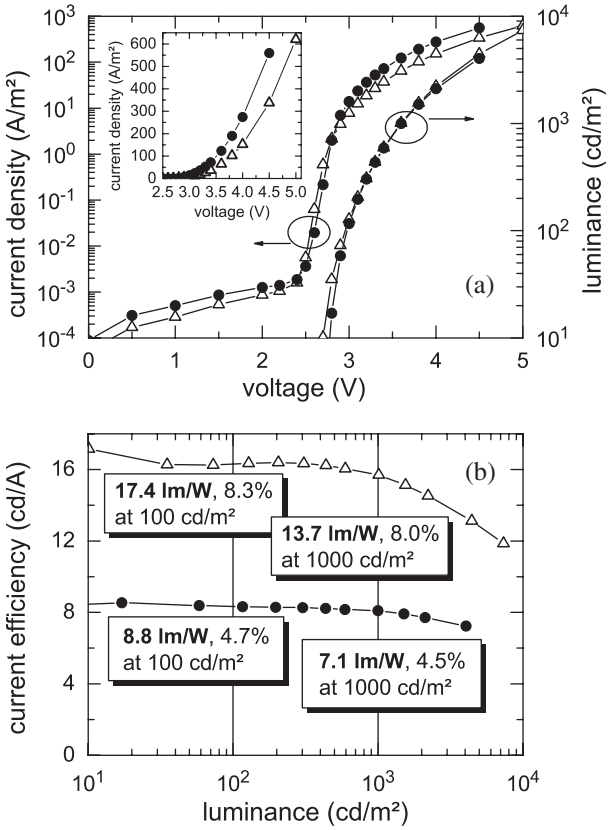

FIG. 18. Characteristics of hybrid white without (filled circles) and with (open triangles) exciton blocking interlayer. Top: Current density and luminance vs voltage. Bottom: Current efficiency as a function of luminance. Additionally, luminous efficacy and EQE are given at brightness values of 100 and 1000 cd m^{-2}. From Schwartz *et al.*, 2006.

Sun *et al.* (2006) reported on a device concept for white OLEDs that shows improvement in the exciton distribution within the emission layer. Their OLEDs are based on the fluorescent blue emitter BCzVBi and the green and red phosphors Ir(ppy)$_3$ and PQIr, respectively, all embedded into a common host at different spatial locations. They claim that their device concept enables 100% internal quantum efficiency as a result of a decoupling of singlet and triplet exciton channels. This enables one to use only the 25% fraction of singlets for fluorescence whereas the remaining 75% of the generated triplets are directed to the green and red phosphors (cf. Sec. I.A.3). Furthermore, with a finely tuned EML, thermalization losses prior to photon emission can be reduced to decrease the operating voltage and increase the luminous efficacy (Sun *et al.*, 2006). Their device concept is based on the experimental finding that excitons are mainly formed at both EML interfaces to adjacent transport layers, forming a U-shaped exciton generation profile (Sun *et al.*, 2006). Both regions of exciton formation are therefore doped with the fluorescent blue emitter BCzVBi at 5 wt %. There singlets recombine while triplets diffuse away from the site of exciton generation into the center of the EML. The energy

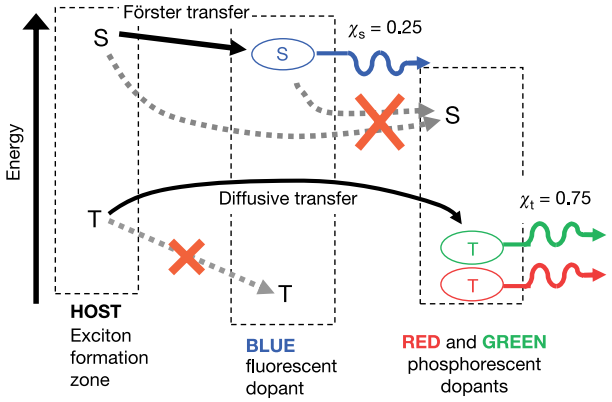

FIG. 19 (color online). Exciton transfer scheme for hybrid fluorescence and phosphorescence white OLEDs. Exciton formation mainly occurs on the CBP host material. Solid lines represent allowed and dashed lines suppressed energy transfers. From Sun *et al.*, 2006.

transfer scheme is shown in Fig. 19. As proof of both, the exciton generation at the interfaces forming a U shape and the ability for triplet excitons to diffuse into the center of the EML are given in Fig. 20. Comparing a device with an undoped (device I) and on with a BCzVBI-doped (device II) middle section does not show differences in the emitted blue intensity. If the center section is doped with the green emitter $Ir(ppy)_3$ (device III) instead, an additional high-intensity green signal is detected in the electroluminescence. Because the blue fluorescent intensity remains unchanged between devices I and III, it is valid to assume that only triplet excitons are transferred to the phosphor while the singlets recombine solely on BCzVBi. However, it cannot be excluded from these data that a constant fraction of triplet excitons remains trapped on the blue fluorophore [comparable in undoped and $Ir(ppy)_3$-doped devices]. Furthermore, a thin undoped CBP layer is sandwiched between blue and green layers to prevent singlet exciton transfer from BCzVBi to $Ir(ppy)_3$ (see Fig. 19).

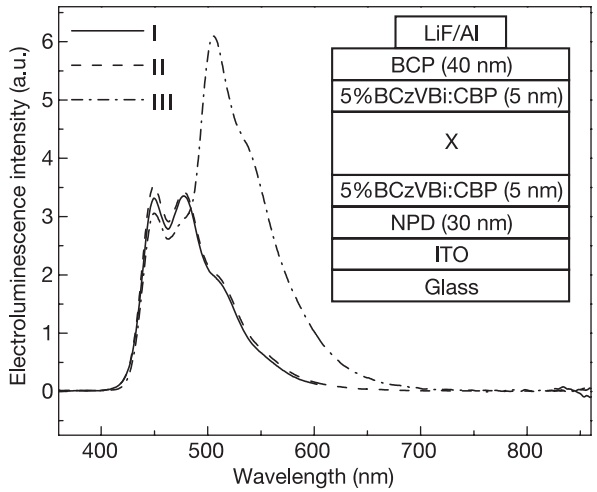

FIG. 20. Electroluminescence spectra of three different device structures having variations in the spacer X. I: $X = 16$ nm CBP, II: $X = 15$ nm CBP:BCzVBi (5 wt %), and III: $X = 4$ nm CBP + 20 nm CBP: $Ir(ppy)_3$ (3 wt %). The inset shows the device layout. From Sun *et al.*, 2006.

Sun *et al.* (2006) stated that the triplet exciton transfer from the CBP host to the blue emitter BCzVBi is suppressed as shown in Fig. 19 [see also Schwartz *et al.* (2009)]. However, it is fairly unlikely that this Dexter-type energy transfer (cf. Sec. I.A.5) does not occur as the BCzVBi concentration is at a sufficiently high level of 5 wt %. This transfer is energetically favorable, since the triplet excited state of BCzVBi is at 1.81 eV (Deaton *et al.*, 2008), which is noticeably smaller than the respective T_1 levels of $Ir(ppy)_3$ (2.42 eV) and PQIr (2.06 eV). Thus, the BCzVBi triplet states form a triplet exciton trap that introduces a nonradiative loss channel. Therefore, the theoretical limit for the internal quantum efficiency of this concept is below 100%. Note that at 5 wt % of BCzVBi in the region of exciton formation, even direct triplet exciton generation on the emitter molecules cannot be excluded, which similarly populates the nonradiative BCzVBi triplet state. Recently, Schwartz *et al.* (2009) presented a calculation made for devices based on triplet harvesting, which will be discussed in the next section, where EQE values of 10% are possible even when the triplets on the blue emitter are lost nonradiatively. With all triplets harnessed, the EQE limit is in the range of 16%. The device efficiencies reported by Sun *et al.* (2006) are 10.8% EQE at 500 cd m^{-2} (14 lm W^{-1}), with corresponding color coordinates of (0.40, 0.41) ($\alpha_{CIE} = +0.02$) and a very high CRI of 85. The efficiency data alone, however, do not prove that the majority of nonradiative host triplets are harnessed by the lower-energy phosphors in their device concept.

2. Phosphor-sensitized fluorescence

In order to overcome the bottleneck that only 25% of the excitons are electrically excited in singlet states (cf. Sec. I.A.3), Baldo, Thompson, and Forrest (2000) proposed a cascade excitation scheme to promote triplets back to emissive singlet states of a fluorophore. This is achieved by additionally introducing a phosphorescent molecule [i.e., $Ir(ppy)_3$] into the system that acts as a sensitizer, denoted as X. As the subsequent discussion will show, white OLEDs based on this concept either are designed to have substantial emission from the sensitizer X or are combined with additional phosphors to achieve white light emission. Thus, this concept is discussed here in Sec. III.B, even though it was originally promoted to achieve highly efficient fluorescent devices (Baldo, Thompson, and Forrest, 2000).

The transfer scheme is shown in Fig. 21. The cascade energy transfers from host donor singlet ($^1D^*$) and triplet ($^3D^*$) level are [see Baldo, Thompson, and Forrest (2000)]

$$^1D^* + {}^1X \xrightarrow{\text{Förster}} {}^1D + {}^1X^*, \tag{24}$$

$$^1X^* \xrightarrow{\text{ISC}} {}^3X^*, \tag{25}$$

$$^3X^* + {}^1A \xrightarrow{\text{Förster}} {}^1X + {}^1A^*, \tag{26}$$

and

$$^3D^* + {}^1X \xrightarrow{\text{Dexter}} {}^1D + {}^3X^*, \tag{27}$$

$$^3X^* + {}^1A \xrightarrow{\text{Förster}} {}^1X + {}^1A^*. \tag{28}$$

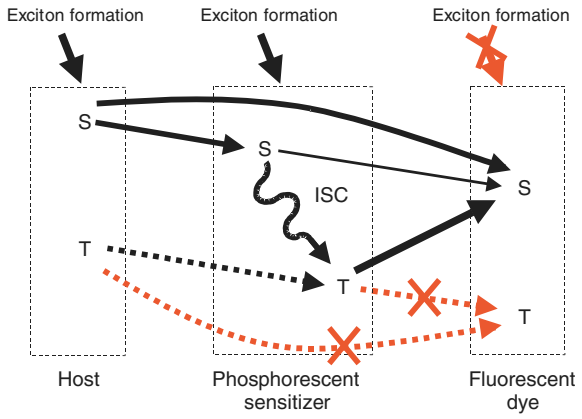

FIG. 21 (color online). Energy transfer mechanisms for a phosphor-sensitized fluorescence system. Triplet transfer from host and sensitizer molecules to the fluorescent dye is suppressed by highly diluting the fluorophore. Triplet excitons from the sensitizer are transferred to the singlet state of the fluorophore via Förster energy transfer. From Baldo, Thompson, and Forrest, 2000.

Finally, the photon is emitted via ${}^1A^* \rightarrow {}^1A + h\nu$ from the singlet state of the fluorescent acceptor. Note that triplet transfer via Förster energy exchange [Eqs. (26) and (28)] is possible only because X is a phosphorescent donor (cf. Sec. I.A.5). Triplet exciton transfer from the donor (host) D and sensitizer X to the triplet level of the fluorophore needs to be avoided because it presents quenching channels. Both, being Dexter-type transfers requiring orbital overlap, can be suppressed by increasing the intermolecular distance between the respective donors (D or X) and the acceptor. In their early report, Baldo, Thompson, and Forrest (2000) increased the device efficiency of a red fluorescent OLED based on DCM2 by a factor of 3 compared to a reference device by incorporating $Ir(ppy)_3$ as a sensitizing molecule. Since the singlet excited-state lifetime of DCM2 is in the range of a few nanoseconds, which is orders of magnitude longer compared to $Ir(ppy)_3$ (Adachi *et al.*, 2000), the transient signal of DCM2 resembles the decay of the phosphor (Baldo, Thompson, and Forrest, 2000), giving direct evidence for the proposed excitation scheme.

Following the fundamental finding of Baldo, Thompson, and Forrest (2000), $Ir(ppy)_3$ has been widely used so far to sensitize red fluorescent emission (Cheng *et al.*, 2003; Cheng, Zhang, Zhao, Liu, and Ma, 2006; Kanno, Sun, and Forrest, 2006; Xue *et al.*, 2010). Here the red fluorophores were either rubrene (Cheng, Zhang, Zhao, Liu, and Ma, 2006; Xue *et al.*, 2010) or DCJTB (Cheng *et al.*, 2003; Kanno, Sun, and Forrest, 2006). The highest efficiency and color quality based on phosphor-sensitized fluorescence was reported by Kanno, Sun, and Forrest (2006). In their concept, CBP is used as a common host for all emitting materials, which were laterally distributed to achieve emission from all colors. BCzVBi is used for the high-energy blue emission in their devices. A double-doped film comprising $Ir(ppy)_3$ (8 wt %) as a sensitizer and DCJTB (0.08 wt %) as a red fluorophore is positioned in the center of the emission layer. Here as in Baldo, Thompson, and Forrest (2000), the emission of the green phosphor $Ir(ppy)_3$ is not fully quenched, which is utilized in this white concept to fill the spectral gap between blue and red emission bands to achieve high-quality white emission. This device reaches 8.5% external quantum efficiency (maximum value), which corresponds to 18.1 $\mathrm{lm\,W^{-1}}$, with CIE color coordinates of (0.38, 0.42) ($\alpha_{\mathrm{CIE}} = +0.03$). Omitting $Ir(ppy)_3$ in the device structure strongly decreases the EQE values to approximately 3% (Kanno, Sun, and Forrest, 2006).

In contrast to many reports based on $Ir(ppy)_3$, Lei, Wang, and Qiu (2004) introduced the light-blue emitter FIrpic as a sensitizer. Here FIrpic (8%) and DCJTB (0.4%) are diluted in a wide-gap material (DCB), where FIrpic acts as both a blue emitter and a phosphorescent sensitizer for the red DCJTB molecules. These devices reach a maximum efficiency of 9.2 $\mathrm{cd\,A^{-1}}$ with CIE coordinates of (0.32, 0.36) ($\alpha_{\mathrm{CIE}} = +0.02$).

Even though phosphor sensitization seems to be a promising route to make use of short-lifetime fluorophores that enable higher efficiency at high brightness (Baldo, Thompson, and Forrest, 2000) because of reduced triplet quenching, this concept has not drawn much attention. This might be due to the complex, cascade energy transfer that has to be controlled to achieve white light emission. Putting the limited stability of blue phosphorescent materials aside for a moment (Kanno, Sun, and Forrest, 2006; Sun *et al.*, 2006; Reineke, Lindner *et al.*, 2009; Schwartz *et al.*, 2009), it might be worth investigating phosphor-sensitized white OLEDs, where a high-energy (deep blue) triplet emitter distributes all excitons to longer-wavelength fluorescent materials. This would enable the creation of a fully fluorescent white OLED with internal efficiencies of unity.

3. Triplet harvesting

In order to reduce the losses in triplet states of blue fluorescent emitters scaling with $q(1 - r_{\mathrm{ST}})$ (see Fig. 17), these excited states need to be passed on to other sites, as their generation cannot fully be excluded. The only way to achieve this is to incorporate fluorescent materials with a triplet level that is equal to or higher than the T_1 state of at least one of the phosphorescent emitters used. Assuming a blue fluorescence at 450 nm and a red phosphorescence at 600 nm, the key requirement for blue fluorophores to act as a triplet donor in white OLEDs translates into a singlet-triplet energy gap of <0.7 eV. Note that the fluorescent emitter BCzVBi that was discussed in Sec. III.A has a fluorescence peak at 450 nm and a singlet-triplet splitting of approximately 0.95 eV (Sun *et al.*, 2006; Deaton *et al.*, 2008).

From quantum mechanical principles, it is known that the singlet-triplet splitting ΔE_{ST} is proportional to the exchange integral K between spatial overlap of the HOMO and LUMO (Endo *et al.*, 2009, 2011; Schwartz *et al.*, 2009): $\Delta E_{\mathrm{ST}} \sim 2K$. By localizing HOMO and LUMO wave functions to different regions of the molecular structure, the singlet-triplet splitting can be strongly reduced even down to 0.11 eV (Endo *et al.*, 2011). Once the triplet state of the fluorophore is higher than the triplet level of a phosphor incorporated, the quenching rate $k_{\mathrm{P\text{-}F}}$ transforms into an additional path to excite a phosphor $k_{\mathrm{F\text{-}P}}$ [cf. Figs. 17(a) and 17(b)], because the different relations of the energy levels reverse the direction of the energy transfer. Thus, when triplet harvesting is incorporated into a device concept for white OLEDs, internal quantum efficiencies of 100% are possible, because the fluorophore

triplet state is changed from a nonradiative trap to an intermediate state that participates in the excitation of the phosphors.

The concept of triplet harvesting in white OLEDs was introduced by Schwartz *et al.* (2007). Their work is based on a special fluorescent blue emitter 4P-NPD, shown in Fig. 22, that has its fluorescent peak at 426 nm and a singlet-triplet splitting of ~0.6 eV (cf. Fig. 22). Another important property of 4P-NPD is its very high pure-film PLQY (Schwartz *et al.*, 2007), making it possible to use it as a bulk emitter. The working principle is shown in Fig. 23. With the triplet level of 4P-NPD at approximately 2.3 eV, it is sufficiently high to excite the red phosphor $Ir(MDQ)_2(acac)$ (2.06 eV). However, the green emitter $Ir(ppy)_3$ with a triplet level at 2.42 eV would still be quenched by 4P-NPD.

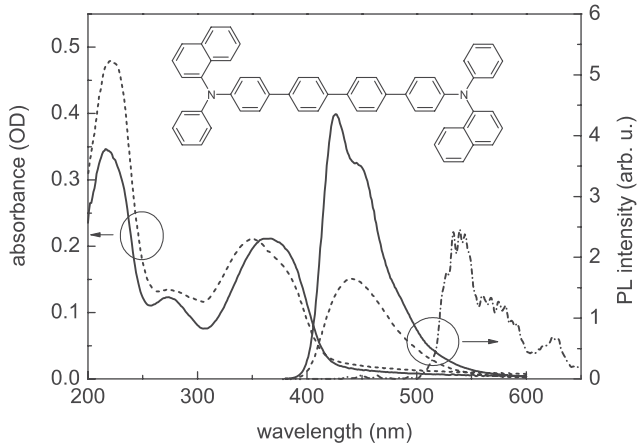

FIG. 22. Absorbance and photoluminescence data of 30 nm pure films of NPB (dashed) and 4P-NPD (solid, chemical structure shown in the inset). Photoluminescence is recorded at an excitation wavelength where absorbance data of both materials intersect (356 nm), so that the intensities reflect the relative quantum yields of the materials. Additionally, the phosphorescence spectrum of 4P-NPD is plotted as obtained at 77 K for the diluted form in a solid polystyrene matrix (2 wt %). From Schwartz *et al.*, 2007.

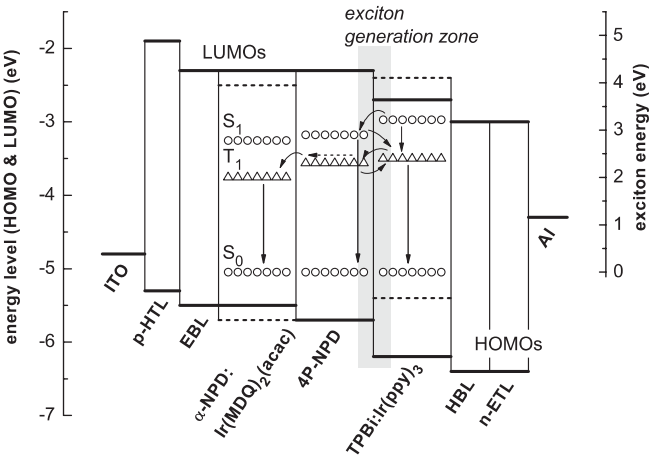

FIG. 23. Energy-level diagram [HOMOs and LUMOs (lines), and triplet energies (open symbols)] of the white OLED making use of the triplet-harvesting concept. From Schwartz *et al.*, 2007.

Consequently, triplet harvesting is realized with the combination of 4P-NPD and $Ir(MDQ)_2(acac)$, while an additional layer for conventional green phosphorescence is added. Excitons are formed at a double emission layer interface (Zhou *et al.*, 2002) between a composite α-NPD: $Ir(MDQ)_2(acac)$/4P-NPD system and TPBi: $Ir(ppy)_3$. This concept makes use of the ability of triplet excitons being able to diffuse farther than singlets (Schwartz *et al.*, 2007; Rosenow *et al.*, 2010). For 4P-NPD, a triplet diffusion length of 11 nm (Wünsche *et al.*, 2010) was determined. While singlet excitons recombine in the close proximity of the exciton generating interface [cf. 4P-NPD singlet diffusion length of ~4 nm (Hofmann *et al.*, 2012)], the triplet excitons diffuse away from this interface ultimately reaching the phosphor-doped α-NPD: $Ir(MDQ)_2(acac)$ layer. There they are efficiently transferred via $k_{F\text{-}P}$ to the emissive $Ir(MDQ)_2(acac)$ triplet state. The devices of the first report by Schwartz *et al.* (2007) already reached high efficiency values of 10.4% EQE and 22.0 lm W^{-1} at 1000 cd m^{-2} with CIE coordinates of (0.44, 0.47) ($\alpha_{CIE} = +0.06$) with a CRI = 86.

The effect of triplet harvesting is best seen in Fig. 24. It shows a series of samples with a bilayer EML architecture of 4P-NPD: $Ir(MDQ)_2(acac)$ [5 wt %]/4P-NPD with different intrinsic 4P-NPD layer thickness from 0 to 30 nm. Excitons are created at the interface between the 4P-NPD layer and the adjacent hole-blocking layer (HBL) (Rosenow *et al.*, 2010). Without an intrinsic 4P-NPD layer (0 nm), the device is a conventional red phosphorescent OLED showing solely red emission and high EQE. With increasing 4P-NPD layer

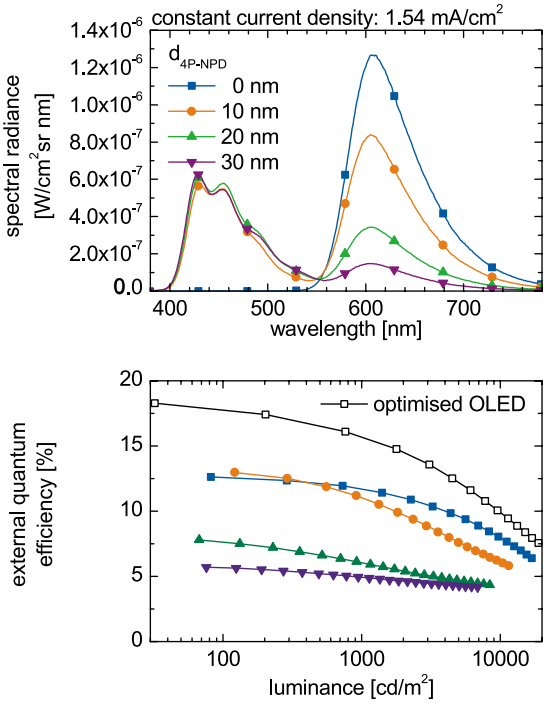

FIG. 24 (color online). Top: Absolute electroluminescence spectra of triplet-harvesting devices showing a variation in the 4P-NPD spacer thickness from 0 to 30 nm measured at a fixed current density. Bottom: Corresponding EQE vs luminance characteristics. Additionally plotted is the EQE of an optimized device that is further used for integration in the two-unit white OLEDs. From Rosenow *et al.*, 2010.

thickness, the red intensity decreases and additional blue fluorescence is observed. Note here that the spectra shown are not normalized but rather plotted in absolute units, clearly indicating that additional triplets can be harvested by $Ir(MDQ)_2(acac)$ when the 4P-NPD layer thickness is adjusted correctly (this is also reflected in the EQE on the bottom of Fig. 24).

Since the triplet level of 4P-NPD cannot excite green phosphorescent emitters, Rosenow *et al.* (2010) incorporated this triplet-harvesting system into a two-unit stacked OLED, where the second unit is a double-doped phosphorescent green or yellow unit based on the emitters $Ir(ppy)_3$ and $Ir(dhfpy)_2(acac)$. Without going into the details of this device layout, they could improve the efficiency and color quality to 26% EQE[12] and 33 lm W^{-1} at 1000 cd m^{-2}. The corresponding color coordinates are (0.506, 0.422) ($\alpha_{CIE} < +0.01$), very close to the Planckian locus. This improvement in color quality can mainly be attributed to the possibility to optimize the triplet harvesting and green or yellow units independently, whereas in the report of Schwartz *et al.* (2007) multiple exciton transfer steps at the exciton generating interface (cf. Fig. 23) complicated the color control.

The triplet-harvesting concept is based on the fact that nonradiative triplets formed on the fluorescent material can find accessible sites for recombination which are spatially separated and reached only via diffusion. Taking into account the fact that the triplet excited lifetime in 4P-NPD is long [in the range of ms (Schwartz *et al.*, 2007)], a correspondingly high triplet exciton density n_T is formed in the 4P-NPD layer. Since triplet-triplet annihilation scales with the square of n_T, it will be much stronger than observed in state-of-the-art phosphorescent systems (Reineke, Walzer, and Leo, 2007), where the triplet lifetime is in the range of microseconds. The consequence is that triplets diffusing to the emissive phosphorescent sites are likely to annihilate with other triplets [or even charges (Reineke, Walzer, and Leo, 2007)], so that the quantum efficiency of the red emission is strongly reduced as a function of the excitation level (current density) (Schwartz *et al.*, 2007). Thus, triplet-harvesting systems typically have a strong EQE roll-off (compare for instance the EQE characteristics of devices with and without 10 nm intrinsic 4P-NPD layer, shown in Fig. 24, bottom). In order to reduce the triplet density n_T, Schwartz, Reineke *et al.* (2008) merged the bilayer triplet-harvesting system to one blend layer of 4P-NPD: $Ir(MDQ)_2(acac)$, so that the average distance a triplet has to travel to reach a phosphor is reduced. Fluorescence is still observed, because the doping concentration of the phosphor is reduced by 1 or 2 orders of magnitude (~ 0.1 wt %) compared to conventional phosphorescent OLEDs ($\sim$ 5–10 wt %). The effect is shown in Fig. 25 comparing bilayer and blended systems incorporated into white devices (Schwartz, Reineke *et al.*, 2008). While the EQE of the bilayer device steadily decreases as a function of current density j, the blend system shows a noticeable range of j (almost 3 orders of magnitude), where the EQE remains at a relatively constant value. Only at high j is the EQE roll-off

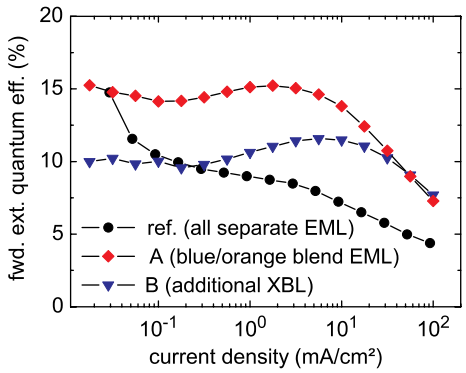

FIG. 25 (color online). External quantum efficiency vs current density for different triplet-harvesting integrations (bilayer and blended systems) showing strong differences in the efficiency roll-off. XBL is the exciton blocking layer. From Schwartz, Reineke *et al.*, 2008.

observed, similar to standard phosphorescent devices (Reineke, Walzer, and Leo, 2007). The blend system reaches very high device efficiencies at 1000 cd m^{-2} of 15.2% EQE and 31.6 lm W^{-1} with CIE coordinates of (0.49, 0.41) matching the Planckian locus ($\alpha_{CIE} = 0$). This conceptional improvement is important because, especially for lighting applications, brightness values of a few thousand cd m^{-2} are required. The only drawback of the blend approach is the very low emitter concentration down to $\sim$0.1 wt %, raising the question whether this process can be controlled in large-scale manufacturing.

Relying on the special properties of fluorescent blue emitters having a noticeably reduced singlet-triplet splitting ΔE_{ST}, the progress based on the triplet-harvesting concept is rather slow. Still, in recent years, first reports were published discussing new materials with even improved properties compared to 4P-NPD. Here the ultimate goal is to reduce ΔE_{ST} to values where also green phosphors ($\sim$ 510 nm) can be excited from the fluorophore triplet state. Recently, Kondakova *et al.* (2010) reported on another fluorescent blue emitter MQAB with small singlet-triplet splitting of 0.27 eV (singlet 2.82 eV and triplet 2.55 eV). Presumably, because its PLQY as a pure film is not high, Kondakova *et al.* (2010) used MQAB in a host-guest system together with the well-known CBP host (triplet 2.61 eV). Thus, with respect to their triplet energies, both MQAB dopant and CBP host are almost in resonance so that triplet movement throughout the layer is possible. In contrast to the work presented above, Kondakova *et al.* (2010) always used a spacer material, i.e., $Ga(pyimd)_3$ (experimental triplet level 2.71 eV, in dilute form), between blue fluorescent and phosphor-doped layers. The host for the phosphors used is $Ga(pyimd)_3$ also. In total, the EML layer (from hole injection side) is CBP: $MQAB/Ga(pyimd)_3/Ga(pyimd)_3$:
phosphor. Using time-resolved spectroscopy, Kondakova *et al.* (2010) gave experimental evidence for the presence of triplet harvesting in their devices as shown in Fig. 26. Here the prompt fluorescence and delayed phosphorescence are separately shown, clearly displaying a time delay between the two. The inset shows the delay between fluorescence and phosphorescence peaks as a function of $Ga(pyimd)_3$ spacer

[12]Note that the EQE values in two-unit stacked OLEDs can theoretically be doubled, because for every electron that is injected, two photons can be emitted.

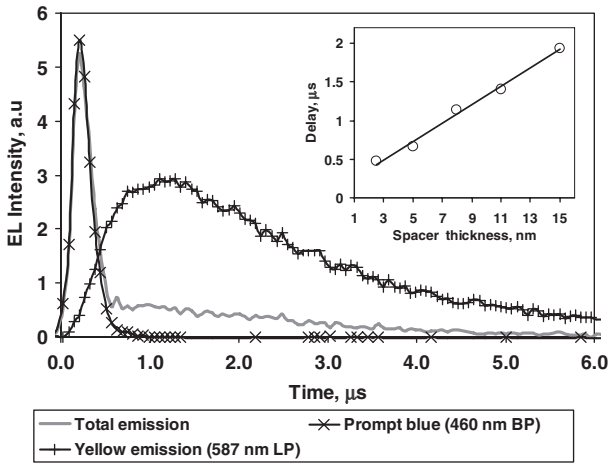

FIG. 26. Time-resolved electroluminescence of a device with blue fluorescence (MQAB) and yellow phosphorescence [$Ir(ppy)_2pc$, triplet: 2.34 eV] of a triplet-harvesting system. Inset: Delay between time-resolved maxima of prompt and delayed features as a function of spacer thickness. From Kondakova *et al.*, 2010.

thickness, indicating the diffusively promoted excitation of the phosphor. In their study, they investigated different phosphorescent emitters varying in emission wavelength, spanning from red [$Ir(1-piq)_3$] to green [$Ir(ppy)_3$]. For all the phosphors used, Kondakova *et al.* (2010) demonstrated triplet harvesting with overall device efficiencies >10% EQE at low current densities. To our knowledge, this is the first time triplet harvesting has been reported to work in conjunction with $Ir(ppy)_3$ as a phosphorescent acceptor (Kondakova *et al.*, 2010). Three-color white devices were also fabricated based on two phosphorescent emitters $Ir(ppy)_3$ and $Ir(phq)_3$ for green and orange, respectively, and MQAB for blue. At 1000 cd m^{-2} the efficiencies are 12.6% EQE and 21.4 lm W^{-1} with CIE coordinates of (0.317, 0.317) ($\alpha_{CIE} < -0.01$).

Another report about a material capable of exciting green phosphors in a triplet-harvesting configuration was by Hung *et al.* (2010). The fluorophore CPhBzIm has its EL fluorescence maximum at approximately 430 nm (2.88 eV) and triplet level at 2.48 eV, resulting in $\Delta E_{ST} = 0.4$ eV. The T_1 of CPhBzIm should be sufficiently high to be used together with $Ir(ppy)_3$ in a triplet-harvesting concept. Instead they used a slightly different phosphor $Ir(pbi)_2(acac)$ (Hung *et al.*, 2010). They fabricated a two-color white device by blending CPhBzIm with $Ir(pbi)_2(acac)$ at a low concentration of 0.1 wt%. The efficiency reached 5.1% EQE at 1000 cd m^{-2} (7% EQE maximum value), which cannot be used as an indication of whether triplet harvesting actually occurs or not.

To summarize, triplet harvesting is a promising concept for future high-efficiency white OLEDs with high color quality. Once the right materials are found it will also allow one to simplify the device structure, because in general all materials could be blended into one uniform emission layer. One key challenge to date is that triplet harvesting itself does not limit the long-term stability of the devices but rather materials need to be developed that meet the stability and conceptual requirements at the same time.

C. Phosphorescent devices

Among the various concepts for white OLEDs, by far the most effort has been spent on research dealing with devices based solely on phosphorescence-emitting materials. This is probably due to the fact that phosphors inherently offer internal efficiencies of unity (Baldo *et al.*, 1998), so that in general the only remaining task in device engineering is the distribution of excitons to different emitters for white emission. The high internal efficiency is important for white OLEDs to be competitive with existing lighting technologies, i.e., fluorescent tubes and white LEDs (Steele, 2007). In this section, conventional phosphorescent OLEDs will be discussed first, where the discussion will be split between two- and three-color concepts. This is followed by a discussion of systems with reduced band gap that aim to reduce the operating voltage of the devices, and finally white phosphorescent concepts are introduced based on combined monomer or excimer emission.

In contrast to fluorophores, where examples of high-PLQY emitters exist (Xie, Liu, and Zhao, 2003; Schwartz *et al.*, 2006, 2007; Tong *et al.*, 2007), the vast majority of phosphorescent emitters needs to be embedded into a host material to avoid concentration quenching (Kawamura *et al.*, 2005, 2006; Kobayashi *et al.*, 2005). The key requirement for a suitable host material of a phosphorescent emitter is to have a higher triplet level than the phosphor. By that, the triplet excitons are efficiently confined to the emissive states (Goushi *et al.*, 2004), which are, due to the nature of phosphorescent molecules, long-living excited states with lifetimes in the range of microseconds (Thompson, 2007). The excitonic confinement is especially a challenge for blue emitters, as they require host materials with widest band gap.

One good example of the importance of the right choice of matrix material is given by Tokito *et al.* (2003). They use the

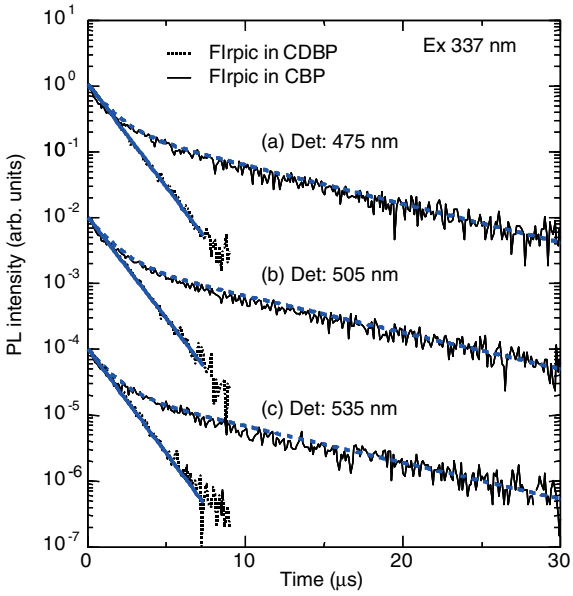

FIG. 27 (color online). Photoluminescence decay curves for two host materials (CBP and CDBP) doped with 3% FIrpic each as taken at different detection wavelengths. The lines correspond to mono-exponential and biexponential decays. From Tokito *et al.*, 2005.

archetype blue phosphorescent emitter FIrpic ($T_1 = 2.7$ eV) and compare its efficiency when embedded in either CBP ($T_1 = 2.6$ eV) or CDBP ($T_1 = 3.0$ eV). The photoluminescence (PL) transients of both CBP:FIrpic and CDBP:FIrpic (both doped with 3 wt %) are plotted in Fig. 27. While the CDBP system shows monoexponential decay with a time constant of 1.4 μs, the CBP:FIrpic PL decay shows a long-living delayed component which can be attributed to energy back transfers between host and guest, which lowers the PLQY (Kawamura *et al.*, 2005) and consequently the device efficiency. Tokito *et al.* (2003) prepared identical blue OLEDs based on FIrpic with either CBP or CDBP as host material that reach 5.1 and 10.4% EQE (at 0.1 mA cm^{-2}), respectively, showing the importance of excitonic confinement in case of phosphorescence.

CDBP with a triplet level of 3.0 eV is just one of many wide-band-gap materials suitable to host blue phosphorescent emitters. The most common host materials with high triplet energies are mCP [$T_1 = 2.91$ eV (Kawamura *et al.*, 2005)], UGH2 [$T_1 = 3.5$ eV (Giebink, Sun, and Forrest, 2006; Lai *et al.*, 2010)], CzSi [$T_1 = 3.01$ eV (Tsai *et al.*, 2006)], and TCTA [$T_1 = 2.81$ eV (Reineke, Schwartz, Walzer, and Leo, 2009)].

1. Conventional architectures: Two-color devices

White light can be mixed using two colors that are complementary in the sense that their straight connection in the CIE 1931 (cf. Fig. 7) color space crosses the desired white point on the Planckian locus. Most of the research in this field used the archetype phosphorescent blue emitter FIrpic in connection with various emitters. With its rather light-blue emission corresponding to CIE coordinates of (0.17, 0.34) (Yeh *et al.*, 2005), the FIrpic spectrum is typically mixed with the emission of a red emitter (PL maximum ~600 nm) (Lei, Wang, and Qiu, 2006; Kim, Jang, and Lee, 2007; Su *et al.*, 2008; Wang *et al.*, 2009a). Lai *et al.* (2010) reported on white two-color OLEDs, where the common red emitter is replaced by a yellow emitter with reasonably high PLQY. However, as the yellow emission has CIE coordinates of ~(0.44, 0.53), it is not possible to cross the Planckian locus when FIrpic (and most other blue phosphors) are used as a complementary blue emitter (cf. Fig. 7). Thus, to use yellow phosphorescent emitters in a two-color approach requires deep-blue emitters with CIE coordinates (<0.2, <0.2).

The highest device performance of two-color white OLEDs based on FIrpic was reported by Su *et al.* (2008). PQ2Ir is used as a complementary red emitter in their study. Their EML is designed to form a strong carrier- and exciton-confining structure. Figure 28 shows the triplet energy diagram of their device structure and the phosphorescence spectra of the important materials used (Su *et al.*, 2008). In order to confine triplet excitons of the blue emitter FIrpic ($T_1 = 2.62$ eV), they composed the device structure solely with materials having higher triplet levels (see Fig. 28). Their basic concept is based on a double EML layout (Zhou *et al.*, 2002) to pin the exciton generation zone to an interface in the center of the EML (TCTA/DCzPPy interface). This device when doped with FIrpic reaches only the highest efficiencies reported to date for FIrpic-based OLEDs: 25% EQE and 46 lm W^{-1} at 1000 cd m^{-2} (Su *et al.*, 2008). In order to achieve white light, ultrathin layers of TCTA and DCzPPy (0.25 nm each) are doped with the red emitter PQ2Ir instead of FIrpic. Both its triplet and HOMO and LUMO levels function to achieve excitonic (cf. Fig. 28) and charge carrier confinement at the TCTA:DCzPPy interface. The white device reaches 25% EQE and 44 lm W^{-1} at 1000 cd m^{-2}. The corresponding CIE coordinates are (0.335, 0.396) ($\alpha_{CIE} = +0.04$) with a CRI of 68.

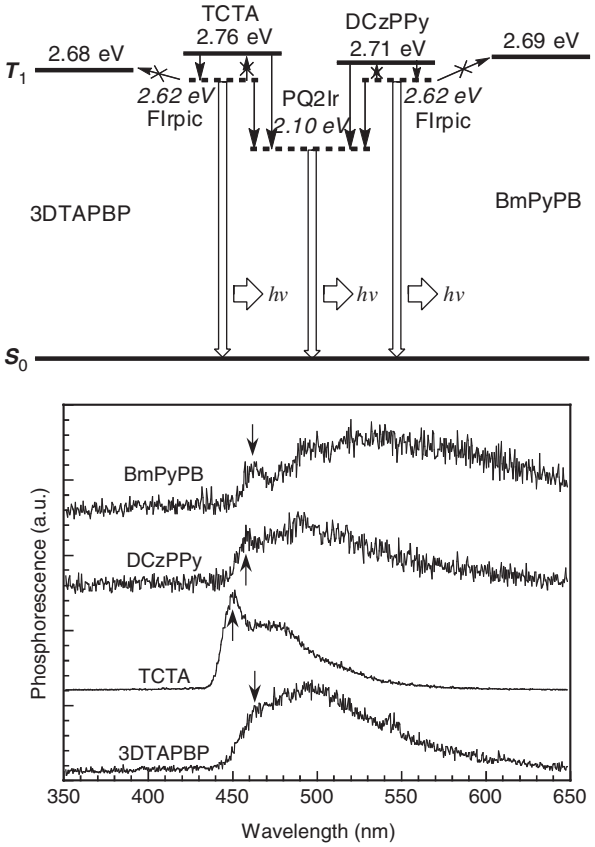

FIG. 28. Top: Triplet energy-level diagram for the EML concept. Bottom: Phosphorescence spectra of the nonemitting materials used for host and exciton blocking layers (cf. top) as measured at 4.2 K for the vacuum deposited films. Arrows indicate the estimated triplet levels. From Su *et al.*, 2008.

The lack of green emission in the spectrum of two-color white devices results in poor color quality, where the color rendering index typically is limited to values of CRI ~ 70 (Su *et al.*, 2008; Wang *et al.*, 2009a). Furthermore, the two-color approach limits the luminous efficacy because the dip in the spectrum strongly overlaps with the response curve of the human eye $V(\lambda)$, which artificially lowers the luminance efficacy of radiation K_r (cf. Sec. I.B.2).

The highest color quality of two-color phosphorescent white OLEDs was reported by Chang, Chen *et al.* (2010). They used an iridium complex Ir(dfbppy)(fbppz)$_2$ as a blue phosphorescent emitter combined with a red-emitting osmium heavy metal complex Os(bptz)$_2$(dppee). The blue emitter with PL maximum at 450 nm and strong vibronic sidebands at approximately 480 and 520 nm can alleviate the lack of green emission, resulting in a high CRI = 79. At 100 cd m^{-2}, a white device based on these emitters reached 6.8% EQE and 10.0 lm W^{-1} with color coordinates

of (0.324, 0.343), closely matching the standard illuminant E ($\alpha_{CIE} = 0$).

2. Conventional architectures: Three-color devices

In order to increase the color quality and luminous efficacy of phosphorescent OLEDs, three primary colors need to be employed. D'Andrade, Holmes, and Forrest (2004) reported on the first high-efficiency three-color devices, based on FIr6 (0.1 eV higher T_1 compared to FIrpic), $Ir(ppy)_3$, and PQIr. Based on earlier reports (Holmes *et al.*, 2003) on direct charge injection and trapping by FIr6 when dispersed into the inert wide band gap host UGH2 (band gap of 4.4 eV), the EML (9 nm in total) was designed to host all three emitters simultaneously. With a high concentration of 20 wt %, FIr6 is used to capture both electrons and holes. The other two dopants are highly diluted into the system with 0.5 and 2 wt % for $Ir(ppy)_3$ and PQIr, respectively. The doping ratio of the green and red emitters is adjusted in such a way that only parts of the FIr6 excitons are transferred to them. This excitation scheme is analyzed in time-resolved measurements, where the triple-doped film is excited with a short laser pulse and recorded in a streak camera (D'Andrade, Holmes, and Forrest, 2004), as shown in Fig. 29. Additionally shown is the FIr6 transient signal for a single-doped UGH2:FIr6 system. By introducing the green and red emitters, the lifetime of FIr6 is reduced from 1.60 to 0.75 μs, clearly indicating the energy transfer occurring from FIr6 to lower-energy triplet states of $Ir(ppy)_3$ and PQIr. Furthermore, the study shows that the $Ir(ppy)_3$ decay rate remains unchanged compared to solely $Ir(ppy)_3$-doped devices, indicating that the energy transfer from $Ir(ppy)_3$ to PQIr is weak. White devices based on the EML layout reach efficiencies of 7.5% EQE and 11 lm W^{-1} at 1000 cd m^{-2} with color coordinates of (0.41, 0.46)[13] ($\alpha_{CIE} = +0.06$) and a CRI = 78.

In contrast to the energy transfer excitation scheme of D'Andrade, Holmes, and Forrest (2004), Sun and Forrest (2008a) proposed a different EML design with multiple exciton formation zones while using exactly the same emitter molecules. A scheme of their concept is shown in Fig. 30. Here the red, green, and blue sub-EMLs are spatially separated, i.e., each sub-EML consists of a different host-guest system. The energy levels of the host materials are chosen to form a stepped energy barrier sequence for both charge carrier types. The host materials are TCTA, mCP, and UGH2 as ordered from the hole injecting side of the device (see Fig. 30). By the introduction of these moderate energy barriers, electrons and holes will accumulate at each of these interfaces where they can form excitons with the opposite carrier type. A detailed investigation of the exciton distribution within this multilayer emission layer is given by Sun and Forrest (2008b). As indicated in Fig. 30, additional energy transfer from high- to low-energy phosphors can occur at the respective sub-EML interfaces. At 1000 cd m^{-2}, a white OLED based on this concept yields efficiencies of 12.9% EQE and 20 lm W^{-1}. The color rendering index is high (CRI = 81) with color coordinates of (0.37, 0.41) ($\alpha_{CIE} = +0.04$).

[13]Estimated to 1000 cd m^{-2}.

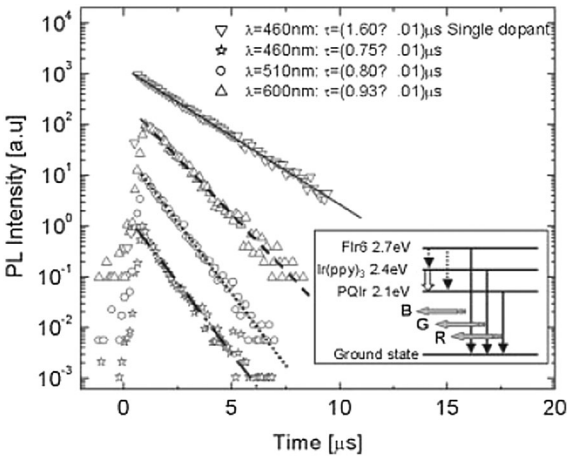

FIG. 29. Photoluminescence decay curves spectrally resolved to show the transients of the three emitters [FIr6, $Ir(ppy)_3$, and PQIr] embedded in the common host UGH2. Inverted triangles refer to a blue system, i.e., UGH2:FIr6. Lines correspond to monoexponential decays. The inset shows the proposed energy transfer scheme. From D'Andrade, Holmes, and Forrest, 2004.

Finally, Wang *et al.* (2009b) combined the two concepts from above, discussing white phosphorescent OLEDs based on one common host with spatially different emitter doping, i.e., either sequential red, green, and blue or red + green or

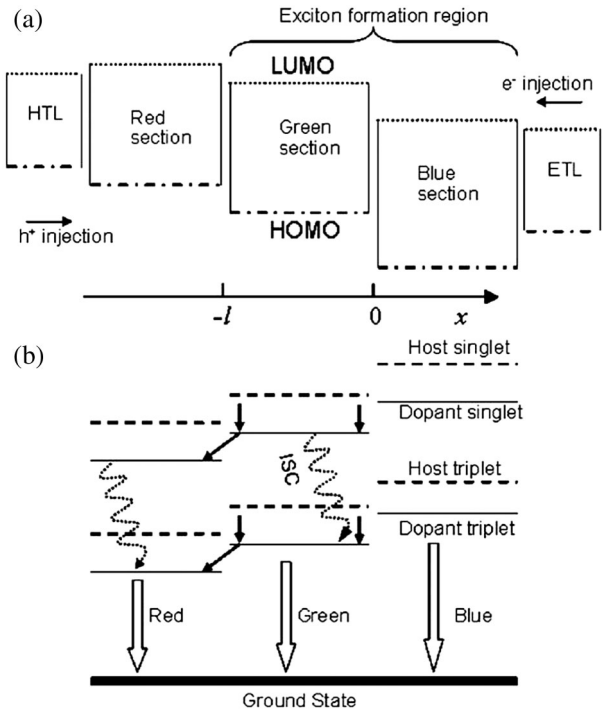

FIG. 30. (a) Energy-level diagram of the host materials incorporated in the three-section EML. Dotted lines are LUMO, and dash-dotted lines are HOMO levels. The three host materials form a stepped energy barrier sequence for both electrons and holes. (b) Proposed energy transfers within the EML. Solid arrows indicate energy transfer from host to dopant and from high- to low-energy dopants across an interface. Dotted curved arrows indicate ISC. Dashed lines are host singlet and triplet levels, and solid lines are dopant singlet and triplet levels. From Sun and Forrest, 2008b.

blue. They used the wide gap material mCP as the host material. They carefully discussed the influences of charge distribution and carrier trapping leading to different effects on device efficiency and color quality. With a blended red or green, followed by a blue-doped mCP region, device efficiencies at 1000 cd m^{-2} are reported to be 13.6% EQE with CIE coordinates of (0.39, 0.42) ($\alpha_{CIE} = +0.03$, CRI = 80). Unfortunately, no luminous efficacy is reported at illumination relevant brightness. Similar studies on a combined red + green EML were carried out by Seo *et al.* (2010); however, in this report two matrix materials (mCP and TPBi for blue and red + green) were employed.

The highest device efficiency of white OLEDs based on three phosphorescent emitters was recently reported by Sasabe *et al.* (2010). Their report is based on their earlier study of high-efficiency two-color devices (Su *et al.*, 2008), emphasizing the need for deeper-blue phosphorescent emitters to incorporate an additional green phosphor. A new iridium carbene complex Ir(dbfmi)$_3$ was introduced having a PL maximum at 445 nm (2.79 eV). This emitter was used together with a new host material PO9, having a triplet level of 2.95 eV. At an emitter concentration of 10 wt %, this PO9: Ir(dbfmi)$_3$ system has a very high PLQY of 70%. The device concept is similar to the two-color approach, basically using a blue phosphorescent OLED with additional ultrathin layers for red and green. Here the total EML is CBP: $PQ_2Ir(dim)$ (1 nm, 2 wt %)/CBP: Ir(ppy)$_3$ (1 nm, 6 wt %)/ PO9:Ir(dbfmi)$_3$ (10 nm, 10 wt %). The only difference of the two-color device layout is the position of the lower energy phosphors that has been moved from the center to the side of the EML [cf. Su *et al.* (2008)]. The device based on this EML sequence reached very high efficiencies of 21.5% EQE and 43.3 lm W^{-1} at 1000 cd m^{-2}. Compared to the two-color OLEDs, the color quality is improved to a CRI = 80.2 with CIE coordinates of (0.43, 0.43) ($\alpha_{CIE} = +0.03$).

The highest color rendering index to date for a three-emitter system was reported by Chang, Tien *et al.* (2010). Their devices, optimized for emission close to standard illuminant *E*, have a very high CRI = 94 at 1000 cd m^{-2} with color coordinates of (0.322, 0.349) ($\alpha_{CIE} = +0.01$, 8% EQE at 100 cd m^{-2}).

3. Resonant triplet-level blue host-guest systems

The results from the preceding sections have shown that it is generally possible to incorporate blue phosphorescent emitters in OLEDs to achieve efficient white light. However, in order to achieve excitonic confinement necessary for high PLQY, host materials with extremely wide band gap have to be employed. The use of high-band-gap materials like UGH2, mCP, or CzSi in turn increase the operating voltages of OLEDs, ultimately leading to reduced luminous efficacies. One way to circumvent this problem is to directly inject charges into the blue emitter, which then functions as charge carrying and emissive material (D'Andrade, Holmes, and Forrest, 2004). The additional transport functionality, however, may likely further decrease the operational stability of the blue phosphor, which already is the bottleneck for realizing long-term stable phosphorescent white OLEDs.

Another route is to reduce the transport band gap by choosing a host material in such a way that the triplet levels of host and blue emitter are in resonance (Reineke, Lindner *et al.*, 2009). This, however, introduces the general problem that a host-guest system with resonant triplet energies has a smaller PLQY in the mixed film. This effect is even more pronounced when the triplet level of the emitter is higher compared to the matrix material (Kawamura *et al.*, 2005). In a resonant system, the excitons are free to move, so that the capture efficiency of excitons on the phosphor is reduced. A common signature of a resonant or endothermic ($T_{1,host} \leq T_{1,emitter}$) is a delayed component in the transient signal. For instance, for a CBP:FIrpic system ($T_{1,host} = 2.56$ eV $< T_{1,emitter} = 2.6$ eV), the PL decay shows a noticeable delayed component as plotted in Fig. 27, which is attributed to back energy transfer between host and guest molecules (Adachi, Kwong *et al.*, 2001).

Incorporating a resonant triplet energy blue system into a white EML is more complicated, because (i) the excitons are likely to escape the EML, where they might be transferred to quenching sites, and (ii) it must be taken into consideration that the resonant system is inherently less efficient compared to an exothermic system ($T_{1,host} > T_{1,emitter}$) [compare, for instance, the PLQY of FIrpic dispersed in either CBP or mCP ($T_1 = 2.91$ eV) at 4.1 mol%: 55 and 98% (Kawamura *et al.*, 2005)]. Thus, in order to achieve intense blue emission, the blue resonant EML must be made thicker to counteract the small PLQY of the film. D'Andrade, Thompson, and Forrest (2002) used this CBP:FIrpic system in a three-color phosphorescent white device. Their CBP:FIrpic 6 wt % layer had a thickness of 20 nm. Furthermore, it was located at the exciton generation zone adjacent to a NPB electron-blocking layer. NPB has a triplet level of 2.29 eV (Goushi *et al.*, 2004), much lower than the emissive state of FIrpic, clearly functioning as an effective quenching channel for excitons freely moving in the CBP:FIrpic film. Thus, a white OLED based on this system reached a low device efficiency of 5.2% EQE (maximum value) (D'Andrade, Thompson, and Forrest, 2002).

Cheng, Zhang, Zhao, Lin *et al.* (2006) also used CBP: FIrpic in a three-color device; however, they situated the blue sub-EML in the center of the EML [spatially separated from the site of exciton generation (D'Andrade, Thompson, and Forrest, 2002)], sandwiched between doped CBP layers hosting either a green [Ir(ppy)$_3$] or a red [Ir(ppq)$_2$(acac)] phosphor (5 nm each). In order to achieve sufficient blue emission, the central layer had to have a thickness of 30 nm, where the less efficient endothermic CBP:FIrpic loses a great amount of excitons (Cheng, Zhang, Zhao, Lin *et al.*, 2006). Unfortunately, they do not state EQE values, making it hard to evaluate their data.

Reineke, Lindner *et al.* (2009) improved this device concept by readdressing the emission layer design. The energy level diagram of their EML architecture is depicted in Fig. 31. In contrast to the device reported by Cheng, Zhang, Zhao, Lin *et al.* (2006) based on the common host CBP, the EML is based on the double EML concept, incorporating a hole- and an electron-transporting host material to locate the exciton generation to the center of the EML (Zhou *et al.*, 2002; Reineke, Lindner *et al.*, 2009). Instead of using CBP, TPBi is used as the electron-transporting host material having a triplet energy of 2.6 eV, exactly matching the FIrpic T_1 state.

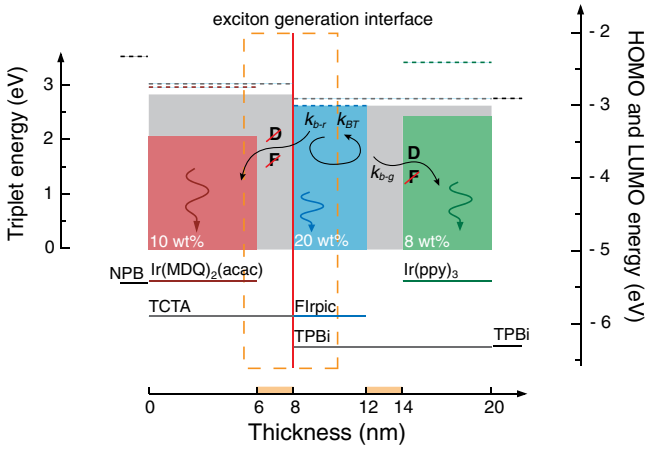

FIG. 31 (color online). Energy-level diagram of the phosphorescent white emission layer concept. Dashed lines are LUMO and solid lines HOMO levels. The filled boxes indicate the respective triplet levels of host (gray) and emitter (colored) materials. The dashed box indicates the exciton formation zone. D and F denote Dexter and Förster energy transfers, respectively. Furthermore, the rates refer to blue-to-red transfer $k_{b\text{-}r}$, backtransfer k_{BT}, and blue-to-green transfer $k_{b\text{-}g}$. From Reineke, Lindner *et al.*, 2009.

TPBi is well known to form an efficient double EML system together with the hole-transporting matrix TCTA (T_1 = 2.83 eV) (Q. Huang *et al.*, 2006; Meerheim, Nitsche, and Leo, 2008). Placing the blue sub-EML at the position of exciton generation (cf. Fig. 31), the total layer thickness can be reduced because the exciton density is accordingly higher. Thus, the TPBi:FIrpic layer is only 4 nm thick. Furthermore, the concentration of FIrpic is increased to 20 wt %, because in a resonant system, the highest PLQY is obtained at higher concentrations[14] (Kawamura *et al.*, 2005) as a result of a higher probability that an exciton can find a site for recombination. For instance, the PLQY of TPBi:FIrpic is increased from 13% to 32% as the concentration is increased from 1.7 to 10 wt % (Reineke, Lindner *et al.*, 2009). For comparison, the exothermic system TCTA:FIrpic at a concentration of 1.7 wt % yields a PLQY = 81%.

The red emitter Ir(MDQ)$_2$(acac) is doped into the TCTA matrix, the green Ir(ppy)$_3$ is embedded also into the TPBi host, but spatially separated from the exciton generation interface (see Fig. 31). In order to suppress complete energy transfer $k_{b\text{-}r}$ from FIrpic to Ir(MDQ)$_2$(acac), a thin intrinsic interlayer of TCTA (2 nm) is inserted acting as a triplet energy barrier and spacer (Kawamura *et al.*, 2006) to suppress Dexter- and Förster-type energy transfers (cf. Sec. I.A.5), respectively. To reduce Förster-type energy transfer $k_{b\text{-}g}$ from FIrpic to Ir(ppy)$_3$, which would artificially reduce the blue intensity, a 2 nm thin intrinsic TPBi interlayer—large enough to exceed the Förster radius of FIrpic (Kawamura *et al.*, 2006)—is inserted between blue and green sub-EML.

Time- and spectrally resolved measurements performed by Reineke, Lindner *et al.* (2009) on a resonant triplet energy system provide experimental evidence for the energy backtransfer k_{BT}. The results are plotted in Fig. 32. Color filters are used to alter the emission of a white OLED based on the above concept from a solely red emission stepwise to the full spectrum [spectra 1 to 5 in Fig. 32(a)]. The time decay of the transmitted spectrum following an EL excitation pulse is recorded as shown in Fig. 32(b). Additionally, response curves of monochromatic devices are plotted for comparison. A monoexponential decay is observed, when only the red part of the spectrum is transmitted, nicely agreeing with the time constant of the reference device (time constant of 1.4 μs). With increasing transmission, a second delayed component with a time constant of 3.0 μs is observed, much longer than any of the reference decay signals. This delayed signal can be attributed to the energy backtransfer k_{BT}, as it is linked to the blue emission of FIrpic.

The motivation for the use of reduced-band-gap materials is to reduce the operation voltage of the device. With the EML structure of Reineke, Lindner *et al.* (2009), very low voltages of 3.22 and 3.95 V are obtained for 1000 and 10 000 cd m^{-2}, respectively, operating close to the thermodynamic limit (He, Pfeiffer *et al.*, 2004; Su *et al.*, 2010). The corresponding device efficiencies are 13.1% EQE and 30 lm W^{-1} at 1000 cd m^{-2} with CIE color coordinates of (0.45, 0.47) (α_{CIE} = +0.06, CRI = 80).

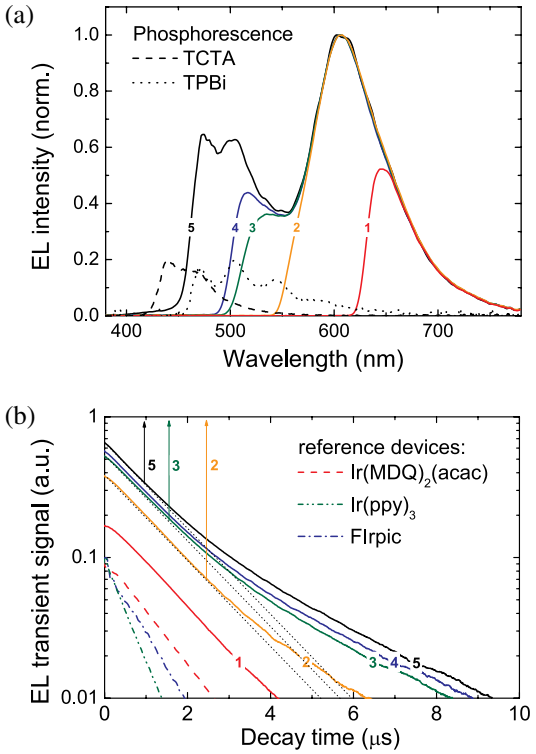

FIG. 32 (color online). (a) EL spectra of device B as obtained through different color filters (numbered from 1: solely red emission to 5: complete emission spectrum). Dashed and dotted lines are phosphorescence spectra of the hosts TCTA and TPBi, respectively, as measured at 77 K. (b) EL decay curves measured for the respective spectra of (a). Arrows indicate the time when a slower component sets in. Additionally, the decay curves of reference monochrome devices are shown (dashed, dotted, dash-dotted) for red, green, and blue. From Reineke, Lindner *et al.*, 2009.

[14]Upon a further increase of emitter concentration, the PLQY decreases again as dominated by concentration quenching (Kawamura *et al.*, 2006).

Even if this structure reaches very high efficiencies, the color quality is limited due to the use of the light-blue emitter FIrpic. Here it is not possible to reach emission with CIE coordinates close to the Planckian locus, i.e., $\alpha_{CIE} \equiv 0$, with a well-balanced contribution from all three emitters (cf. Sec. I.B.2). In order to improve the color quality, Weichsel *et al.* (2012) replaced the blue sub-EML TPBi: FIrpic by an electron-transporting mixed system SPPO1: FIr6, where the triplet energy of SPPO1 ($T_1 = 2.8$ eV) is slightly higher compared to FIr6 ($T_1 = 2.7$ eV), still coming close to being a resonant system. Furthermore, a fourth phosphor emitting in the yellow region, i.e., $Ir(dhfpy)_2(acac)$, is incorporated in the EML structure, being codoped with $Ir(ppy)_3$ into the SPPO1 host (Weichsel *et al.*, 2012). An optimized device based on these changes reaches 10.0% EQE and 17.4 lm W^{-1} at 1000 cd m^{-2}. More importantly, the CIE color coordinates changed to (0.444, 0.409) with a CRI = 81.9, representing a Planckian radiator ($\alpha_{CIE} = 0$) emitting at standard illuminant *A*.

4. Single-dopant combined monomer-excimer emission

From the device engineering point of view, it is always desirable to simplify the OLED structure. However, especially for white OLEDs, the number of layers needed solely for the emission layer can be as high as five (Reineke, Lindner *et al.*, 2009). This is mainly a result of the need to address all differently emitting molecules within the EML.

D'Andrade *et al.* (2002) observed efficient electrophosphorescent excimer emission from a organometallic platinum (Pt) complex FPt1. Here, Pt-Pt coupling (Connick *et al.*, 1996; Zheng and Rillema, 1998) forms emissive excimer states at longer wavelengths compared to the monomer emission of the corresponding isolated molecule. Together with the blue emitter FIrpic, white emission could be realized based on FIrpic and FPt1-excimer phosphorescent emission. Because the FPt1 excimer is also a triplet emitting state, 100% internal quantum efficiency in OLEDs is possible based on this approach. D'Andrade *et al.* (2002) even suggested a white OLED based solely on combined monomer-excimer emission of the similar platinum complex FPt2. However, the EL spectrum also comprised a strong peak attributed to a NPB hole-transport layer, which strongly limits the device efficiency.

Adamovich *et al.* (2002) picked up the general concept of combined monomer-excimer electrophosphorescence investigating further variants of the platinum FPt1 complex. Photoluminescence of three different emitters having small ligand variations (denoted as **1**, **2**, and **4**) are shown in Fig. 33. The relative intensities of the high-energy monomer and the long-wavelength excimer bands are continuously altered as a function of doping concentration, which determines the fraction of excimers formed. Thus, this approach offers a simple route to realize broadband white emission from one single molecule by adjusting its doping concentration within an appropriate host material, strongly simplifying the device structure. For a device based on FPt1 doped in mCP host material, 4.3% EQE could be obtained at 500 cd m^{-2}. A more detailed investigation of the exciton formation and trapping in such a device is given by D'Andrade and Forrest (2003), discussing a mCP:FPt2 system.

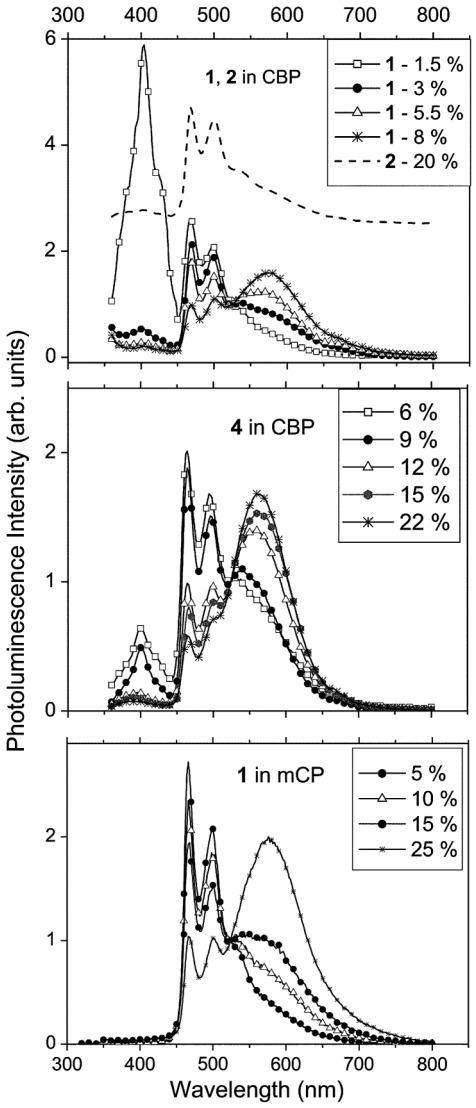

FIG. 33. Photoluminescence spectra of platinum complexes as doped in either CBP (top and middle) or mCP (bottom) host materials under a variation of the emitter concentration. The blue emission at approximately 400 nm is the CBP host fluorescence. **1**, **2**, and **4** refer to different molecular structures of the platinum complexes. From Adamovich *et al.*, 2002.

By further optimizing the host (using 26mCPy, a mCP derivative) and adjacent blocking materials, Williams *et al.* (2007) further improved the device efficiency based on the emitter FPt1. At 500 cd m^{-2}, an EQE of 15.9% was reached for an EML doped with approximately 12 wt % of FPt1. This corresponds to 12.6 lm W^{-1} with CIE coordinates of (0.46, 0.47) ($\alpha_{CIE} = +0.07$) and a CRI = 69.

The effect of the heavy metal atom coupling (Connick *et al.*, 1996; Zheng and Rillema, 1998), which has to date only been effectively observed for platinum-cored emitters, leading to the formation of excimer states, was shown by Ma *et al.* (2006). In their study, they investigated binuclear platinum complexes as shown in Fig. 34 designed to have different Pt-Pt spacing, by that altering the strength of their coupling. For compound **1** with a Pt-Pt distance of 3.376 Å, solely the monomeric emission in the blue spectral region is observed, while compound **3** with a spacing of 2.834 Å shows

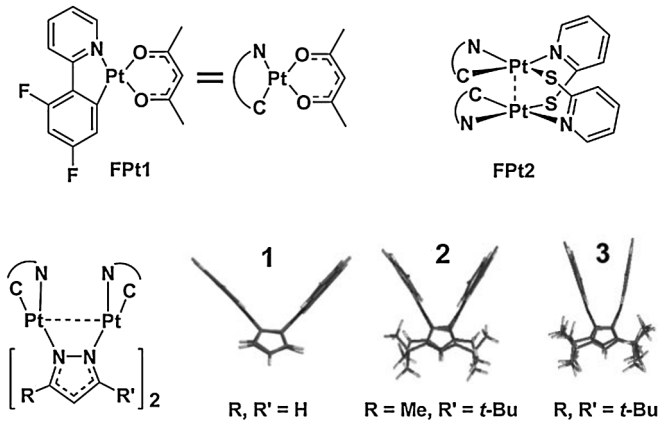

FIG. 34. Molecular structures of the binuclear platinum complexes (**1**, **2**, and **3**) of Ma *et al.* (2006). Additionally, the reference structures are shown at the top (Koshiyama, Omura, and Kato, 2004). The Pt-Pt distances for **1**, **2**, and **3** are 3.376, 3.064, and 2.834 Å, respectively, corresponding to PL maxima at 466, 546, and 630 nm. From Ma *et al.*, 2006.

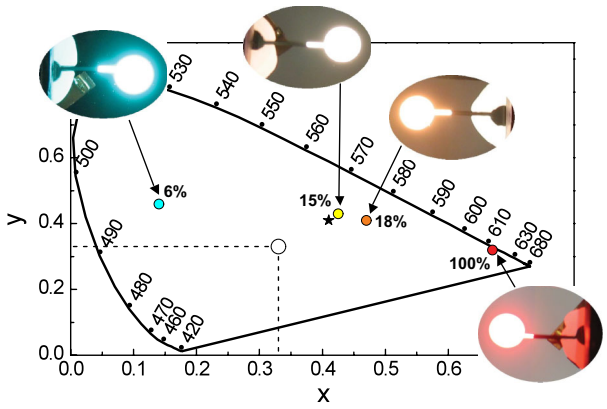

FIG. 35 (color online). CIE 1931 chromaticity diagram showing the electroluminescence color coordinates of devices differing in the PtL^2Cl emitter concentration. Open white circle indicates the standard illuminant *E*, and the star refers to color coordinates of a specific incandescent lamp; they used for comparison [(0.41, 0.41)]. From Cocchi *et al.*, 2007.

solely red excimer emission. The EQE of the devices ranges between approximately 4% and 6% for blue, green, and red emissions from compounds **1**, **2**, and **3**, respectively (Ma *et al.*, 2006). For pure films of compound **1**, red emission is also observed, which is attributed to emission originating from distorted complexes with compressed Pt-Pt distances (Ma *et al.*, 2006).

Based on these binuclear platinum complexes, it is possible to realize white emission by combining two or more emitters with different Pt-Pt spacing, whereas the emission of the respective phosphor does not sensitively depend on the dopant concentration (Ma *et al.*, 2006), as seen from the previous reports by Adamovich *et al.* (2002) and D'Andrade *et al.* (2002). The other alternative is a combination of compound **1** in dilute form (doped in mCP) and pure film, arranged in a dual layer architecture (Ma *et al.*, 2006). Both approaches were exemplarily shown by Ma *et al.* (2006), reaching maximum EQE values of 7.7% and 4.2% for either mCP : **1**/mCP : **3** or mCP : **1**/neat **1** EML layouts.

Cocchi *et al.* (2007) introduced an improved N^C^N-coordinated platinum (II) complex for this monomer-excimer approach. OLEDs based in this PtL^2Cl emitter with different concentrations, doped in a mixed host system CBP:OXA, nicely sweep the CIE color space from light blue (low concentration) to red (high concentration), as shown in Fig. 35. At a PtL^2Cl concentration of 15%, CIE coordinates of (0.43, 0.43) ($\alpha_{CIE} = +0.03$) are obtained. The corresponding efficiencies are 13.5% EQE and 12.6 cd A^{-1} at 1000 cd m^{-2} (Cocchi *et al.*, 2007). Based on the same emitter PtL^2Cl, Kalinowski *et al.* (2007) improved the color quality of white OLEDs by combining the monomer-excimer emission with an additional exciplex emission that occurs between the hole-transporting material m-MTDATAs HOMO and PtL^2Cls LUMO, filling the spectral gap in the green region. However, with 6.5% at 500 cd m^{-2}, the EQE is much lower compared to the devices presented by Cocchi *et al.* (2007).

Further studies by Cocchi *et al.* (2009) discussed the influence of the ligand structure of the emitters with the general structure PtL^xCl on their photophysical properties. The corresponding chemical structures of emitter series is shown in Fig. 36 (also showing both the monomeric and excimeric PL). While the PLQY of the monomer emission from compounds PtL^{21}Cl to PtL^{23}Cl are comparable in the range of 70%–90%, the PLQY of the pure film drastically increases from 5% (PtL^{21}Cl) to 65% (PtL^{23}Cl). OLEDs based on the PtL^{23}Cl with high PLQY in the neat film reach very high external quantum efficiencies in the range of 15%–18% at 500 cd m^{-2}, slightly depending on the emitter concentration (Cocchi *et al.*, 2009). For instance at a concentration of 20% PtL^{23}Cl doped in the host TCTA, the OLEDs achieve 14.9% EQE and 8.3 lm W^{-1} at 500 cd m^{-2} with CIE coordinates of (0.45, 0.38) ($\alpha_{CIE} = -0.02$).

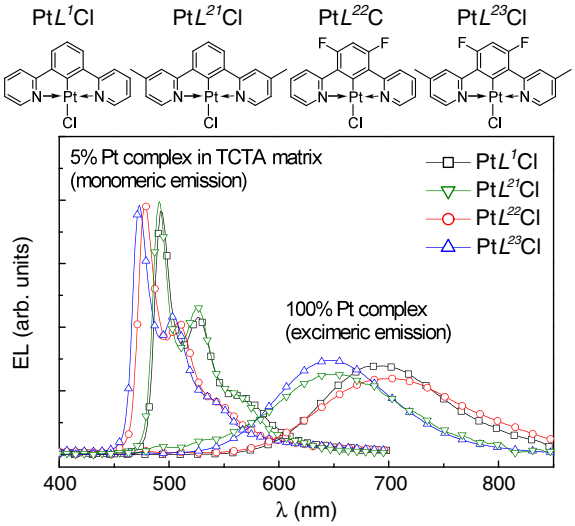

FIG. 36 (color online). Top: Molecular structures of different emitters. Corresponding EL spectra of all emitters obtained for a 5 wt % host-guest system (TCTA host) and a pure film EML formed by the platinum complexes. Each spectrum is normalized to the integrated intensity. From Cocchi *et al.*, 2009.

TABLE II. Summary of selected, high performance devices based on different device concepts as discussed in Sec. III. Device efficiencies are maximum values; additional values at higher brightness or specific current density are given in parentheses.

Concept	η_{EQE} (%)	η_{CE} (cd A^{-1})	η_{LE} (lm W^{-1})	CIE (x, y); α_{CIE}	Reference
Fluorescent					
Fluorescent emitters	(4.7)[a]	(10.9)[a]	11.2 (6.0)[a]	(0.329, 0.353); +0.02	Tsai and Jou (2006)
	5.6 (5.2)[a]	14.0	9.2 (4.8)[a]	(0.332, 0.336); 0	Yang *et al.* (2011)
Fluorescent emitters (with exciplexes)	···	···	9.0	(0.31, 0.36); +0.02	Tong *et al.* (2007)
Hybrid fluorescent or phosphorescent					
Conventional	(8.0)[b]	···	(13.7)[b]	(0.47, 0.42); +0.02	Schwartz *et al.* (2006)
	11.0 (10.8)[c]	···	22.1 (14)[c]	(0.41, 0.40); +0.02	Sun *et al.* (2006)
Phosphor-sensitized fluorescence	8.5	···	18.1	(0.38, 0.42); +0.03	Kanno, Holmes *et al.* (2006)
Triplet harvesting	(26)[b,d]	···	(33)[b]	(0.506, 0.422); < + 0.01	Rosenow *et al.* (2010)
Phosphorescent					
Conventional: two color	(25)[b]	···	(44)[b]	(0.335, 0.396); +0.04	Su *et al.* (2008)
Conventional: three color	21.6 (21.5)[b]	49.9 (49.6)[b]	59.9 (43.3)[b]	(0.43, 0.43); +0.03	Sasabe *et al.* (2010)
Resonant triplet-level blue	(13.1)[b]	···	(30)[b]	(0.45, 0.47); +0.06	Reineke, Lindner *et al.* (2009)
Combined monomer or excimer	(16.6)[c]	···	(9.6)[c]	(0.42, 0.38); −0.02	Cocchi *et al.* (2010)

[a]At 10 mA cm^{-2}.
[b]At 1000 cd m^{-2}.
[c]At 500 cd m^{-2}.
[d]Two-unit stacked device, 200% internal quantum efficiency limit (Rosenow *et al.*, 2010).

Cocchi *et al.* (2010) discussed in detail the mixing of molecular excitonic and excimeric phosphorescence to alter efficiency and color of the devices based on PtL^xCl complexes. In this report, they also introduced another similar Pt complex, PtL^{21}Cl, which can be used in devices reaching 16.6% EQE and 9.6 lm W^{-1} at 500 cd m^{-2}. The corresponding CIE coordinates are (0.42, 0.38) ($\alpha_{CIE} = -0.02$). Furthermore, a comprehensive study on the high brightness nonlinearities, i.e., exciton quenching leading to the efficiency roll-off (cf. Sec. I.A.7), is given by Kalinowski *et al.* (2010).

The highest color rendering index based on the monomer-excimer approach was reported by Zhou *et al.* (2009) for a Pt-Ge emitter doped into CBP host material. At a high emitter concentration of 10 wt % of Pt-Ge, CIE coordinates of (0.354, 0.360) are obtained with a very high CRI = 97. Note that this device qualifies as a Planckian radiator ($\alpha_{CIE} = 0$). The corresponding peak EQE value is 4.13% (Zhou *et al.*, 2009).

D. Summary

Table II summarizes the key figures of high-quality devices based on the various concepts discussed in this section. The external quantum efficiencies of the concepts listed from top to bottom noticeably increase from fluorescence to fully phosphorescence-based white OLEDs with hybrid concepts ranking at an intermediate efficiency level. Table II shows that both fluorescent and phosphorescent OLEDs have been demonstrated to reach their expected EQE levels of 5% and 20% (cf. Sec. I.A.3), respectively.

In order to be competitive with existing light sources (Steele, 2007), OLEDs need to be designed to allow the highest possible internal quantum efficiency. Thus clearly, it is unlikely that fluorescent devices, with approximately 75% recombination losses (Segal *et al.*, 2003) within the device, will be able to compete with phosphorescence-based designs.

The above discussion showed that the highest possible device efficiencies need sophisticated, sometimes highly complex device layouts (cf. Secs. III.B.1, III.B.2, III.C.1, III.C.2, and III.C.3,). These designs are not desirable for upscaling the device production to reasonable OLED panel sizes. Thus, devices offering high-efficiency and large-area controllable device architectures are the concepts of choice.

Even though the first reports on triplet harvesting (cf. Sec. III.B.3) employed rather complex emission layer designs (Schwartz *et al.*, 2007, 2009), the layer complexity has recently been greatly reduced. Rosenow *et al.* (2010) introduced a triplet-harvesting EML consisting of two simple 5 nm thick sublayers, offering great reproducibility.

Another attractive concept promising high efficiency is the combined monomer-excimer phosphorescence (cf. Sec. III.C.4). Especially the possibility to design a white OLED based on a single emitter that is dispersed into a matrix material at a certain concentration offers unmet simplicity. The reports have shown (cf. Table II) that this approach can reach similar high EQE values than conventional phosphorescent devices. To date, their corresponding luminous efficacies are smaller than the corresponding values of other concepts. This is mainly due to the superior electrical performance of the respective devices (Su *et al.*, 2008; Reineke, Lindner *et al.*, 2009; Sasabe *et al.*, 2010).

IV. CONCEPTS FOR IMPROVED LIGHT OUTCOUPLING

Many of the reports from the previous sections show results that come rather close to 100% internal quantum efficiency. Still the external quantum efficiency of conventional OLEDs is limited to 20%–25% (Adachi, Baldo, Thompson, and Forrest, 2001; Su *et al.*, 2008; Sasabe *et al.*, 2010), which is due to the thin-film layered structure of the OLED, introducing trapped light modes.

Figure 37 shows a scheme of an OLED's cross section, illustrating the different light modes (Lu and Sturm, 2002). Organic materials used for the functional layers in the device typically have refractive indices of $n_{org} \sim 1.7$–1.8 (Greiner, 2007). Conventionally, standard glass is used as a transparent substrate with a refractive index of $n_{sub} = 1.51$, forming an optical interface between organics and substrate. Because of

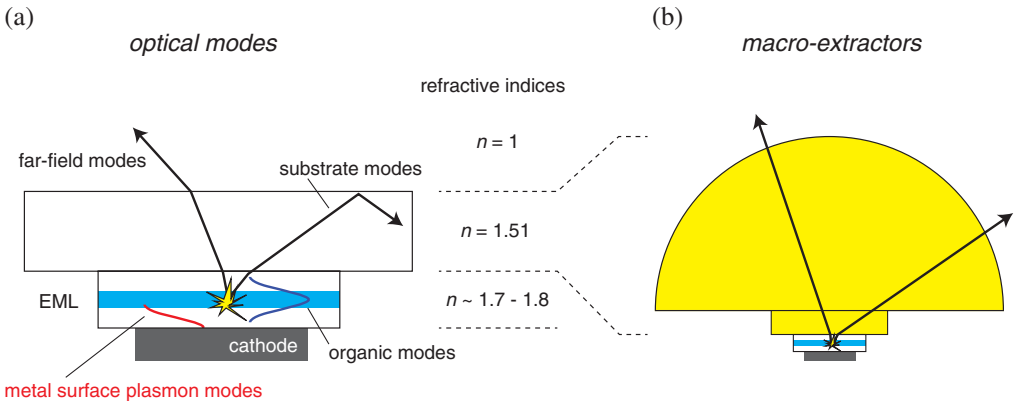

FIG. 37 (color online). (a) Different light modes in a conventional bottom-emitting OLED. Typical refractive indices of the different OLED sections are given. In this configuration, only the far-field modes reach the observer. Substrate and organic modes are trapped in the device, where they dissipate. In addition, the emitting dipoles can couple to surface plasmon modes of the metal cathode, which decrease exponentially with distance. (b) Application of a macroextractor matching the refractive index of the substrate used. Here all modes that are coupled to the substrate can be extracted to air.

the difference in refractive indices, total internal reflection (TIR) occurs at that interface, leading to a noticeable portion of light being waveguided in the organic layers. Here the critical angle θ_c of TIR is in the range of $57°-63°$, depending on the actual n_{org}. Ultimately these modes dissipate in the system. Similarly the difference in refractive indices between glass substrate and air introduces losses due to TIR ($\theta_c = 41.5°$), as so-called substrate modes are formed.

In addition to organic and substrate modes, the coupling of the radiating dipoles to the plasmon states of the metal cathode is another severe loss channel in OLEDs. The fields of the metal surface plasmon modes decay exponentially with distance (cf. Fig. 37). Thus, the efficiency of the emission is strongly decreased, if the EML is placed in the proximity of a metal layer.

Based on a comprehensive optical model (Neyts, 1998; Furno *et al.*, 2010, 2012), Meerheim *et al.* (2010) analyzed the different loss channels in a model OLED comprising a red phosphorescent emitter. In their study, they varied the thickness of the ETL to map the first and second field antinodes. The quantification of the loss channels as a function of ETL thickness is shown in Fig. 38. First, this plot shows that the outcoupled fraction can be as high as ~20%, when the interference condition for the emitter is met, which agrees with the expected EQE limit (Greenham, Friend, and Bradley, 1994; Forrest, Bradley, and Thompson, 2003). Note that this calculation is taking the imperfection of the OLED and emitter used into account, as it considers electrical, nonradiative, and absorptive losses (cf. Fig. 38). The substrate modes follow almost the same modulation as the far-field modes showing distinct peaks. In contrast, the losses to surface plasmon modes decrease notably with increasing ETL thickness, reaching a negligible level for thicknesses >200 nm, which is due to a weaker coupling between emitting dipoles and the surface plasmon mode. Similar studies were reported by Nowy *et al.* (2008) and Krummacher *et al.* (2009). On the contrary, as the ETL layer thickness increases, the fraction of the light being waveguided in organic modes increases substantially. Thus, the device does not gain outcoupled photons by avoiding losses to surface plasmons, as waveguides become dominant when placing dipoles far away from the cathode.

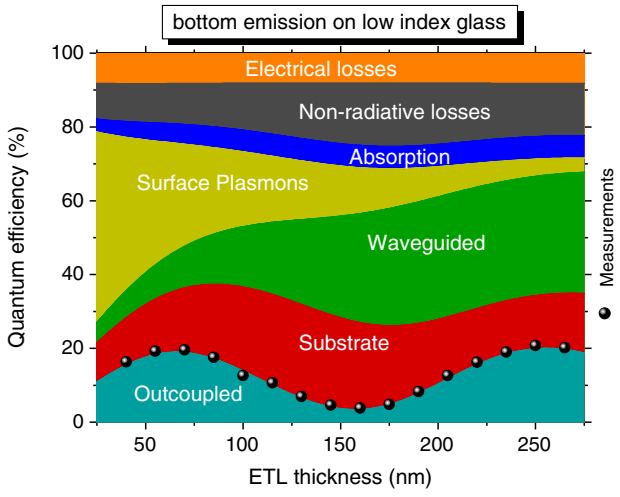

FIG. 38 (color online). Distribution of light modes and loss channels of a red phosphorescent OLED as a function of electron-transport layer (ETL) thickness that spaces the EML from the metal cathode. Dots are measurement points. Calculation is based on a comprehensive optical OLED model established by Furno *et al.* (2010, 2012). From Meerheim *et al.*, 2010.

In the following, we address concepts that aim to improve the outcoupled fraction of photons in OLEDs. Since only every fifth photon leaves the device in a standard architecture, much efficiency can be gained by providing efficient ways to enhance the light outcoupling. Here it is important to focus on methods that offer enhancement over the complete visible spectrum to be suitable for white OLEDs. In contrast, selective and directional concepts, e.g., the introduction of microcavities (Meerheim, Nitsche, and Leo, 2008), detrimental for obtaining high-efficiency, white OLEDs.

A. Improving outcoupling for bottom-emitting white OLEDs

The vast amount of research dealing with improved light outcoupling focuses on bottom-emitting OLEDs. This is

mainly due to the fact that the OLED itself is placed on a robust, thick substrate which can be easily manipulated. Furthermore, the preparation of the organic layers is the last processing step so that posttreatment, potentially damaging the device, is not necessary.

1. Macroextractors

Figure 38 shows that a substantial amount of light is trapped in substrate modes that simply cannot escape to air because of total internal reflection at the substrate/air interface. This light can easily be accessed by applying a macroextractor to the substrate surface, matching the refractive index of the latter. The ideal structure is a half sphere (Greiner, 2007; Mladenovski *et al.*, 2009; Reineke, Lindner *et al.*, 2009; Rosenow *et al.*, 2010) with dimensions much greater than the active area of the OLED so that the source of light can be treated as a point source. As shown in Fig. 37, this configuration assures that all the light entering the substrate from the organic layers is able to escape to air, as it is hitting the half-sphere surface under normal angle of incidence.

Other designs of macroextractors are truncated square-pyramid (D'Andrade and Brown, 2006) or "flowerpot"-shaped (Greiner, 2007) luminaires. It is worth noting that their use is meaningful only to quantify the amount of substrate-trapped light. For real applications involving large-area OLEDs, thin and scalable concepts need to be applied to enhance the light outcoupling. Thus, efficiency values stated using macroextractor elements should be handled with care and be seen only as the upper limit for concepts that enhance the outcoupling of substrate modes, fully unlocking the potential of a given OLED stack.

2. Structured substrate surfaces

The easiest way to improve the total light output of bottom-emitting OLEDs is to incorporate structured substrate surfaces. The surface structure can be either arbitrary, e.g., as achieved by sandblasting, or periodic. Typical examples for ordered structures are pyramidal or lens arrays (Madigan, Lu, and Sturm, 2000; Möller and Forrest, 2002; Nakamura *et al.*, 2005; Greiner, 2007). In contrast to the planar substrate, the use of a structured surface reduces the losses due to TIR, because the condition for TIR will be altered locally as the normal to the surface repeatingly changes. An example of a microlens array made from PDMS is shown in Fig. 39 (Möller and Forrest, 2002). It comprises lenslike features with a base dimension of approximately 10 μm in a square lattice.

Madigan, Lu, and Sturm (2000) showed that the integrated emission of an OLED can be improved by factors ranging from 1.6 to 3.0, depending on the substrate and lens materials as well as the dimensions of the lens array. In their study, the lenses used still had macroscopic dimensions with sphere radii of ~3 mm. Möller and Forrest (2002) reported on an 1.5-fold improvement achieved using the microlens array shown in Fig. 39 with much smaller lens dimensions. The light propagation within the substrate and the outcoupling structures is incoherent, thus conventional ray-tracing methods can be applied to optimize such structures for maximum light output for a respective OLED structure as shown by Greiner (2007).

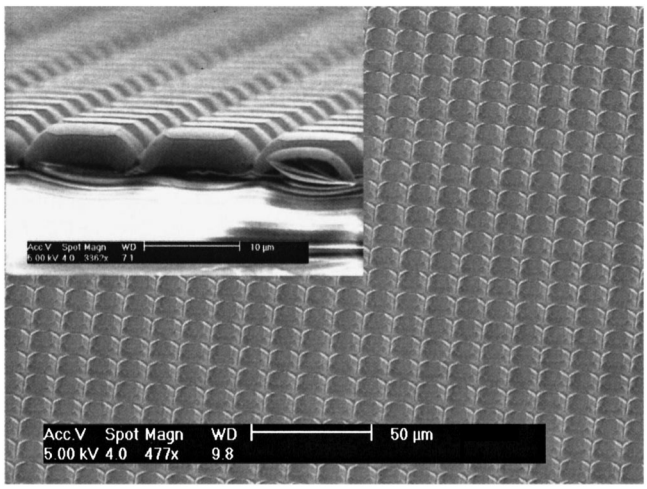

FIG. 39. Scanning electron micrograph of a PDMS microlens array using an etched SiN_x mold. Inset: Side view. The base lengths of the lenses are approximately 10 μm. From Möller and Forrest, 2002.

It is worth noting at this point that structured substrate surfaces are often combined with other concepts applied internally that aim to reduce waveguiding within the organic layers (Sun and Forrest, 2008a; Reineke, Lindner *et al.*, 2009; Koh *et al.*, 2010; Rosenow *et al.*, 2010). Such concepts will be discussed subsequently.

3. Low-refractive-index layers

Equally as important as extracting substrate modes, but at the same time much harder to achieve, is the outcoupling of light that is trapped in the organic layers (waveguide modes). This light, traveling in the plane of the OLED, is absorbed and dissipated in the end, introducing heat to the system.

Sun and Forrest (2008a) introduced a novel concept to convert a waveguide into extractable modes by inserting a square grid of low-refractive-index material [low-index grid (LIG)] between the transparent anode ITO and the organic layers by means of photolithography. A scheme illustrating this approach is shown in Fig. 40. Here the width of the grid material (in their study SiO_2 having a refractive index of $n_{LIG} = 1.45$) is 1 μm, with 6×6 μm squared openings. Embedded into a high-refractive-index surrounding, this grid material redirects light rays according to Snell's law (cf. Fig. 40). Originally traveling with a large angle to the OLED normal, these modes are converted to light having a smaller angle to the normal, entering the escape cone of the device. In comparison to a reference white OLED, the light output from a device with a LIG structure increases by a factor of 1.32. Additionally applying a microlens array (cf. Sec. IV.A.2), yields a 2.3-fold total improvement. Note that the microlens array as placed onto the reference device yields only a factor of 1.68. They additionally provided simulation data showing that the overall outcoupling enhancement can be increased by a factor of 3.4 when incorporating grid materials with even lower refractive indices (Sun and Forrest, 2008a).

Another way to utilize materials with low refractive index was developed by Koh *et al.* (2010). Instead of structuring the

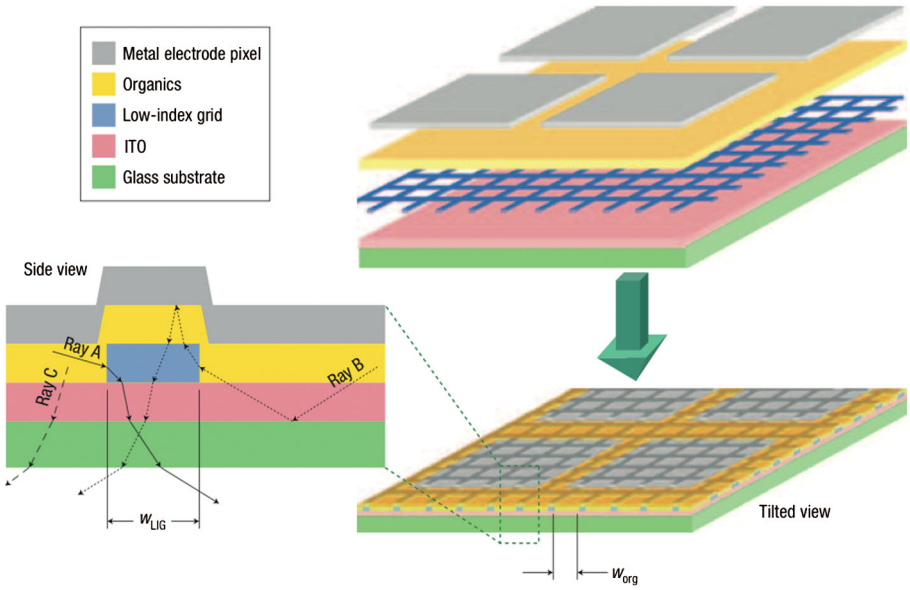

FIG. 40 (color online). Scheme showing an OLED with embedded low-index grid between ITO and organic layers. The inset illustrates the mechanism leading to the outcoupling of organic modes. The active area of the pixels is 1 order of magnitude larger compared to the grid period. From Sun and Forrest, 2008a.

low-index material as in the work of Sun and Forrest (2008a), they structured the ITO by photolithography to form truncated pyramids as shown in Fig. 41 in the cross-sectional view. This ITO grid is then coated with the highly conductive polymer PEDOT:PSS (Fehse *et al.*, 2007), having a low refractive index of $n_{\mathrm{PEDOT:PSS}} = 1.42$. On top of this layer, the remaining OLED is processed in a conventional manner. With its low refractive index, the PEDOT:PSS introduces an index contrast between organic materials and the ITO. Improved light outcoupling is now an interplay between waveguiding on both sides of the low-index polymer [cf. Fig. 41(b)] and the truncated pyramidal shape of the ITO electrodes. It results in an increased fraction of light originally propagating in waveguide modes that reduces its angle to the device normal and by that is able to escape to air. The enhancement is highly dependent on the angle between the substrate plane and the side face of the truncated pyramid [cf. Fig. 41(a)]. Because the PEDOT:PSS is highly lateral conductive (Fehse *et al.*, 2007), light is generated not only in between the ITO base electrode and the metal cathode but also in areas not having ITO beneath the polymer. At high current densities, where the electrical influence of the PEDOT:PSS can be neglected (Koh *et al.*, 2010), the enhancement over the reference OLED is 125%. Again, similar to other approaches, applying an additional microlens array increases the outcoupling enhancement to 167%.

4. Corrugated OLEDs

Instead of introducing a structured layer to the device layer sequence, Koo *et al.* (2010) developed a way to process a complete OLED with corrugation. Also aiming to couple out the organic modes, their approach is based on a subwavelength periodic, corrugated structure that allows one to efficiently Bragg scatter the organic modes to the far field of the OLED.

The corrugation is formed spontaneously after cooling down a bilayer of Al on thermally expanded PDMS (at 100 °C during Al deposition), as a result of different thermal expansion coefficients of Al and PDMS (Koo *et al.*, 2010). Atomic force microscope images of these layers can be seen

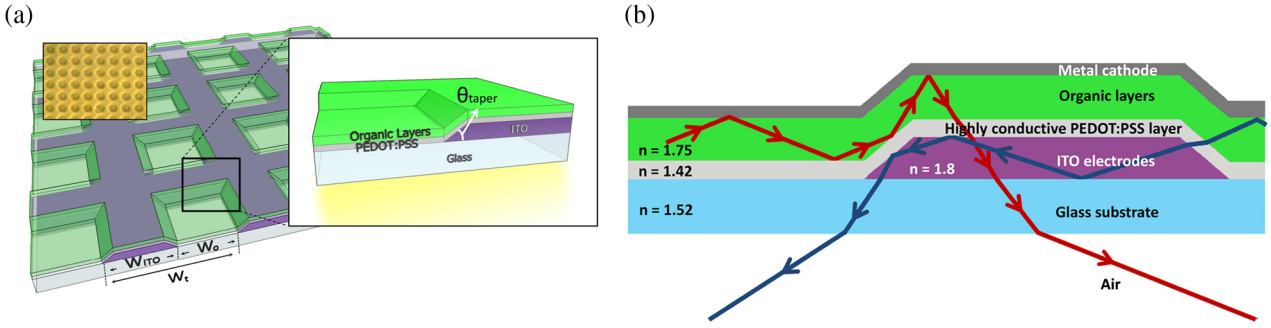

FIG. 41 (color online). (a) 3D scheme of the ITO electrode structure used in connection with the highly conductive PEDOT:PSS film. The size of the patterned ITO openings is roughly 3 μm with a grid period of 6 μm. (b) Cross section of the complete layer structure. The PEDOT:PSS is introducing a refractive index contrast between the otherwise well-matching organic layers and ITO introducing waveguiding. The edges of the ITO electrodes enable enhanced outcoupling of the waveguided modes. From Koh *et al.*, 2010.

in Figs. 42(a)–42(c), and the depths of the buckles increase from 25–30 to 50–70 nm, which is achieved by repeated deposition of 10-nm-thick Al layers on to the thermally expanded PDMS and cooling down afterward. In general, the extraction of organic modes becomes more efficient with increasing buckle depth. The insets in Fig. 42 show the fast Fourier transforms (FFTs) of the structures, clearly indicating a periodic pattern with a characteristic wavelength and a wide distribution without preferred orientation (ring shape) (Koo *et al.*, 2010). Figure 42(d) shows the power spectrum of all patterns, obtained from the FFTs, indicating the unchanged peak wavelength of ~410 nm and the increasing distribution with increasing feature depth.

Koo *et al.* (2010) discussed monochrome OLEDs prepared on flat and corrugated surfaces prepared by dual and triple Al evaporation. Figure 43(a) shows the EL spectra of all three devices obtained at a constant current density of 5 mA cm^{-2}. Dividing the spectra of the buckled samples by the reference spectrum results in the spectral enhancement for each structure, as shown in Fig. 43(b). Important to the application to white OLEDs, the enhancement is seen over the complete visible spectrum with a minimum enhancement of a factor of ~2 (for the triple buckling device) in the blue region, even further increasing to a peak enhancement of >4 in the red spectral region, where the TE_0 and TM_0 of the devices are located. Additionally this plot supports the fact that the extraction efficiency of the corrugation increases with increasing buckle depth as achieved by multiple buckling formation cycles (Koo *et al.*, 2010). Figure 43(c) shows the angular emission profile of all the devices. The data show that the Lambertian emission characteristics of the reference device is conserved by the corrugation. The broad spectral enhancement and the uniform angular emission make this approach suitable for white OLEDs. The integrated enhancement of the current efficiency η_{CE}, obtained at 2000 cd m^{-2}, reaches high values of 1.8 and 2.2 for the double and triple formed buckling OLEDs.

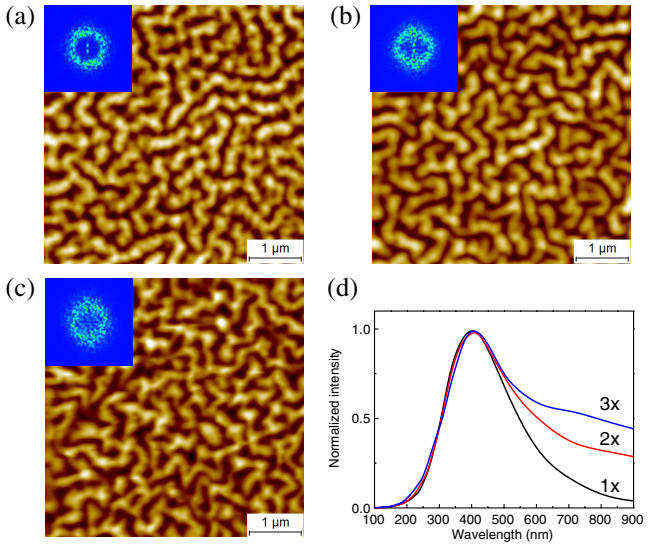

FIG. 42 (color online). Atomic force microscope images of buckling patterns obtained by cooling down a 10-nm-thick aluminum (Al) film, which has been deposited onto a PDMS film heated to 100°C, for 1 (a), 2 (b), and 3 (c) times. Insets: Fast Fourier transform (FFT) patterns. (d) Power spectra from the FFTs as a function of wavelength (1×, 2×, and 3× Al deposition). From Koo *et al.*, 2010.

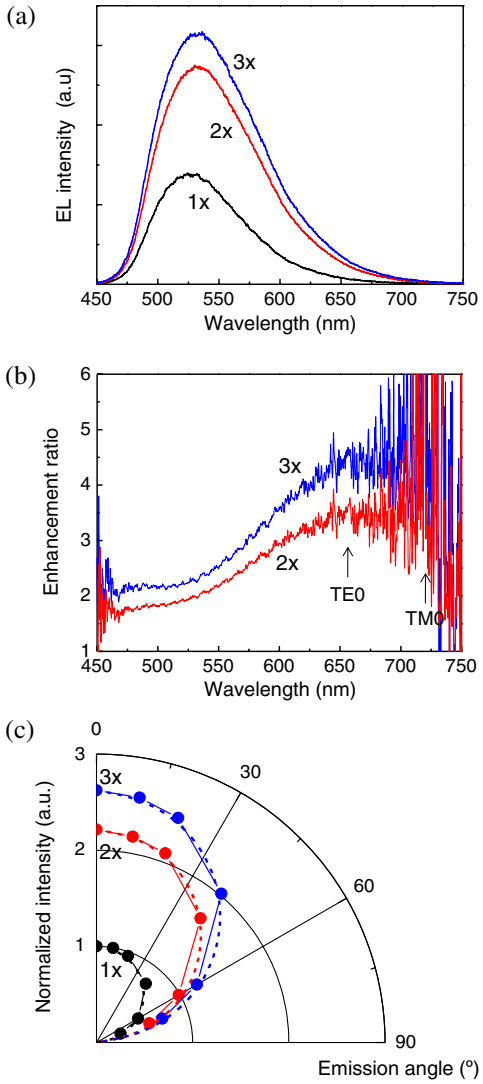

FIG. 43 (color online). (a) Electroluminescence spectra of the reference 1×, 2×, and 3× buckling OLEDs, measured at a constant current density of 5 mA cm^{-2}. (b) Enhancement ratio obtained by dividing the spectra as of (a) of the buckling OLEDs by the one of the reference device. Additionally, the spectral position of the TE_0 and TM_0 modes are indicated. (c) Angular dependence of the light intensity of all three devices. The dashed lines indicate Lambertian emission characteristics. Adapted from Koo *et al.*, 2010.

5. High-refractive-index substrates

The use of high-refractive-index substrates to suppress organic modes was suggested many years ago (Madigan, Lu, and Sturm, 2000), generally offering an easy route to substantially increase the amount of light in the substrate (Lu and Sturm, 2002; Nakamura *et al.*, 2005). Figure 44 schematically shows the differences between the use of standard and high-index substrates.

By matching the refractive index of the substrate of choice closely to the respective indices of the organic materials [$n_{org} \sim 1.7$–1.8 (Greiner, 2007)], the optical contrast at the

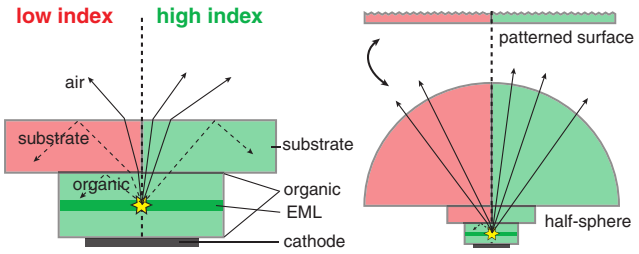

FIG. 44 (color online). Left: Light modes in an OLED structure using low ($n_{low} = 1.51$) and high ($n_{high} \sim 1.8$) refractive index substrates. Right: Application of outcoupling structures, i.e., either a macroextractor or a patterned surface of matching substrate refractive index. Adapted from Reineke, Lindner *et al.*, 2009.

ITO-substrate interface vanishes in first approximation (Gärtner and Greiner, 2008). Thus, the propagation of light, generated in the organic layer stack, into the substrate is not hindered. Consequently organic modes are minimized [cf. Meerheim *et al.* (2010)]. At the same time, as a result of the large index difference at the substrate/air interface, the escape cone of high-refractive-index substrates is noticeably reduced from $\theta_{c,n=1.51} = 41.5°$ to $\theta_{c,n=1.8} = 33.7°$. Thus, even though a larger fraction of light is coupled into the substrate, TIR at the substrate/air interface counteracts this improvement, typically leading to comparable or even slightly lower far-field extraction efficiencies using the high-index substrates (Lu and Sturm, 2002; Nakamura *et al.*, 2005; Reineke, Lindner *et al.*, 2009). In order to overcome this limiting factor, the use of outcoupling structures (cf. Fig. 44) gains importance, because their use can strongly reduce the effect of TIR.

To demonstrate the effect of high-refractive-index glass substrates, Fig. 45 plots the external quantum efficiency of two identical white OLEDs[15] differing in the substrate type used: standard glass ($n_{low} = 1.51$) or high index glass with $n_{high} = 1.78$. The EQE is determined using different outcoupling structures at a constant current density of 5 mA cm^{-2}: (i) a large index-matched half sphere and (ii), for the high-index case, a pyramidal structure (Reineke, Lindner *et al.*, 2009; Rosenow *et al.*, 2010). Applying the half sphere to the reference, low-index substrate OLED results in a 1.76-fold increase in light output. The same measurement setup shows a substantial increase in the high-index case, where an enhancement of 2.32 over the flat measurement is obtained. Applying an outcoupling structure comprising pyramids in a square lattice with a height of 250 μm and a base length of 500 μm still reaches a 1.77-fold enhancement. Note that this is almost identical to the value obtained using the half sphere in the low-index case, clearly showing the potential of using refractive-index-matched substrates.

Similar studies on monochrome green OLEDs are discussed by Mladenovski *et al.* (2009). Rosenow *et al.* (2010) combined the concept of high-refractive-index substrates with white stacked OLEDs, where the optics become more complex.

[15]The transport layer thicknesses of the ETL and HTL slightly differ to meet the field antinode, accounting for the different optical properties of the two substrate types.

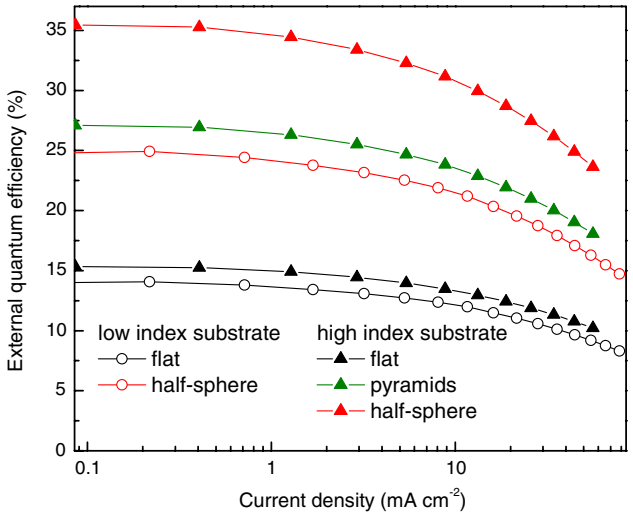

FIG. 45 (color online). External quantum efficiency of white OLEDs processed on standard ($n_{low} = 1.51$) (open symbols) and high ($n_{high} = 1.78$) refractive index (filled symbols) substrates. Different sets of data correspond to different outcoupling methods used. The data displayed are obtained from devices by Reineke, Lindner *et al.* (2009) (devices LI and HI-1).

6. Losses to metal surface plasmons

Whenever methods are successfully applied to efficiently couple organic modes to the far field, the remaining loss in OLEDs is the coupling to surface plasmon states of the highly reflective metal cathode. Figure 38 already showed the magnitude of this effect for different distances between the EML and the cathode. Using high refractive index materials qualitatively shows a similar dependency of the coupling to surface plasmons on the spacing distance (Gärtner and Greiner, 2008; Mladenovski *et al.*, 2009; Meerheim *et al.*, 2010).

In order to reduce these losses, Lin *et al.* (2006) suggested increasing the distance between EML and the metal electrode to distances meeting the second field antinode of the system. However, even though coupling to surface plasmon modes is strongly reduced with thickness (cf. Fig. 38), their improvement based on a thick transport layer was only marginal (120% enhancement for the integrated intensity). This observation can be explained by the increasing fraction of organic modes with increasing distance between EML and metal, which is observed when using standard glass substrates.

Two key points needing to be met practically exploit the suppressed coupling to surface plasmon modes in OLEDs: (i) The transport layer that is to be increased needs to either be electrically doped (Walzer *et al.*, 2007) or have a very high charge conductivity to assure that Ohmic losses and changes of charge carrier balance can be excluded. The studies of Lin *et al.* (2006) and Meerheim *et al.* (2010) made use of doped transport layers. (ii) Substrates matching the refractive indices of the organic materials need to be employed to prevent the formation of an increased number of organic modes with increasing thickness (Gärtner and Greiner, 2008; Mladenovski *et al.*, 2009; Reineke, Lindner *et al.*, 2009; Meerheim *et al.*, 2010).

Similar to the discussion of using high index substrates, data of two white OLEDs by Reineke, Lindner *et al.* (2009) are exemplarily used and plotted in Fig. 46. They

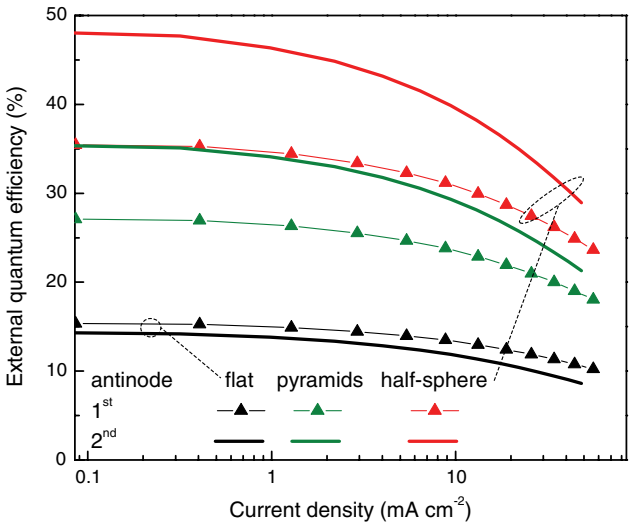

FIG. 46 (color online). External quantum efficiency of white OLEDs processed on high ($n_{high} = 1.78$) refractive index substrates having a variation in the ETL thickness, meeting first (ETL = 45 nm) and second (ETL = 205 nm) field antinodes, respectively. Different sets of data correspond to different outcoupling methods used. The data displayed are obtained from devices by Reineke, Lindner *et al.* (2009) (devices HI-1 and HI-2)].

have different ETL thicknesses of 45 and 205 nm which meet the interference criteria for the first and second field antinodes, respectively. Both processed on high-index substrates ($n_{high} = 1.78$), measurements in flat, half sphere, and pyramid pattern configuration can be directly compared to see the effect of reduced plasmonic losses. The current density versus voltage characteristics of both devices are almost identical (Reineke, Lindner *et al.*, 2009). In the second field antinode, the outcoupling enhancement obtained at 5 mA cm^{-2} with the half sphere increases to a factor of 3.37 (42.4% EQE) from 2.32 (32.5% EQE) for the device in the first maximum. Even using the pyramid pattern as an outcoupling structure yields 31.3% EQE, corresponding to a 2.48-fold increase in outcoupling efficiency (Reineke, Lindner *et al.*, 2009). It is worth noting that the second order white OLEDs undergo a noticeable change in their optical properties, which is mainly due to diverging interference conditions with increasing device thickness for the primary colors (Reineke, Lindner *et al.*, 2009). Consequently, the white OLEDs with thick transport layers require one to readdress the exciton-color management to attain a high-quality white emission.

7. Orientation of the molecular dipoles

As mentioned in Sec. IV.A.6, the coupling of the emitting dipoles to the metal surface plasmons contributes substantially to the loss in a typical OLED. Another way to reduce the losses to plasmon modes is the alignment of the emitting molecules and by that their transition dipole with respect to the metal layer plane. In general, the orientation of the emitter ensemble within the OLED is treated to be isotropic (Furno *et al.*, 2012). However, it was shown that preferential alignment of emitter dipoles can be achieved for both fluorescent (Yokoyama *et al.*, 2009; Frischeisen *et al.*, 2010) and, more recently, phosphorescent (Flaemmich *et al.*, 2011; Schmidt *et al.*, 2011; Taneda, Yasuda, and Adachi, 2011) emitter molecules.

The ensemble of emitting dipoles in an OLED emission layer is composed of three fundamental dipole orientations (Neyts, 1998; Furno *et al.*, 2012; Brütting *et al.*, 2013): $P_{\perp,TM}$, $P_{\parallel,TM}$, and $P_{\parallel,TE}$, where TM and TE stand for transverse magnetic and transverse electric, respectively. In the case of isotropic orientation, these contributions are weighted equally, i.e., $P_i = 1/3$. It can be shown that the $P_{\perp,TM}$ dipoles only very weakly couple to the metal surface plasmon mode, even when the dipoles are close to the metal (Brütting *et al.*, 2013). Thus, emitter molecules which preferentially orient parallel to the metal surface do not couple effectively to the plasmon mode so that, consequently, the fraction of outcoupled light can be increased. Frischeisen *et al.* (2011) estimated recently that the external quantum efficiency of OLEDs could be increased from 20% to about 45% by engineering the emission layer to have ideal horizontal dipole orientation. Despite the fact that this concept will heavily depend on the actual material design, it provides an elegant and effective way to suppress the losses to surface plasmon modes.

8. Stacked OLEDs

Stacked white OLEDs (Shen *et al.*, 1997; Kanno, Giebink *et al.*, 2006; Kanno, Holmes *et al.*, 2006; Rosenow *et al.*, 2010) have not been discussed in Secs. II and III due to their structural difference from single-unit OLEDs. Stacked OLEDs are based on the concept of depositing more than one OLED on top of each other, serially interconnected with either a metal electrode (Shen *et al.*, 1997) or a charge-generation (also termed charge-conversion) layer (Kanno, Giebink *et al.*, 2006; Kanno, Holmes *et al.*, 2006; Rosenow *et al.*, 2010). Their structural complexity and variability qualify for an independent review. Because the EMLs used in stacked devices fully make use of either monochrome or multicolor systems that have been discussed in previous sections, we point out only key differences from single-unit devices.

Stacked OLEDs still are transparent devices; thus in first approximation the brightness and color emitted from each unit can be added to form the total emission. If these devices are fabricated with charge-generation layers, more than one photon can be emitted per injected electron. Note that even though the EQE values add up, the LE ideally remains constant for stacking identical units as the driving voltage increases accordingly. As brightness adds up, the individual units need to sustain less current density to achieve a given luminance level compared to the single-unit OLEDs. This benefits the long-term stability of the devices.

One key advantage of stacked OLEDs is the possibility of designing a white device by placing the different EMLs comprising primary colors into their respective field antinodes within the layer structure, which enables operation of all emitters at maximum outcoupling efficiency. This is in contrast to single-unit devices, where some of the colors are likely to be suppressed (Reineke, Lindner *et al.*, 2009).

One drawback of this concept is the increased thickness of the complete device, which may increase the fraction of waveguided organic modes, as shown in Fig. 38. This again is overcome by using high-index glass substrates. Rosenow *et al.* (2010) discussed two-unit stacked devices based on a

triplet-harvesting blue or red (cf. Sec. III.B.3) and a phosphorescent green or yellow (cf. Sec. III.C) unit also employing glass substrates with $n_{high} = 1.78$. At 1000 cd m^{-2}, white stacked OLEDs reach 75.8% and 41.6% EQE when using an index-matched half sphere and pyramidal patterned structure, respectively. With respect to a reference device on standard glass measured without outcoupling structures, these values correspond to a 2.9- and 1.6-fold increase in outcoupling efficiency.

B. Concepts for top-emitting devices

In contrast to bottom-emitting OLEDs, top-emitting devices can mostly be optically influenced by manipulating the top layers made of soft, organic materials and thin metal layers (Chen *et al.*, 2010). This in turn complicates the task of developing efficient strategies for improved light outcoupling, because the organic layer stack likely will not withstand many postprocessing steps that would be necessary to improve the outcoupling of light.

Kanno, Sun, and Forrest (2005) reported on highly efficient top-emitting white OLEDs based on two primary colors, where they employ the transparent conductor ITO as the top cathode, providing sufficient transparency similar to bottom-emitting devices. However, as ITO and similar conductors are processed by sputtering techniques, such processing introduces a high risk of damaging the underlying organic layers. To avoid techniques with high impact on the organics, thin metal layers have become the top electrode of choice, having sufficient lateral conductivity while maintaining sufficient transparency (Chen *et al.*, 2010). They turn the OLED into a microresonator. This even complicates the realization of white OLEDs, because the resonances of the optical structure become narrower and angle dependent (Meerheim, Nitsche, and Leo, 2008; Hofmann *et al.*, 2010).

1. Dielectric capping layer

The concept of a dielectric capping layer applied on top of the thin, semitransparent metal cathode was introduced by Hung *et al.* (2001). Hung *et al.* evaluated a variety of inorganic and organic materials with different refractive indices with respect to their outcoupling effect. By introducing a capping layer, the transmittance of the top metal layer can be increased. Early work on monochrome, top-emitting OLEDs showed that the concept of dielectric capping layers can substantially increase the amount of outcoupled light (Riel *et al.*, 2003; Q. Huang *et al.*, 2006).

In addition to the outcoupling enhancement, the capping layer helps to realize high-quality white light (Hsu *et al.*, 2005; Freitag *et al.*, 2010). As stated, top-emitting OLEDs employing thin metal top electrodes have a much stronger cavity compared to standard bottom-emitting devices, negatively affecting their optical properties. Figure 47 shows the calculated extractable power $A(\lambda, \theta)$ of a model OLED consisting of a single organic layer (Thomschke *et al.*, 2009). The EML is located in the bulk of this model OLED. Figure 47(a) shows $A(\lambda, \theta)$ of this structure without a capping layer for different angles of observation. This extractable mode is very narrow with a FWHM of 83 nm at 0°, in addition to shifting to shorter wavelength with increasing observation angle.

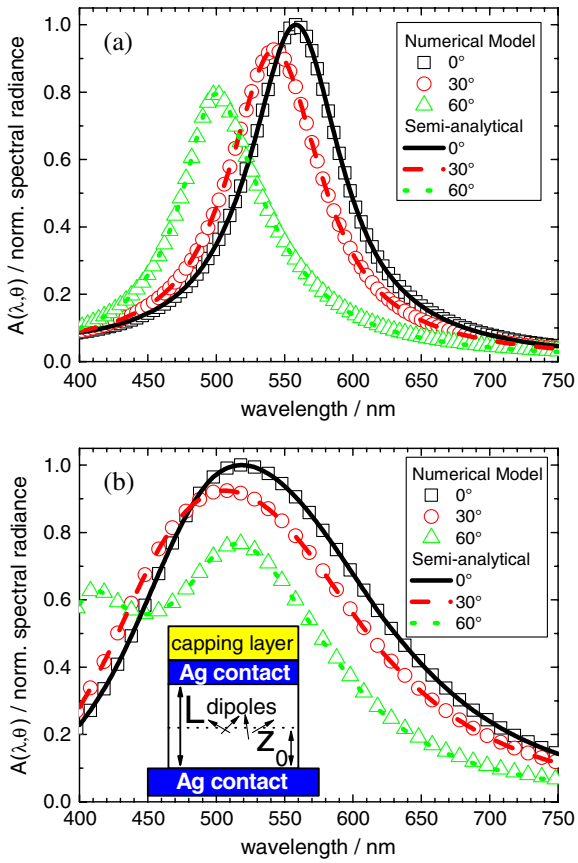

FIG. 47 (color online). Calculated extractable power $A(\lambda, \theta)$ of two model OLED structures having the following layer sequence: (a) 100 nm Ag/100 nm organic ($n = 1.8$)/15 nm Ag. (b) Layer structure of (a) followed by an additional 50 nm organic capping layer. Emitters are placed in the field antinode corresponding to a resonance wavelength of approximately 560 nm. From Thomschke *et al.*, 2009.

Figure 47(b) shows the calculation made for the same model OLED with additionally applied organic capping layer. This layer effectively reduces the color shift of $A(\lambda, \theta)$ and at the same time broadens the extractable mode (FWHM at 0°: 190 nm). In comparison to the device without a capping layer, the FWHM is more than doubled, which is mandatory for coupling a broad white spectrum to air (Hsu *et al.*, 2005; Thomschke *et al.*, 2009; Freitag *et al.*, 2010). Even with the applied capping layer, top-emitting OLEDs based on semitransparent metal electrodes are very sensitive to optical changes. Freitag *et al.* (2010) compared the performance of two identical white OLEDs with different, highly reflective anode metals (single-layer Al versus a bilayer of Al/Ag) having slightly different reflectivity. The effect on the extractable mode [see Fig. 48(c)] and the resulting emitted OLED spectrum [see Figs. 48(a) and 48(b)] is significant.

Thomschke *et al.* (2009) discussed white OLEDs based on a hybrid EML concept (Schwartz *et al.*, 2006) without and with the capping layer applied. The external quantum efficiency, obtained at 5.4 mA cm^{-2}, increased from 5.4% (without) to 7.8% (with). In addition, the OLEDs with an additional capping layer emit a broad white spectrum, which only weakly varies as a function of the observation angle. In contrast, the reference OLED does not even emit white light

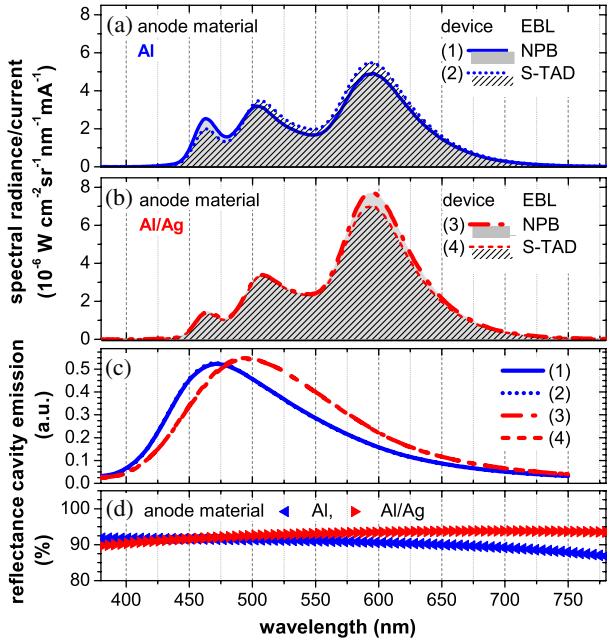

FIG. 48 (color online). Forward EL spectra of white OLEDs based on an (a) Al and (b) Al/Ag anode, obtained at 1000 cd m^{-2} (additional variations of the EBL are shown). (c) Calculated extractable mode for all devices. (d) Reflectance of both anodes used (Al vs Al/Ag). From Freitag *et al.*, 2010.

at any angle, which is a result of the narrow $A(\lambda, \theta)$ and points to the need of capping layers for realizing white top-emitting OLEDs based on thin metal electrodes.

2. Laminated microlens arrays

A concept for improved outcoupling for top-emitting white OLEDs that goes beyond the application of a dielectric capping layer was recently introduced by Thomschke *et al.* (2012). Their reference device already has an organic capping layer applied having a refractive index that is similar to the rest of the layers used in the OLED. Now they coat a polymer microlens film with high refractive index ($n_{\text{microlens}} = 1.71$) with the same material used for the capping layer, to finally merge the two organic layers in a lamination process. Thus, a top-emitting OLED is fabricated that is refractive index matched throughout the device.

To show this concept, Thomschke *et al.* (2012) used a highly efficient two-unit stacked OLED as a reference device, which makes use of a phosphorescent yellow and a triplet-harvesting blue or red unit [modified from Rosenow *et al.* (2010)]. The emitted spectrum of the reference device is shown in Fig. 49(a) as a function of viewing angle. Strong color shifts are observed, where both cavity modes sweep from lower to higher photon energies with increasing angle of observation. Not for a single angle, a white spectrum is emitted. Application of the microlens foil drastically improves the optical properties of the device, as is shown in Fig. 49(b). Now the emitted spectrum only changes slightly with viewing angle and represents a broadband, balanced white spectrum. The laminated microlens has two functions in this concept: (i) it acts as an integrating element, effectively mixing all photons so that the spectrum becomes

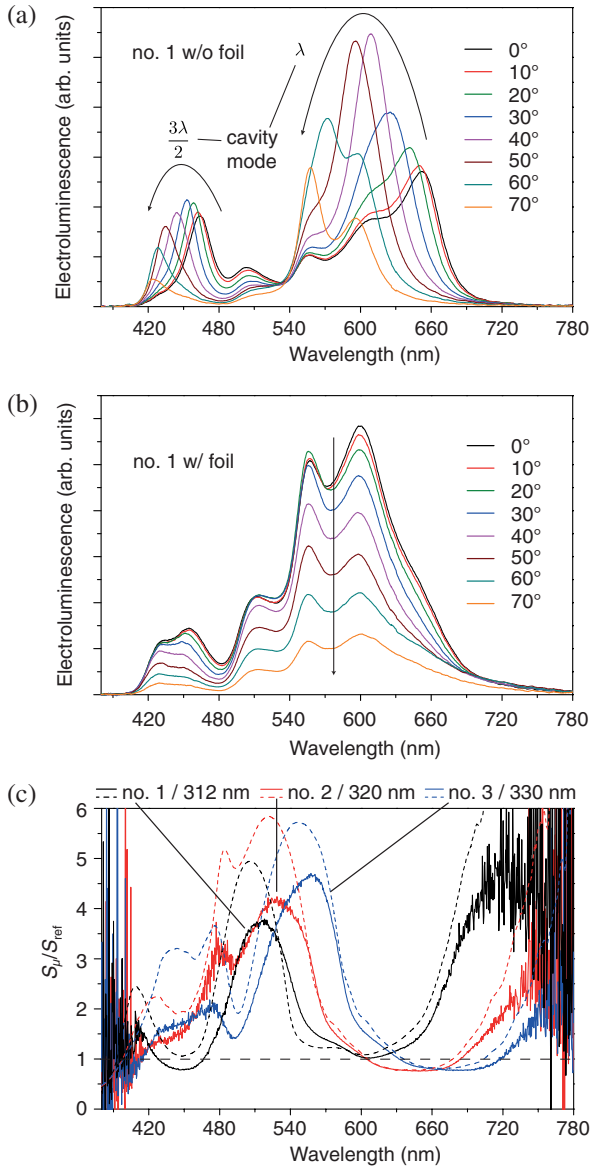

FIG. 49 (color online). (a) Electroluminescence of a two-unit stacked top-emitting OLED as a function of viewing angle. (b) Identical OLED architecture as in (a) with additional application of refractive-index-matched microlens film. (c) Experimental and calculated spectral enhancement factor between device without (a) and with (b) microlens film (data shown for three different total cavity thicknesses). From Thomschke *et al.*, 2012.

independent of the viewing angle, and (ii) it functions as an outcoupling structure for modes that are not able to escape the thin-film structure. The latter is seen in Fig. 49(c), where the spectral outcoupling enhancement factor is plotted as derived between reference and microlens laminated OLED. It shows an outcoupling enhancement up to a factor of roughly 4 in the green spectral region, where the planar reference structure is unable to couple out efficiently [cf. Fig. 49(a)].

The highest EQE[16] for a laminated OLED is 26.8% (30.1 lm W^{-1}) with color coordinates of (0.542, 0.416) ($\alpha_{\text{CIE}} = +0.02$, CRI = 75). The highest CRI of 93 was

[16]Note that this is a two-unit stacked device potentially having 200% internal quantum efficiency.

reached with a slightly different cavity length; unfortunately no efficiency data are available for this device (Thomschke *et al.*, 2012).

C. Summary

Besides improving the internal OLED performance to realize internal quantum efficiencies approaching unity, which has been realized for specific white OLED concepts, the improvement of the light outcoupling is of great interest. This inherently offers the largest potential for performance enhancement up to a factor of 5 (cf. Sec. I.A.6).

Many promising and effective concepts for bottom-emitting white OLEDs have been proposed. The currently reported enhancement factors are 1.67 [low-index layer, Sec. IV.A.3 (Koh *et al.*, 2010)], 2.2 [corrugated OLEDs (monochrome), Sec. IV.A.4 (Koo *et al.*, 2010)], 2.3 [low-index grid, Sec. IV.A.3 (Sun and Forrest, 2008a)], and 2.48 [high-index substrate with thick ETL, Sec. IV.A.6 (Reineke, Lindner *et al.*, 2009)]. All these concepts promise a spectrally broad gain, which is necessary for white light emission. At the same time the improvement values reported to date indicate that there still is a noticeable gap between experimental results and the amount of light that can potentially be gained (as a rule of thumb a factor of 5). Furthermore, the enhancement factors are often achieved based on reference devices which are not optically optimized and thus have to be taken not seriously. Also, as an important future factor, the scalability of these outcoupling concepts strongly determines their acceptance.

The discussion of concepts for top-emitting white OLEDs showed that the outcoupling enhancement is expected to have a much smaller margin compared to bottom-emitting devices. Here the capping layer concept is to date the only concept providing substantial outcoupling enhancement [1.44-fold (Thomschke *et al.*, 2009)]. Apparently it is still a challenge to realize broadband white OLEDs with emission that does not change strongly as a function of the observation angle (Freitag *et al.*, 2010). The concept of laminating a microlens foil on top of the capping layer (Thomschke *et al.*, 2012) seems promising, especially as it alleviates the general problem of white top-emitting OLEDs that compromises between high efficiency and high color quality must be made. Still more research is needed to test its feasibility on a larger scale.

V. ESTIMATION OF EFFICIENCY LIMIT FOR WHITE OLEDs

It is not easy to make predictions that aim to answer the question: What level of efficiency can white OLEDs reach in the future? Still we want to make a serious attempt in trying to estimate a realistic upper limit for the efficiency of white OLEDs. We specifically focus here on the luminous efficacy, given in lumens per watt ($\mathrm{lm\,W^{-1}}$), that is widely used to compare white OLED performance to existing, mature technologies.

In order to do so, we base our estimation on a published white OLED, hereinafter called the reference device, serving as a baseline [device HI-2 from Reineke, Lindner *et al.* (2009)]. Its performance data are 34% EQE and 90 $\mathrm{lm\,W^{-1}}$ at 1000 $\mathrm{cd\,m^{-2}}$ with CIE color coordinates of (0.41, 0.49) ($\alpha_{\mathrm{CIE}} = +0.09$). In the following, we discuss different aspects that influence the overall efficiency. Figure 50 displays a table that lists all these aspects with their anticipated change on the device efficiency.

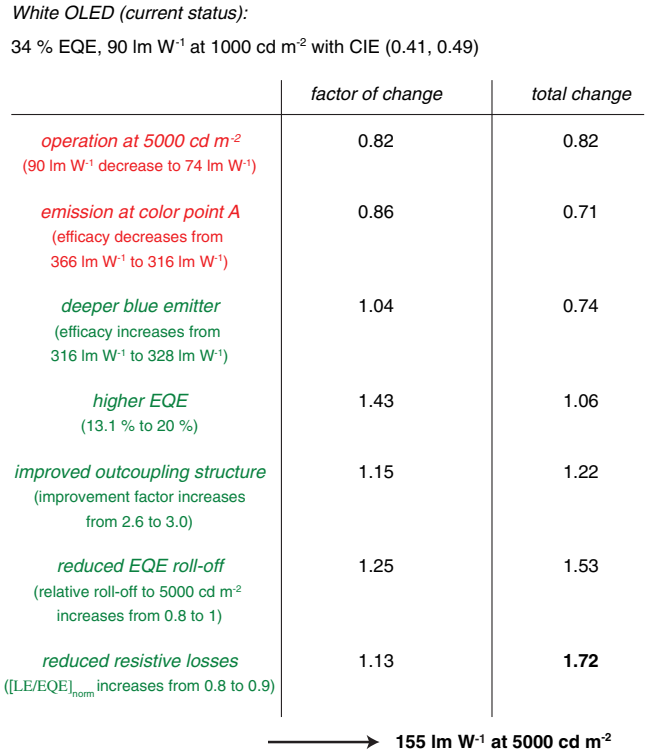

FIG. 50 (color online). Based on a reference white OLED, representing the current status; different aspects influencing the device efficiency are listed to estimate a realistic upper limit. For each aspect, the estimated potential change is given. Efficiency reduction is encountered to meet color quality and lighting application requirements. From Reineke, Lindner *et al.*, 2009 (device HI-2).

First we see that it is necessary for real applications to raise the brightness level of the OLED to 5000 instead of the commonly used 1000 $\mathrm{cd\,m^{-2}}$. The luminous efficacy of the reference OLED rolls off from 90 $\mathrm{lm\,W^{-1}}$ at 1000 $\mathrm{cd\,m^{-2}}$ to 74 $\mathrm{lm\,W^{-1}}$ at 5000 $\mathrm{cd\,m^{-2}}$; thus we account for this change by the factor of 0.82 (cf. Fig. 50).

Furthermore, the emitted color of the reference device used in this argument is by far too green ($\alpha_{\mathrm{CIE}} = +0.09$) to meet white light requirements, which we simply see as being a Planckian radiator (cf. Sec. I.B.2). Based on the three emitters used, i.e., FIrpic, $\mathrm{Ir(ppy)_3}$, and $\mathrm{Ir(MDQ)_2(acac)}$ (Reineke, Lindner *et al.*, 2009), we calculated the luminous efficacy of radiation K_r for the reference white OLED and for a simulated spectrum based on the same emitters that has emission at standard illuminant A in the CIE color space, i.e., CIE (0.448, 0.408). Here K_r drops from 366 to 316 $\mathrm{lm\,W^{-1}}$ (factor of 0.86). The use of FIrpic introduces an unbalanced ratio of blue, green, and red emissions, barely having green intensity (cf. Fig. 8[17]). By incorporating a

[17]Note that the absolute numbers of K_r differ for the spectra shown in Fig. 8 and for the values displayed in Fig. 50. While the latter are based on OLED spectra, the simulation of Fig. 8 takes only the PL spectra of the emitters into account, giving rise to slight differences.

deeper blue emitter, the green intensity can be increased, which increases K_r again from 316 to 328 lm W^{-1} (cf. Fig. 8).

The external quantum efficiency of the reference device is 13.1% EQE at 1000 cd m^{-2} when processed on standard glass substrates and measured without outcoupling enhancement.[18] We anticipated that by using emitters with the highest possible PLQY in connection with the right EML concept, 20% EQE can be reached—the typical limit seen for phosphorescent OLEDs or equivalent concepts with the potential of 100% internal quantum efficiency. Note that this limit even seems conservative, given the fact that various reports suggest EQE values significantly exceeding 20% (Tanaka, Agata *et al.*, 2007; Tanaka, Sasabe *et al.*, 2007; Su *et al.*, 2008; Sasabe *et al.*, 2010).

With a theoretical potential to increase the outcoupled light by a factor of 5 (cf. Sec. I.A.6) and considering the amount of high-performance concepts reported (Sun and Forrest, 2008a; Reineke, Lindner *et al.*, 2009; Koh *et al.*, 2010; Koo *et al.*, 2010), we see it is feasible to increase the current outcoupling enhancement obtained for the reference white OLED[19] of 2.6 to a factor of 3.

Much effort is spent on reducing the efficiency roll-off induced by nonlinearities at high excitation levels (Baldo, Adachi, and Forrest, 2000; Kalinowski *et al.*, 2002; Reineke, Walzer, and Leo, 2007). Especially phosphorescent emitters seem to have the potential to extend their operation range where no annihilation is present (Namdas *et al.*, 2005; Kang *et al.*, 2007; Staroske *et al.*, 2007; Han *et al.*, 2008; Schwartz, Reineke *et al.*, 2008; Su *et al.*, 2008; Reineke *et al.*, 2010). Thus, we simply assume in this estimation that future research will enable white OLED to be operated at 5000 cd m^{-2} without suffering a decrease in EQE up to this brightness.

The last aspect we discuss is the contribution of resistive losses within an OLED to the luminous efficacy roll-off, which has not drawn much attention in current research. Figure 51 plots the relative roll-off of EQE and LE as normalized to an initial brightness of 100 cd m^{-2} for a white OLED. Clearly the luminous efficacy shows a more pronounced decrease with increasing luminance compared to the EQE. While the EQE solely accounts for the intensity dependency of the internal quantum efficiency, the LE also quantifies changes due to transport related properties of the device, i.e., conductivity of the layers and possible energy barriers within the device that need to be overcome. Their impact on the LE roll-off can be calculated by determining the ratio of the normalized LE and EQE curves, $[\mathrm{LE/EQE}]_{\mathrm{norm}}$, yielding the solid line for this specific device (cf. Fig. 51). For the device considered here, the resistive losses already contribute to as much as 20% of the LE roll-off at 5000 cd m^{-2}. Further research on high-conductivity transport materials (Sasabe and Kido, 2011; Sasabe *et al.*, 2011), doped transport layers (Walzer *et al.*, 2007), and even investigation of homojunction OLEDs (Harada *et al.*, 2005; Cai *et al.*, 2011a, 2011b), barely having any energy barriers within the device, will help to reduce this loss. We assume here that the relative decrease of $[\mathrm{LE/EQE}]_{\mathrm{norm}}$ can be increased from 0.8 to at least 0.9 at 5000 cd m^{-2}.

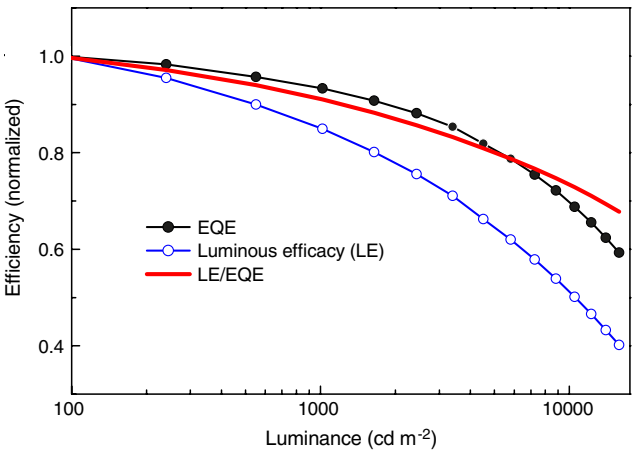

FIG. 51 (color online). The drop of EQE and LE as a function of luminance as normalized to a brightness of 100 cd m^{-2}. Device data are from Reineke, Lindner *et al.* (2009) (device HI-1). To quantify the resistive losses in the OLED, the normalized trends of LE and EQE are divided: $[\mathrm{LE/EQE}]_{\mathrm{norm}}$.

Of course it is most challenging to address and improve all aspects given in Fig. 50 in one future OLED. Still, considering all these factors, we believe that for high-quality white OLEDs luminous efficacies of 155 lm W^{-1} will be in reach, even at a high operating brightness of 5000 cd m^{-2}. If these values really can be achieved, then the future of white OLEDs might be bright, as they will by far outperform existing lighting technologies such as halogen lamps, fluorescent tubes, and compact fluorescent lamps (Steele, 2007). At the same time, the OLED technology enters our everyday life with an exciting new form factor, redefining the way we use and perceive artificial light.

However, one should also keep in mind that the OLED lighting technology might have unexpected competitors: While it is unlikely that inorganic thin-film electroluminescence will reach similar parameters in terms of efficiency, brightness, and lifetime, the inorganic LED in combination with light-distributing sheets might be a serious competitor. Such technologies are currently intensively developed for liquid crystal display backlighting. The current efficiency advantage of the white LED, in combination with the low-cost potential of the light-distribution sheets, might yield a product that is for the end user similarly or more attractive than the much more elegant solution offered by the OLED.

ACKNOWLEDGMENTS

We are indebted to many co-workers and colleagues with whom we had the pleasure to interact. For our own results presented here Karsten Fehse, Patricia Freitag, Mauro Furno, Simone Hoffmann, Frank Lindner, Rico Meerheim, Thomas Rosenow, Gregor Schwartz, Caroline Weichsel, Julia Wünsche, and many others made important contributions. We enjoyed helpful discussions with Chihaya Adachi, Marc Baldo, Herbert Börner, Stephen Forrest, Georg Gärtner, Horst

[18]Note that the reference device is an optimized OLED employing high refractive index substrates and thick electron-transport layers.

[19]This increase with respect to the flat device was obtained in the LE using the pyramid pattern.

Greiner, Junji Kido, Kristiaan Neyts, Ching Tang, and Mark Thompson. Furthermore, we thank Novaled AG for continuous support. This work would not have been possible without the continuous support of the funding agencies: the European Commission with projects "OLLA" (No. IST-2002-004607) and "OLED100.eu" (No. FP7-224122) within the sixth and seventh frameworks IST program, respectively; the Bundesminesterium für Bildung und Forschung (BMBF) with projects "ROLLEX" (No. 13N 8855) and "R2FLEX" (No. 13N11060); and the state of Saxony with the project "NKOE" (No. 12712). We received further funding via the Leibniz prize of the Deutsche Forschungsgemeinschaft (DFG). S. R. gratefully acknowledges the support of the Deutsche Forschungsgemeinschaft through a research fellowship (Grant No. RE3198/1-1).

APPENDIX: INTERNATIONAL UNION OF PURE AND APPLIED CHEMISTRY (IUPAC) NAMES OF THE MATERIALS DISCUSSED

If the full chemical name is not specifically important in the main text of this review, only the material's common abbreviation found in the literature is used to improve readability. Here the full IUPAC chemical names of all materials discussed are listed. In Tables III and IV, redundancies might occur, i.e., multiple abbreviations for one material. We display them both, as we use the abbreviation found in the respective reference.

TABLE III. Small-molecular-weight materials.

Abbreviation	IUPAC name	Function
4P-NPD	*N*, *N*′-di-(1-naphthalenyl)-*N*, *N*′-diphenyl-[1, 1′ : 4′, 1″ : 4″, 1‴-quaterphenyl]-4, 4‴-diamine	Blue fluor. emitter
α-NPD	*N*, *N*′-bis(naphthalen-1-yl)-*N*, *N*′-bis(phenyl)-benzidine	HTL + host
BBOT	2,5-bis(5-tert-butyl-2-benzoxazolyl)thiophen	ETL
BCzVBi	4, 4′-bis(9-ethyl-3-carbazovinylene)-1, 1′-biphenyl	Blue fluor. emitter
$Bepp_2$	bis(2-(2-hydroxyphenyl)-pyridine)beryllium	Host
BPhen	4,7-diphenyl-1,10-phenanthroline	ETL
$Bt_2Ir(acac)$	bis(2-phenylbenzothiozolato-*N*, $C^{2'}$)(acetylacetonate)Ir(III)	Yellow phos. emitter
$Btp_2Ir(acac)$	bis(2-(2′-benzothienyl)-pyridinato-*N*, $C^{3'}$)(acetylacetonate)Ir(III)	Red phos. emitter
CBP	4, 4′-bis(carbazol-9-yl)biphenyl	Host
CDBP	4, 4′-bis(carbazol-9-yl)-2, 2′-dimethylbiphenyl	Host
CPhBzIm	bis(N-phenylbenzimidazole)carbazole	Host
CzSi	9-(4-tert-butylphenyl)-3,6-bis(triphenylsilyl)-9H-carbazole	Host
DCB	1,4-bis((9H-carbazol-9-yl)methyl)benzene	Host
DCJTB	4-(dicyanomethylene)-2-tert-butyl-6-(1,1,7,7-tetramethyljulolidin-4-yl-vinyl)-4H-pyran	Red fluor. emitter
DCM	2-(2-(4-(dimethylamino)styryl)-6-methyl-4H-pyran-4-ylidene)malononitrile	Red fluor. emitter
DCM1	2-(2-(4-(dimethylamino)styryl)-6-methyl-4H-pyran-4-ylidene)malononitrile	Red fluor. emitter
DCM2	4-(dicyanomethylene)-2-methyl-6-julolidyl-9-enyl-4H-pyran	Red fluor. emitter
DCzPPy	2,6-bis(3-(9H-carbazol-9-yl)phenyl)pyridine	Host
DPAN	4-diphenylamino-1,8-naphthalimide	Green fluor. emitter
DPAVBi	4, 4′-bis[4-(di-p-tolylamino)styryl]biphenyl	Blue fluor. emitter
DTPA	(4-(2-[2,5-dibromo-4-(2-(4-diphenylamino-phenyl)-vinyl)-phenyl]-vinyl)-phenyl)-diphenylamine	Green fluor. emitter
FIr6	bis(2,4-difluorophenylpyridinato)tetrakis(1-pyrazolyl)borate iridium(III)	Blue phos. emitter
FIrpic	bis(3,5-difluoro-2-(2-pyridyl)phenyl-(2-carboxypyridyl)iridium(III)	Blue phos. emitter
FPt1	platinum(II)(2-(4′, 6′-difluorophenyl)pyridinato-*N*, $C^{2'}$)(2, 4-pentanedionato)	Blue phos. emitter
FPt2	platinum(II)(2-(4′, 6′-difluorophenyl)pyridinato-*N*, $C^{2'}$)(6-methyl-2, 4-heptanedionato-*O*, *O*)	Blue phos. emitter
$Ga(pyimd)_3$	tris(2-(2-pyridyl)imidazole)gallium(III)	Host
$Ir(1\text{-}piq)_3$	tris(1-phenyl-isoquinolinato-*N*, $C^{2'}$)iridium(III)	Red phos. emitter
$Ir(Bu\text{-}ppy)_3$	fac-tris(2-(4′-ter-butyl)phenylpyridine)iridium(III)	Green phos. emitter
Ir(dbfmi)	mer-tris(*N*-dibenzofuranyl-*N*′-methylimidazole)iridium(III)	Blue phos. emitter
$Ir(dhfpy)_2(acac)$	bis(2-(9,9-dihexylfluorenyl)-1-pyridine)(acetylacetonate)iridium(III)	Yellow phos. emitter
$Ir(dfbppy)(fbppz)_2$	bis(4-tert-butyl-2-(2,4-difluorophenyl)pyridinato)(3-(trifluoro-methyl)-5-(4-tert-butylpyridyl)pyrazolate)iridium(III)	Blue phos. emitter
$Ir(HFP)_3$	tris(2, 5-bis-2′-(9′, 9′-dihexylfluorene)pyridine)iridium(III)	Red phos. emitter
$Ir(MDQ)_2(acac)$	bis(2-methyldibenzo[f,h]quinoxaline)(acetylacetonate)iridium (III)	Red phos. emitter
$Ir(pbi)_2(acac)$	bis(phenyl-benzoimidazole)(acetylacetonate)iridium(III)	Yellow phos. emitter
$Ir(ppy)_3$	fac-tris(2-phenylpyridine)iridium(III)	Green phos. emitter
$Ir(ppy)_2pc$	fac-bis(2-phenylpyridyl)(2-pyridylcoumarin)iridium(III)	Yellow phos. emitter
$Ir(SBFP)_2(acac)$	iridium(III)bis(2-(9, 9′-spirobi[fluorene]-7-yl)pyridine-*N*, $C^{2'}$)acetylacetonate	Orange phos. emitter
MB-BT-ThTPA	4-(5-(4-(diphenylamino)-phenyl)-thienyl-2-)-7-(4-methoxybenzene)-2,1,3-benzothiadiazole	Red fluor. emitter

TABLE III. (*Continued*)

Abbreviation	IUPAC name	Function
mCP	1,3-bis(carbazol-9-yl)benzene	Host
MPD	(2-methyl-6-(2-(2,3,6,7-tetrahydro-1H,5H-benzo[i,j]quinolizin-9-yl)ethenyl)-4H-pyran-4-ylidene)-propanedinitrile	Red fluor. emitter
MQAB	6-mesityl-N-(6-mesitylquinolin-2(1H)-ylidene)quinolin-2-amine-BF2	Blue fluor. emitter
m-MTDATA	4, 4′, 4″-tris(*N*-3-methylphenyl-*N*-phenylamino)triphenylamine	HTL
Nile red	9-diethylamino-5-benzo[α]phenoxazinone	Red fluor. emitter
NPB	*N*, *N*′-bis(naphthalen-1-yl)-*N*, *N*′-bis(phenyl)-benzidine	HTL + host
$Os(bptz)_2(dppee)$	osmium(II)bis(3-tert-butyl-5-(2-pyridyl)-1,2,4-triazolate)cis-1,2-bis(diphenylphosphino)ethene	Orange phos. emitter
Os-R1	osmium(II)bis(3-(trifluoromethyl)-5-(pyridine)-1,2-pyridazine)diphenylmethylphosphine	Red phos. emitter
OXA	(3,5-bis(5-(4-tert-butylphenyl)-1,3,4-oxadiazol-2-yl)-benzene)	ETL
OXD-7	1,3-bis[2-(4-tert-butylphenyl)-1,3,4-oxadiazo-5-yl]benzene	ETL
PBD	2-(4-biphenylyl)-5-(4-tert-butylphenyl)1,3,4-oxadiazole	ETL
$(Piq)_2Ir(acaF)$	bis-(1-phenylisoquinolyl)iridium(III)(1-trifluoro)acetylacetonate	Red phos. emitter
PO9	3,6-bis(diphenylphosphoryl)-9-phenylcarbazole	Host
$(Ppq)_2Ir(acac)$	bis-(1-phenylisoquinolyl)iridium(III)(1-trifluoro)acetylacetonate	Red phos. emitter
PQIr	iridium(III)bis(2-phenyl quinolyl-*N*, $C^{2'}$)acetylacetonate	Red phos. emitter
$PQ_2Ir(dpm)$	iridium bis(2-phenyl-quinoly-*N*, $C^{2'}$)dipivaloylmethane	Red phos. emitter
PtL^2Cl	(platinum II(methyl-3,5-di(2-pyridyl)benzoate)chloride)	Blue phos. emitter
Spiro-DPVBi	2, 2′, 7, 7′-tetrakis(2, 2-diphenylvinyl)spiro-9, 9′-bifluorene	Blue fluor. emitter
SPPO1	9,9-spirobifluoren-2-yl-diphenyl-phosphine oxide	Host
TBADN	2-(*t*-butyl)-9, 10-bis(2′-naphthyl)anthracene	ETL
TCTA	4, 4′, 4″-tris(carbazol-9-yl)-triphenylamine	Host
TPABT	4,7-bis(4-(N-phenyl-N-(4-methylphenyl)amino)phenyl)-2,1-3-benzothiadiazole	Orange fluor. emitter
TPATBT	4,7-bis(5-(4-(N-phenyl-N-(4-methylphenyl)amino)phenyl)-thienyl-2-)-2,1,3-benzothiadiazole	Red fluor. emitter
TPB	1,1,4,4-tetraphenyl-1,3-butadiene	Blue fluor. emitter
TPBi	2, 2′, 2″-(1, 3, 5-benzinetriyl)-tris(1-phenyl-1-H-benzimidazole)	ETL
TPDCM	2-(2-[2-(4-(bis(phenyl-amino)phenyl)-vinyl]-6-tert-butyl-pyran-4-ylidene)-malononitrile	Red fluor. emitter
TPyPA	tris[4-(pyrenyl)-phenyl]amine	Blue fluor. emitter
UGH2	1,4-bis(triphenylsilyl)benzene	Host

TABLE IV. Polymer materials.

Abbreviation	IUPAC name	Function
C12O-PPP	C12O-poly(1,4-phenylene)	Blue fluor. emitter
MEH-PPV	poly[2-methoxy-5-(2-ethylhexyloxy)-1,4-phenylenevinylene]	Green fluor. emitter
P36HCTPSi	n.a.; see Cheng *et al.* (2010) for chemical structure	Host
PDHF	poly(9,9-dihexylfluorene-2,7-diyl)	Blue emitter + host
PDMS	poly(dimethylsiloxane)	Insulator
PEDOT:PSS	poly(3,4-ethylenedioxythiophene) poly(styrenesulfonate)	HTL
PF	polyfluorene	Host
PFO-poss	polyhedral oligomeric silsesquioxane-terminated poly(9,9-dioctylfuorene)	Blue fluor. emitter + host
PF-OH	poly[9,9-bis(2-(2-(2-diethanolamino ethoxy)ethoxy)ethyl)fluorene]	Host
PMMA	poly(methyl 2-methylpropenoate)	Wide band gap insulator
PVK	poly(N-vinylcarbazole)	Host
SY	Super yellow	Yellow fluor. emitter
VB-TCTA	vinylbenzyl-4, 4′, 4″-tris(carbazol-9-yl)-triphenylamine	Host
WPF03	n.a.; see Niu *et al.* (2006) and Tu *et al.* (2006) for chemical structure	White-emitting host

REFERENCES

Adachi, C., M. A. Baldo, S. R. Forrest, S. Lamansky, M. E. Thompson, and R. C. Kwong, 2001, Appl. Phys. Lett. **78**, 1622.

Adachi, C., M. A. Baldo, S. R. Forrest, and M. E. Thompson, 2000, Appl. Phys. Lett. **77**, 904.

Adachi, C., M. A. Baldo, M. E. Thompson, and S. R. Forrest, 2001, J. Appl. Phys. **90**, 5048.

Adachi, C., R. C. Kwong, P. Djurovich, V. Adamovich, M. A. Baldo, M. E. Thompson, and S. R. Forrest, 2001, Appl. Phys. Lett. **79**, 2082.

Adamovich, V., J. Brooks, A. Tamayo, A. M. Alexander, P. I. Djurovich, B. W. D'Andrade, C. Adachi, S. R. Forrest, and M. E. Thompson, 2002, New J. Chem. **26**, 1171.

Anikeeva, P. O., J. E. Halpert, M. G. Bawendi, and V. Bulovic, 2007, Nano Lett. **7**, 2196.

Anthopoulos, T. D., J. P. J. Markham, E. B. Namdas, I. D. W. Samuel, S. C. Lo, and P. L. Burn, 2003, Appl. Phys. Lett. **82**, 4824.

Azuma, T., H. Einhorn, M. Halstead, C. Jerome, J. de Kerf, J. Krtil, W. Münch, E. Barth, J. Ouweitjes, M. Richter, and G. Siljeholm, 1995, CIE Publications **13.3**, 1.

Baek, H. I., and C. H. Lee, 2008, J. Phys. D **41**, 105101.

Baldo, M. A., C. Adachi, and S. R. Forrest, 2000, Phys. Rev. B **62**, 10 967.

Baldo, M. A., and S. R. Forrest, 2000, Phys. Rev. B **62**, 10 958.

Baldo, M. A., V. G. Kozlov, P. E. Burrows, S. R. Forrest, V. S. Ban, B. Koene, and M. E. Thompson, 1997, Appl. Phys. Lett. **71**, 3033.

Baldo, M. A., D. F. O'Brien, M. E. Thompson, and S. R. Forrest, 1999, Phys. Rev. B **60**, 14 422.

Baldo, M. A., D. F. O'Brien, Y. You, A. Shoustikov, S. Sibley, M. E. Thompson, and S. R. Forrest, 1998, Nature (London) **395**, 151.

Baldo, M. A., M. E. Thompson, and S. R. Forrest, 2000, Nature (London) **403**, 750.

Berggren, M., O. Inganas, G. Gustafsson, J. Rasmusson, M. R. Andersson, T. Hjertberg, and O. Wennerstrom, 1994, Nature (London) **372**, 444.

Blochwitz, J., M. Pfeiffer, T. Fritz, and K. Leo, 1998, Appl. Phys. Lett. **73**, 729.

Braslavsky, S. E., E. Fron, H. B. Rodriguez, E. S. Roman, G. D. Scholes, G. Schweitzer, B. Valeur, and J. Wirz, 2008, Photochem. Photobiol. Sci. **7**, 1444.

Brütting, W., J. Frischeisen, T. D. Schmidt, B. J. Scholz, and C. Mayr, 2013, Phys. Status Solidi A **210**, 44..

Bulovic, V., G. Gu, P. E. Burrows, S. R. Forrest, and M. E. Thompson, 1996, Nature (London) **380**, 29.

Burroughes, J. H., D. D. C. Bradley, A. R. Brown, R. N. Marks, K. Mackay, R. H. Friend, P. L. Burns, and A. B. Holmes, 1990, Nature (London) **347**, 539.

Burrows, P. E., S. R. Forrest, S. P. Sibley, and M. E. Thompson, 1996, Appl. Phys. Lett. **69**, 2959.

Cai, C., S.-J. Su, T. Chiba, H. Sasabe, Y.-J. Pu, K. Nakayama, and J. Kido, 2011a, Jpn. J. Appl. Phys. **50**, 040204.

Cai, C., S.-J. Su, T. Chiba, H. Sasabe, Y.-J. Pu, K. Nakayama, and J. Kido, 2011b, Org. Electron. **12**, 843.

Caruge, J. M., J. E. Halpert, V. Wood, V. Bulovic, and M. G. Bawendi, 2008, Nat. Photonics **2**, 247.

Castellani, M., and D. Berner, 2007, J. Appl. Phys. **102**, 024509.

Chang, C. H., C. C. Chen, C. C. Wu, S. Y. Chang, J. Y. Hung, and Y. Chi, 2010, Org. Electron. **11**, 266.

Chang, C. H., K. C. Tien, C. C. Chen, M. S. Lin, H. C. Cheng, S. H. Liu, C. C. Wu, J. Y. Hung, Y. C. Chiu, and Y. Chi, 2010, Org. Electron. **11**, 412.

Chao, C. I., and S. A. Chen, 1998, Appl. Phys. Lett. **73**, 426.

Chen, F. C., Y. Yang, M. E. Thompson, and J. Kido, 2002, Appl. Phys. Lett. **80**, 2308.

Chen, S. F., L. L. Deng, J. Xie, L. Peng, L. H. Xie, Q. L. Fan, and W. Huang, 2010, Adv. Mater. **22**, 5227.

Cheng, G., T. Fei, Y. Duan, Y. Zhao, Y. G. Ma, and S. Y. Liu, 2010, Opt. Lett. **35**, 2436.

Cheng, G., F. Li, Y. Duan, J. Feng, S. Y. Liu, S. Qiu, D. Lin, Y. G. Ma, and S. T. Lee, 2003, Appl. Phys. Lett. **82**, 4224.

Cheng, G., Y. F. Zhang, Y. Zhao, Y. Y. Lin, C. Y. Ruan, S. Y. Liu, T. Fei, Y. G. Ma, and Y. X. Cheng, 2006, Appl. Phys. Lett. **89**, 043504.

Cheng, G., Y. F. Zhang, Y. Zhao, S. Y. Liu, and Y. G. Ma, 2006, Appl. Phys. Lett. **88**, 083512.

Chin, B. D., and C. Lee, 2007, Adv. Mater. **19**, 2061.

Choukri, H., A. Fischer, S. Forget, S. Chenais, M. C. Castex, D. Ades, A. Siove, and B. Geffroy, 2006, Appl. Phys. Lett. **89**, 183513.

Chuang, C. Y., P. I. Shih, C. H. Chien, F. I. Wu, and C. F. Shu, 2007, Macromolecules **40**, 247.

Chuen, C. H., and Y. T. Tao, 2002, Appl. Phys. Lett. **81**, 4499.

Cocchi, M., J. Kalinowski, V. Fattori, J. A. G. Williams, and L. Murphy, 2009, Appl. Phys. Lett. **94**, 073309.

Cocchi, M., J. Kalinowski, L. Murphy, J. A. G. Williams, and V. Fattori, 2010, Org. Electron. **11**, 388.

Cocchi, M., J. Kalinowski, D. Virgili, V. Fattori, S. Develay, and J. A. G. Williams, 2007, Appl. Phys. Lett. **90**, 163508.

Coe, S., W. K. Woo, M. Bawendi, and V. Bulovic, 2002, Nature (London) **420**, 800.

Connick, W. B., L. M. Henling, R. E. Marsh, and H. B. Gray, 1996, Inorg. Chem. **35**, 6261.

D'Andrade, B. W., J. Brooks, V. Adamovich, M. E. Thompson, and S. R. Forrest, 2002, Adv. Mater. **14**, 1032.

D'Andrade, B. W., and J. J. Brown, 2006, Appl. Phys. Lett. **88**, 192908.

D'Andrade, B. W., and S. R. Forrest, 2003, J. Appl. Phys. **94**, 3101.

D'Andrade, B. W., R. J. Holmes, and S. R. Forrest, 2004, Adv. Mater. **16**, 624.

D'Andrade, B. W., M. E. Thompson, and S. R. Forrest, 2002, Adv. Mater. **14**, 147.

Deaton, J. C., M. E. Kondakova, D. J. Giesen, W. J. Begley, and D. Y. Kondakov, 2008, U.S. Patent No. US020080286610A1.

Deaton, J. C., S. C. Switalski, D. Y. Kondakov, R. H. Young, T. D. Pawlik, D. J. Giesen, S. B. Harkins, A. J. M. Miller, S. F. Mickenberg, and J. C. Peters, 2010, J. Am. Chem. Soc. **132**, 9499.

Dexter, D. L., 1953, J. Chem. Phys. **21**, 836.

Duan, Y., M. Mazzeo, V. Maiorano, F. Mariano, D. Qin, R. Cingolani, and G. Gigli, 2008, Appl. Phys. Lett. **92**, 113304.

Edison, T. A., 1880, U.S. Patent No. US223898 (A).

Endo, A., M. Ogasawara, A. Takahashi, D. Yokoyama, Y. Kato, and C. Adachi, 2009, Adv. Mater. **21**, 4802.

Endo, A., K. Sato, K. Yoshimura, T. Kai, A. Kawada, H. Miyazaki, and C. Adachi, 2011, Appl. Phys. Lett. **98**, 083302.

Fehse, K., K. Walzer, K. Leo, W. Loevenich, and A. Elschner, 2007, Adv. Mater. **19**, 441.

Feng, J., F. Li, W. B. Gao, S. Y. Liu, Y. Liu, and Y. Wang, 2001, Appl. Phys. Lett. **78**, 3947.

Fick, A., 1995, J. Membr. Sci. **100**, 33.

Flaemmich, M., J. Frischeisen, D. S. Setz, D. Michaelis, B. C. Krummacher, T. D. Schmidt, W. Bruetting, and N. Danz, 2011, Org. Electron. **12**, 1663.

Forrest, S. R., 1997, Chem. Rev. **97**, 1793.

Forrest, S. R., 2004, Nature (London) **428**, 911.

Forrest, S. R., D. D. C. Bradley, and M. E. Thompson, 2003, Adv. Mater. **15**, 1043.

Förster, T., 1948, Ann. Phys. (Berlin) **437**, 55.

Freitag, P., S. Reineke, S. Olthof, M. Furno, B. Lüssem, and K. Leo, 2010, Org. Electron. **11**, 1676.

Friend, R. H., *et al.*, 1999, Nature (London) **397**, 121.

Frischeisen, J., D. Yokoyama, C. Adachi, and W. Bruetting, 2010, Appl. Phys. Lett. **96**, 073302.

Frischeisen, J., D. Yokoyama, A. Endo, C. Adachi, and W. Bruetting, 2011, Org. Electron. **12**, 809.

Furno, M., R. Meerheim, S. Hofmann, B. Luessem, and K. Leo, 2012, Phys. Rev. B **85**, 115205.

Furno, M., R. Meerheim, M. Thomschke, S. Hofmann, B. Lüssem, and K. Leo, 2010, Proc. SPIE Int. Soc. Opt. Eng. **7617**, 761716.

Gärtner, G., and H. Greiner, 2008, Proc. SPIE Int. Soc. Opt. Eng. **6999**, 69992T.

Gather, M. C., R. Alle, H. Becker, and K. Meerholz, 2007, Adv. Mater. **19**, 4460.

Gather, M. C., A. Koehnen, A. Falcou, H. Becker, and K. Meerholz, 2007, Adv. Funct. Mater. **17**, 191.

Gather, M. C., A. Köhnen, and K. Meerholz, 2011, Adv. Mater. **23**, 233.

Giebink, N. C., Y. Sun, and S. R. Forrest, 2006, Org. Electron. **7**, 375.

Gohri, V., S. Hofmann, S. Reineke, T. Rosenow, M. Thomschke, M. Levichkova, B. Luessem, and K. Leo, 2011, Org. Electron. **12**, 2126.

Gong, X., W. L. Ma, J. C. Ostrowski, G. C. Bazan, D. Moses, and A. J. Heeger, 2004, Adv. Mater. **16**, 615.

Gong, X., S. Wang, D. Moses, G. C. Bazan, and A. J. Heeger, 2005, Adv. Mater. **17**, 2053.
Goushi, K., R. Kwong, J. J. Brown, H. Sasabe, and C. Adachi, 2004, J. Appl. Phys. **95**, 7798.
Goushi, K., K. Yoshida, K. Sato, and C. Adachi, 2012, Nat. Photonics **6**, 253.
Granstrom, M., and O. Inganas, 1996, Appl. Phys. Lett. **68**, 147.
Greenham, N. C., R. H. Friend, and D. D. C. Bradley, 1994, Adv. Mater. **6**, 491.
Greiner, H., 2007, Jpn. J. Appl. Phys. **46**, 4125.
Greiner, M. T., M. G. Helander, W.-M. Tang, Z.-B. Wang, J. Qiu, and Z.-H. Lu, 2012, Nat. Mater. **11**, 76.
Guo, J., N. Koch, S. L. Bernasek, and J. Schwartz, 2006, Chem. Phys. Lett. **426**, 370.
Hamada, Y., C. Adachi, T. Tsutsui, and S. Saito, 1992, Jpn. J. Appl. Phys. **31**, 1812.
Hamada, Y., T. Sang, H. Fujii, Y. Nishio, H. Takanashi, and K. Shibata, 1996, Jpn. J. Appl. Phys. Pt. 2 Letters **35**, L1339.
Han, L. L., D. F. Yang, W. L. Li, B. Chu, Y. Chen, Z. S. Su, D. Y. Zhang, F. Yan, Z. Z. Hu, and Z. Q. Zhang, 2008, Appl. Phys. Lett. **93**, 153303.
Harada, K., A. G. Werner, M. Pfeiffer, C. J. Bloom, C. M. Elliott, and K. Leo, 2005, Phys. Rev. Lett. **94**, 036601.
He, G. F., M. Pfeiffer, K. Leo, M. Hofmann, J. Birnstock, R. Pudzich, and J. Salbeck, 2004, Appl. Phys. Lett. **85**, 3911.
He, G. F., O. Schneider, D. S. Qin, X. Zhou, M. Pfeiffer, and K. Leo, 2004, J. Appl. Phys. **95**, 5773.
Helfrich, W., and W. G. Schneider, 1965, Phys. Rev. Lett. **14**, 229.
Ho, C. L., M. F. Lin, W. Y. Wong, W. K. Wong, and C. H. Chen, 2008, Appl. Phys. Lett. **92**, 083301.
Ho, C. L., W. Y. Wong, Q. Wang, D. G. Ma, L. X. Wang, and Z. Y. Lin, 2008, Adv. Funct. Mater. **18**, 928.
Hofmann, S., T. C. Rosenow, M. C. Gather, B. Luessem, and K. Leo, 2012, Phys. Rev. B **85**, 245209.
Hofmann, S., M. Thomschke, P. Freitag, M. Furno, B. Lüssem, and K. Leo, 2010, Appl. Phys. Lett. **97**, 253308.
Holmes, R. J., B. W. D'Andrade, S. R. Forrest, X. Ren, J. Li, and M. E. Thompson, 2003, Appl. Phys. Lett. **83**, 3818.
Hsu, S. F., C. C. Lee, S. W. Hwang, and C. H. Chen, 2005, Appl. Phys. Lett. **86**, 253508.
Hu, B., and F. E. Karasz, 2003, J. Appl. Phys. **93**, 1995.
Huang, F., P. I. Shih, C. F. Shu, Y. Chi, and A. K. Y. Jen, 2009, Adv. Mater. **21**, 361.
Huang, J. S., W. J. Hou, J. H. Li, G. Li, and Y. Yang, 2006, Appl. Phys. Lett. **89**, 133509.
Huang, J. S., G. Li, E. Wu, Q. F. Xu, and Y. Yang, 2006, Adv. Mater. **18**, 114.
Huang, Q., K. Walzer, M. Pfeiffer, V. Lyssenko, G. F. He, and K. Leo, 2006, Appl. Phys. Lett. **88**, 113515.
Huang, Y. S., J. H. Jou, W. K. Weng, and J. M. Liu, 2002, Appl. Phys. Lett. **80**, 2782.
Hung, L. S., C. W. Tang, M. G. Mason, P. Raychaudhuri, and J. Madathil, 2001, Appl. Phys. Lett. **78**, 544.
Hung, W. Y., L. C. Chi, W. J. Chen, Y. M. Chen, S. H. Chou, and K. T. Wong, 2010, J. Mater. Chem. **20**, 10113.
Hunt, R., 1995, *Measuring Color* (Ellis Horwood, London), 2nd ed.
Jiang, J. X., Y. H. Xu, W. Yang, R. Guan, Z. Q. Liu, H. Y. Zhen, and Y. Cao, 2006, Adv. Mater. **18**, 1769.
Jordan, R. H., A. Dodabalapur, M. Strukelj, and T. M. Miller, 1996, Appl. Phys. Lett. **68**, 1192.
Jou, J. H., Y. S. Chiu, C. P. Wang, R. Y. Wang, and C. Hu, 2006, Appl. Phys. Lett. **88**, 193501.
Kahn, A., J.-J. Pireaux, W. R. Salaneck, and K. Seki, 2001, Eds., *Conjugated Polymer and Molecular Interfaces* (Marcel Dekker, Inc., New York).
Kalinowski, J., M. Cocchi, V. Fattori, L. Murphy, and J. A. G. Williams, 2010, Org. Electron. **11**, 724.
Kalinowski, J., M. Cocchi, D. Virgili, V. Tattori, and J. A. G. Williams, 2007, Adv. Mater. **19**, 4000.
Kalinowski, J., W. Stampor, J. Mezyk, M. Cocchi, D. Virgili, V. Fattori, and P. Di Marco, 2002, Phys. Rev. B **66**, 235321.
Kang, J. W., S. H. Lee, H. D. Park, W. I. Jeong, K. M. Yoo, Y. S. Park, and J. J. Kim, 2007, Appl. Phys. Lett. **90**, 223508.
Kanno, H., N. C. Giebink, Y. R. Sun, and S. R. Forrest, 2006, Appl. Phys. Lett. **89**, 023503.
Kanno, H., R. J. Holmes, Y. Sun, S. Kena-Cohen, and S. R. Forrest, 2006, Adv. Mater. **18**, 339.
Kanno, H., Y. Sun, and S. R. Forrest, 2005, Appl. Phys. Lett. **86**, 263502.
Kanno, H., Y. R. Sun, and S. R. Forrest, 2006, Appl. Phys. Lett. **89**, 143516.
Kawamura, Y., J. Brooks, J. J. Brown, H. Sasabe, and C. Adachi, 2006, Phys. Rev. Lett. **96**, 017404.
Kawamura, Y., K. Goushi, J. Brooks, J. J. Brown, H. Sasabe, and C. Adachi, 2005, Appl. Phys. Lett. **86**, 071104.
Kawamura, Y., S. Yanagida, and S. R. Forrest, 2002, J. Appl. Phys. **92**, 87.
Kepler, R. G., P. Avakian, J. C. Caris, and E. Abramson, 1963, Phys. Rev. Lett. **10**, 400.
Kido, J., K. Hongawa, K. Okuyama, and K. Nagai, 1994, Appl. Phys. Lett. **64**, 815.
Kido, J., M. Kimura, and K. Nagai, 1995, Science **267**, 1332.
Kido, J., H. Shionoya, and K. Nagai, 1995, Appl. Phys. Lett. **67**, 2281.
Kim, C. H., and J. Shinar, 2002, Appl. Phys. Lett. **80**, 2201.
Kim, J. H., P. Herguth, M. S. Kang, A. K. Y. Jen, Y. H. Tseng, and C. F. Shu, 2004, Appl. Phys. Lett. **85**, 1116.
Kim, S. H., J. Jang, and J. Y. Lee, 2007, Appl. Phys. Lett. **91**, 123509.
Kim, T. H., H. K. Lee, O. O. Park, B. D. Chin, S. H. Lee, and J. K. Kim, 2006, Adv. Funct. Mater. **16**, 611.
Klessinger, M., and J. Michl, 1989, *Lichtabsorption und Photochemie organischer Moleküle* (VCH Verlagsgesellschaft mbH, Weinheim).
Kobayashi, T., N. Ide, N. Matsusue, and H. Naito, 2005, Jpn. J. Appl. Phys. **44**, 1966.
Koch, N., 2012, Phys. Status Solidi RRL **6**, 277.
Koch, N., S. Duhm, J. P. Rabe, A. Vollmer, and R. L. Johnson, 2005, Phys. Rev. Lett. **95**, 237601.
Koh, T. W., J. M. Choi, S. Lee, and S. Yoo, 2010, Adv. Mater. **22**, 1849.
Köhnen, A., M. Irion, M. C. Gather, N. Rehmann, P. Zacharias, and K. Meerholz, 2010, J. Mater. Chem. **20**, 3301.
Kondakov, D. Y., 2007, J. Appl. Phys. **102**, 114504.
Kondakova, M. E., J. C. Deaton, T. D. Pawlik, D. J. Giesen, D. Y. Kondakov, R. H. Young, T. L. Royster, D. L. Comfort, and J. D. Shore, 2010, J. Appl. Phys. **107**, 014515.
Koo, W. H., S. M. Jeong, F. Araoka, K. Ishikawa, S. Nishimura, T. Toyooka, and H. Takezoe, 2010, Nat. Photonics **4**, 222.
Koshiyama, T., A. Omura, and M. Kato, 2004, Chem. Lett. **33**, 1386.
Krummacher, B. C., V. E. Choong, M. K. Mathai, S. A. Choulis, F. So, F. Jermann, T. Fiedler, and M. Zachau, 2006, Appl. Phys. Lett. **88**, 113506.
Krummacher, B. C., S. Nowy, J. Frischeisen, M. Klein, and W. Brütting, 2009, Org. Electron. **10**, 478.

Lai, S. L., S. L. Tao, M. Y. Chan, T. W. Ng, M. F. Lo, C. S. Lee, X. H. Zhang, and S. T. Lee, 2010, Org. Electron. **11**, 1511.
Lee, S. K., D. H. Hwang, B. J. Jung, N. S. Cho, J. Lee, J. D. Lee, and H. K. Shim, 2005, Adv. Funct. Mater. **15**, 1647.
Leem, D. S., J. W. Kim, S. O. Jung, S. O. Kim, S. H. Kim, K. Y. Kim, Y. H. Kim, S. K. Kwon, and J. J. Kim, 2010, J. Phys. D **43**, 405102.
Lei, G. T., L. D. Wang, and Y. Qiu, 2004, Appl. Phys. Lett. **85**, 5403.
Lei, G. T., L. D. Wang, and Y. Qiu, 2006, Appl. Phys. Lett. **88**, 103508.
Lin, C. L., T. Y. Cho, C. H. Chang, and C. C. Wu, 2006, Appl. Phys. Lett. **88**, 081114.
Liu, J., X. Guo, L. J. Bu, Z. Y. Xie, Y. X. Cheng, Y. H. Geng, L. X. Wang, X. B. Jing, and F. S. Wang, 2007, Adv. Funct. Mater. **17**, 1917.
Liu, J., Z. Y. Xie, Y. X. Cheng, Y. H. Geng, L. X. Wang, X. B. Jing, and F. S. Wang, 2007, Adv. Mater. **19**, 531.
Liu, J., Q. G. Zhou, Y. X. Cheng, Y. H. Geng, L. X. Wang, D. G. Ma, X. B. Jing, and F. S. Wang, 2005, Adv. Mater. **17**, 2974.
Liu, J., Q. G. Zhou, Y. X. Cheng, Y. H. Geng, L. X. Wang, D. G. Ma, X. B. Jing, and F. S. Wang, 2006, Adv. Funct. Mater. **16**, 957.
Lu, M. H., and J. C. Sturm, 2002, J. Appl. Phys. **91**, 595.
Luo, J., X. Z. Li, Q. Hou, J. B. Peng, W. Yang, and Y. Cao, 2007, Adv. Mater. **19**, 1113.
Ma, B. W., P. I. Djurovich, S. Garon, B. Alleyne, and M. E. Thompson, 2006, Adv. Funct. Mater. **16**, 2438.
Ma, Y. G., H. Y. Zhang, J. C. Shen, and C. M. Che, 1998, Synth. Met. **94**, 245.
Madigan, C. F., M. H. Lu, and J. C. Sturm, 2000, Appl. Phys. Lett. **76**, 1650.
Mattoussi, H., H. Murata, C. D. Merritt, Y. Iizumi, J. Kido, and Z. H. Kafafi, 1999, J. Appl. Phys. **86**, 2642.
Mazzeo, M., D. Pisignano, F. Della Sala, J. Thompson, R. I. R. Blyth, G. Gigli, R. Cingolani, G. Sotgiu, and G. Barbarella, 2003, Appl. Phys. Lett. **82**, 334.
Meerheim, R., M. Furno, S. Hofmann, B. Lüssem, and K. Leo, 2010, Appl. Phys. Lett. **97**, 253305.
Meerheim, R., R. Nitsche, and K. Leo, 2008, Appl. Phys. Lett. **93**, 043310.
Meerheim, R., S. Scholz, S. Olthof, G. Schwartz, S. Reineke, K. Walzer, and K. Leo, 2008, J. Appl. Phys. **104**, 014510.
Meerheim, R., K. Walzer, M. Pfeiffer, and K. Leo, 2006, Appl. Phys. Lett. **89**, 061111.
Mladenovski, S., K. Neyts, D. Pavicic, A. Werner, and C. Rothe, 2009, Opt. Express **17**, 7562.
Möller, S., and S. R. Forrest, 2002, J. Appl. Phys. **91**, 3324.
Murphy, C. B., Y. Zhang, T. Troxler, V. Ferry, J. J. Martin, and W. E. Jones, 2004, J. Phys. Chem. B **108**, 1537.
Nakamura, T., N. Tsutsumi, N. Juni, and H. Fujii, 2005, J. Appl. Phys. **97**, 054505.
Namdas, E. B., A. Ruseckas, I. D. W. Samuel, S. C. Lo, and P. L. Burn, 2005, Appl. Phys. Lett. **86**, 091104.
Narukawa, Y., J. Narita, T. Sakamoto, K. Deguchi, T. Yamada, and T. Mukai, 2006, Jpn. J. Appl. Phys. Pt. 2 Letters **45**, L1084.
Narukawa, Y., M. Sano, T. Sakamoto, T. Yamada, and T. Mukai, 2008, Phys. Status Solidi A **205**, 1081.
Neyts, K., 1998, J. Opt. Soc. Am. A **15**, 962.
Niu, X. D., L. Ma, B. Yao, J. Q. Ding, G. L. Tu, Z. Y. Xie, and L. X. Wang, 2006, Appl. Phys. Lett. **89**, 213508.
Niu, Y. H., *et al.*, 2004, Appl. Phys. Lett. **85**, 1619.
Niu, Y. H., M. S. Liu, J. W. Ka, J. Bardeker, M. T. Zin, R. Schofield, Y. Chi, and A. K. Y. Jen, 2007, Adv. Mater. **19**, 300.
Noh, Y. Y., C. L. Lee, J. J. Kim, and K. Yase, 2003, J. Chem. Phys. **118**, 2853.
Nowy, S., B. C. Krummacher, J. Frischeisen, N. A. Reinke, and W. Brütting, 2008, J. Appl. Phys. **104**, 123109.
Ohno, Y., 2004, Proc. SPIE Int. Soc. Opt. Eng. **5530**, 88.
Ohta, N., and A. R. Robertson, 2005, *Colorimetry: Fundamentals and Applications* (John Wiley & Sons, Ltd., New York).
Okumoto, K., H. Kanno, Y. Hamaa, H. Takahashi, and K. Shibata, 2006, Appl. Phys. Lett. **89**, 063504.
Perumal, A., M. Froebel, S. Gorantla, T. Gemming, B. Luessem, J. Eckert, and K. Leo, 2012, Adv. Funct. Mater. **22**, 210.
Pope, M., and C. E. Swenberg, 1999, Eds., *Electronic Processes in Organic Crystals* (Oxford University Press, New York).
Pschenitzka, F., and J. C. Sturm, 1999, Appl. Phys. Lett. **74**, 1913.
Rack, P. D., and P. H. Holloway, 1998, Materials Science & Engineering R-reports **21**, 171.
Rehmann, N., C. Ulbricht, A. Koehnen, P. Zacharias, M. C. Gather, D. Hertel, E. Holder, K. Meerholz, and U. S. Schubert, 2008, Adv. Mater. **20**, 129.
Reineke, S., and M. A. Baldo, 2012, Phys. Status Solidi A **209**, 2341.
Reineke, S., F. Lindner, G. Schwartz, N. Seidler, K. Walzer, B. Lüssem, and K. Leo, 2009, Nature (London) **459**, 234.
Reineke, S., T. C. Rosenow, B. Lüssem, and K. Leo, 2010, Adv. Mater. **22**, 3189.
Reineke, S., G. Schwartz, K. Walzer, M. Falke, and K. Leo, 2009, Appl. Phys. Lett. **94**, 163305.
Reineke, S., G. Schwartz, K. Walzer, and K. Leo, 2007, Appl. Phys. Lett. **91**, 123508.
Reineke, S., G. Schwartz, K. Walzer, and K. Leo, 2009, Phys. Status Solidi RRL **3**, 67.
Reineke, S., K. Walzer, and K. Leo, 2007, Phys. Rev. B **75**, 125328.
Reinhold, J., 2004, *Quantentheorie der Moleküle: Eine Einführung* (B. G. Teubner Verlag/GWV Fachverlage GmbH, Wiesbaden).
Riel, H., S. Karg, T. Beierlein, B. Ruhstaller, and W. Riess, 2003, Appl. Phys. Lett. **82**, 466.
Rosenow, T. C., M. Furno, S. Reineke, S. Olthof, B. Lüssem, and K. Leo, 2010, J. Appl. Phys. **108**, 113113.
Sasabe, H., and J. Kido, 2011, Chem. Mater. **23**, 621.
Sasabe, H., J. Takamatsu, T. Motoyama, S. Watanabe, G. Wagenblast, N. Langer, O. Molt, E. Fuchs, C. Lennartz, and J. Kido, 2010, Adv. Mater. **22**, 5003.
Sasabe, H., D. Tanaka, D. Yokoyama, T. Chiba, Y.-J. Pu, K.-i. Nakayama, M. Yokoyama, and J. Kido, 2011, Adv. Funct. Mater. **21**, 336.
Schmidt, T. D., D. S. Setz, M. Flaemmich, J. Frischeisen, D. Michaelis, B. C. Krummacher, N. Danz, and W. Bruetting, 2011, Appl. Phys. Lett. **99**, 163302.
Schwab, T., M. Thomschke, S. Hofmann, M. Furno, K. Leo, and B. Luessem, 2011, J. Appl. Phys. **110**, 083118.
Schwartz, G., K. Fehse, M. Pfeiffer, K. Walzer, and K. Leo, 2006, Appl. Phys. Lett. **89**, 083509.
Schwartz, G., T. H. Ke, C. C. Wu, K. Walzer, and K. Leo, 2008, Appl. Phys. Lett. **93**, 073304.
Schwartz, G., M. Pfeiffer, S. Reineke, K. Walzer, and K. Leo, 2007, Adv. Mater. **19**, 3672.
Schwartz, G., S. Reineke, T. C. Rosenow, K. Walzer, and K. Leo, 2009, Adv. Funct. Mater. **19**, 1319.
Schwartz, G., S. Reineke, K. Walzer, and K. Leo, 2008, Appl. Phys. Lett. **92**, 053311.
Segal, M., M. A. Baldo, R. J. Holmes, S. R. Forrest, and Z. G. Soos, 2003, Phys. Rev. B **68**, 075211.
Segal, M., M. Singh, K. Rivoire, S. Difley, T. Van Voorhis, and M. A. Baldo, 2007, Nat. Mater. **6**, 374.

Seidler, N., S. Reineke, K. Walzer, B. Lüssem, A. Tomkeviciene, J. V. Grazulevicius, and K. Leo, 2010, Appl. Phys. Lett. **96**, 093304.
Seo, J. H., S. J. Lee, B. M. Seo, S. J. Moon, K. H. Lee, J. K. Park, S. S. Yoon, and Y. K. Kim, 2010, Org. Electron. **11**, 1759.
Seo, J. H., J. H. Seo, J. H. Park, Y. K. Kim, J. H. Kim, G. W. Hyung, K. H. Lee, and S. S. Yoon, 2007, Appl. Phys. Lett. **90**, 203507.
Shen, Z. L., P. E. Burrows, V. Bulovic, S. R. Forrest, and M. E. Thompson, 1997, Science **276**, 2009.
Shimizu, M., and T. Hiyama, 2010, Chemistry-an Asian Journal **5**, 1516.
Shirasaki, Y., G. Supran, M. Bawendi, and V. Bulovic, 2013, Nat. Photonics **7**, 13.
So, F., and D. Kondakov, 2010, Adv. Mater. **22**, 3762.
Sokolik, I., R. Priestley, A. D. Walser, R. Dorsinville, and C. W. Tang, 1996, Appl. Phys. Lett. **69**, 4168.
Staroske, W., M. Pfeiffer, K. Leo, and M. Hoffmann, 2007, Phys. Rev. Lett. **98**, 197402.
Steele, R. V., 2007, Nat. Photonics **1**, 25.
Stewart, J. S., T. Lippert, M. Nagel, F. Nuesch, and A. Wokaun, 2012, Appl. Phys. Lett. **100**, 203303.
Strukelj, M., R. H. Jordan, and A. Dodabalapur, 1996, J. Am. Chem. Soc. **118**, 1213.
Su, S. J., E. Gonmori, H. Sasabe, and J. Kido, 2008, Adv. Mater. **20**, 4189.
Su, S. J., H. Sasabe, Y. J. Pu, K. Nakayama, and J. Kido, 2010, Adv. Mater. **22**, 3311.
Sun, Y., and S. R. Forrest, 2007, Appl. Phys. Lett. **91**, 263503.
Sun, Y., and S. R. Forrest, 2008a, Nat. Photonics **2**, 483.
Sun, Y. R., and S. R. Forrest, 2008b, Org. Electron. **9**, 994.
Sun, Y. R., N. C. Giebink, H. Kanno, B. W. Ma, M. E. Thompson, and S. R. Forrest, 2006, Nature (London) **440**, 908.
Suna, A., 1970, Phys. Rev. B **1**, 1716.
Swanson, S. A., G. M. Wallraff, J. P. Chen, W. J. Zhang, L. D. Bozano, K. R. Carter, J. R. Salem, R. Villa, and J. C. Scott, 2003, Chem. Mater. **15**, 2305.
Tanaka, D., Y. Agata, T. Takeda, S. Watanabe, and J. Kido, 2007, Jpn. J. Appl. Phys. Pt. 2 Letters **46**, L117.
Tanaka, D., H. Sasabe, Y. J. Li, S. J. Su, T. Takeda, and J. Kido, 2007, Jpn. J. Appl. Phys. **46**, L10.
Tanaka, H., T. Ise, D. Shiomi, K. Sato, and T. Takui, 2006, J. Low Temp. Phys. **142**, 601.
Taneda, M., T. Yasuda, and C. Adachi, 2011, Appl. Phys. Express **4**, 071602.
Tang, C. W., and S. A. VanSlyke, 1987, Appl. Phys. Lett. **51**, 913.
Tasch, S., E. J. W. List, O. Ekström, W. Graupner, G. Leising, P. Schlichting, U. Rohr, Y. Geerts, U. Scherf, and K. Müllen, 1997, Appl. Phys. Lett. **71**, 2883.
Thompson, J., R. I. R. Blyth, M. Mazzeo, M. Anni, G. Gigli, and R. Cingolani, 2001, Appl. Phys. Lett. **79**, 560.
Thompson, M. E., 2007, MRS Bull. **32**, 694.
Thomschke, M., R. Nitsche, M. Furno, and K. Leo, 2009, Appl. Phys. Lett. **94**, 083303.
Thomschke, M., S. Reineke, B. Luessem, and K. Leo, 2012, Nano Lett. **12**, 424.
Tokito, S., T. Iijima, Y. Suzuri, H. Kita, T. Tsuzuki, and F. Sato, 2003, Appl. Phys. Lett. **83**, 569.
Tokito, S., T. Tsuzuki, F. Sato, and T. Iijima, 2005, Curr. Appl. Phys. **5**, 331.
Tong, Q. X., S. L. Lai, M. Y. Chan, J. X. Tang, H. L. Kwong, C. S. Lee, and S. T. Lee, 2007, Appl. Phys. Lett. **91**, 023503.
Tsai, M. H., H. W. Lin, H. C. Su, T. H. Ke, C. C. Wu, F. C. Fang, Y. L. Liao, K. T. Wong, and C. I. Wu, 2006, Adv. Mater. **18**, 1216.
Tsai, M. L., C. Y. Liu, M. A. Hsu, and T. J. Chow, 2003, Appl. Phys. Lett. **82**, 550.
Tsai, Y. C., and J. H. Jou, 2006, Appl. Phys. Lett. **89**, 243521.
Tu, G. L., C. Y. Mei, Q. G. Zhou, Y. X. Cheng, Y. H. Geng, L. X. Wang, D. G. Ma, X. B. Jing, and F. S. Wang, 2006, Adv. Funct. Mater. **16**, 101.
Tu, G. L., Q. G. Zhou, Y. X. Cheng, L. X. Wang, D. G. Ma, X. B. Jing, and F. S. Wang, 2004, Appl. Phys. Lett. **85**, 2172.
Uoyama, H., K. Goushi, K. Shizu, H. Nomura, and C. Adachi, 2012, Nature (London) **492**, 234.
Walzer, K., B. Maennig, M. Pfeiffer, and K. Leo, 2007, Chem. Rev. **107**, 1233.
Wang, Q., J. Q. Ding, D. G. Ma, Y. X. Cheng, L. X. Wang, X. B. Jing, and F. S. Wang, 2009a, Adv. Funct. Mater. **19**, 84.
Wang, Q., J. Q. Ding, D. G. Ma, Y. X. Cheng, L. X. Wang, and F. S. Wang, 2009b, Adv. Mater. **21**, 2397.
Wang, Y. Z., R. G. Sun, F. Meghdadi, G. Leising, and A. J. Epstein, 1999, Appl. Phys. Lett. **74**, 3613.
Weichsel, C., S. Reineke, M. Furno, B. Luessem, and K. Leo, 2012, J. Appl. Phys. **111**, 033102.
Wigner, E., and E. E. Witmer, 1928, Z. Phys. A **51**, 859.
Williams, E. L., K. Haavisto, J. Li, and G. E. Jabbour, 2007, Adv. Mater. **19**, 197.
Wood, V., M. J. Panzer, D. Bozyigit, Y. Shirasaki, I. Rousseau, S. Geyer, M. G. Bawendi, and V. Bulovic, 2011, Nano Lett. **11**, 2927.
Wu, H. B., J. H. Zou, F. Liu, L. Wang, A. Mikhailovsky, G. C. Bazan, W. Yang, and Y. Cao, 2008, Adv. Mater. **20**, 696.
Wu, W. C., W. Y. Lee, and W. C. Chen, 2006, Macromol. Chem. Phys. **207**, 1131.
Wu, Y. S., S. W. Hwang, H. H. Chen, M. T. Lee, W. J. Shen, and C. H. Chen, 2005, Thin Solid Films **488**, 265.
Wünsche, J., S. Reineke, B. Lüssem, and K. Leo, 2010, Phys. Rev. B **81**, 245201.
Xie, W. F., S. Y. Liu, and Y. Zhao, 2003, J. Phys. D **36**, 1246.
Xie, Z. Y., J. S. Huang, C. N. Li, S. Y. Liu, Y. Wang, Y. Q. Li, and J. C. Shen, 1999, Appl. Phys. Lett. **74**, 641.
Xu, Q. F., H. M. Duong, F. Wudl, and Y. Yang, 2004, Appl. Phys. Lett. **85**, 3357.
Xu, Y. H., J. B. Peng, J. X. Jiang, W. Xu, W. Yang, and Y. Cao, 2005, Appl. Phys. Lett. **87**, 193502.
Xue, Q., G. H. Xie, P. Chen, J. H. Lu, D. D. Zhang, Y. N. Tang, Y. Zhao, J. Y. Hou, and S. Y. Liu, 2010, Synth. Met. **160**, 829.
Yamamori, A., C. Adachi, T. Koyama, and Y. Taniguchi, 1998, Appl. Phys. Lett. **72**, 2147.
Yan, B. P., C. C. C. Cheung, S. C. F. Kui, H. F. Xiang, V. A. L. Roy, S. J. Xu, and C. M. Che, 2007, Adv. Mater. **19**, 3599.
Yang, Y., T. Peng, K. Q. Ye, Y. Wu, Y. Liu, and Y. Wang, 2011, Org. Electron. **12**, 29.
Yeh, S. J., M. F. Wu, C. T. Chen, Y. H. Song, Y. Chi, M. H. Ho, S. F. Hsu, and C. H. Chen, 2005, Adv. Mater. **17**, 285.
Yersin, H., 2004, *Transition Metal And Rare Earth Compounds III* (Springer-Verlag, Berlin/Heidelberg), Vol. 241.
Yersin, H., D. Donges, W. Humbs, J. Strasser, R. Sitters, and M. Glasbeek, 2002, Inorg. Chem. **41**, 4915.
Yokoyama, D., A. Sakaguchi, M. Suzuki, and C. Adachi, 2009, Org. Electron. **10**, 127.
Zhang, B. H., C. J. Qin, J. Q. Ding, L. Chen, Z. Y. Xie, Y. X. Cheng, and L. X. Wang, 2010, Adv. Funct. Mater. **20**, 2951.
Zhang, L. J., Y. L. Hua, X. M. Wu, Y. Wang, and S. G. Yin, 2008, Chin. Phys. B **17**, 3097.

Zhang, Z. L., X. Y. Jiang, W. Q. Zhu, B. X. Zhang, and S. H. Xu, 2001, J. Phys. D **34**, 3083.
Zheludev, N., 2007, Nat. Photonics **1**, 189.
Zheng, G. Y., and D. P. Rillema, 1998, Inorg. Chem. **37**, 1392.
Zhou, G. J., Q. Wang, C. L. Ho, W. Y. Wong, D. G. Ma, and L. X. Wang, 2009, Chem. Commun. 3574.
Zhou, T. X., T. Ngo, J. J. Brown, M. Shtein, and S. R. Forrest, 2005, Appl. Phys. Lett. **86**, 021107.
Zhou, X., J. Blochwitz, M. Pfeiffer, A. Nollau, T. Fritz, and K. Leo, 2001, Adv. Funct. Mater. **11**, 310.
Zhou, X., *et al.*, 2002, Appl. Phys. Lett. **81**, 4070.
Zhou, Y. C., L. L. Ma, J. Zhou, X. M. Ding, and X. Y. Hou, 2007, Phys. Rev. B **75**, 132202.
Zuniga, C. A., S. Barlow, and S. R. Marder, 2011, Chem. Mater. **23**, 658.